Max-Planck-Institut für
Hirnforschung

Technische Universität
Darmstadt

VISUAL HEMINEGLECT AND LESION-INDUCED CHANGES OF TOP-DOWN ACTIVITY IN THE PRIMARY VISUAL CORTEX

Vom
Fachbereich Biologie
der Technischen Universität Darmstadt
zur
Erlangung des akademischen Grades
eines Doctor rerum naturalium
genehmigte Dissertation von
Dipl. Biol. Miriam Carolin Müller
aus Frankfurt am Main

1. Referent: Prof. Dr. Ralf A. W. Galuske
2. Referent: Prof. Dr. Gerhard Thiel
Tag der Einreichung: 08.11.2016
Tag der mündlichen Prüfung: 20.01.2017
Darmstadt 2017
D 17

SUMMARY

Visual selective attention is the fundamental cognitive ability to filter out irrelevant sensory information in favor of relevant information. In order to make this possible, an integration of exogenous, stimulus-dependent, and endogenous, context-dependent, attentional factors is necessary. The anatomical basis for this integration is formed by a highly complex network of cortical feedforward and feedback projections which connect areas at every sensory processing level. Lesions in distinct areas of this attention network lead to the clinical pathology of visual unilateral neglect, in which the failure of one network component results in the inability to orient or respond to stimuli appearing in the visual field contralateral to a lesion. Frequently, in humans as well as in animal models, a gradual improvement up to a complete restoration of the behavioral performance can be observed some time after the initial lesion. Based on findings from behavioral studies, it has been suggested that a significant imbalance of neuronal activity levels between the two hemispheres and a resulting unequal distribution of limited attention capacities could be the neural basis of visual neglect. Accordingly, a functional recovery would be accompanied by a restoration of the activity balance between the two hemispheres.

Current concepts of the underlying mechanisms of neglect are mainly based on results from behavioral experiments or data collected in anesthetized animals. To date, there are no neurophysiological studies in awake animals which consider the neglect syndrome and its recovery in the behavioral context. The aim of the present study was to close this gap on the one hand, and on the other, to provide a detailed characterization of feedback-mediated attention signals in the early visual cortex.

For this purpose, bilateral electrophysiological recordings from the primary visual cortex of the cat were made while the animal was performing an active behavioral task. After some time, a unilateral lesion was set in the posterior middle suprasylvian (pMS) cortex to induce a visual neglect. The recordings were made until the completion of the recovery period.

The subsequent analysis of the prelesional activity patterns revealed a late characteristic signature in response to perceived stimuli which was characterized by a significant bilateral increase in oscillatory theta and alpha activity. In addition, latency modulations in the event related potential of the characteristic signature were observed which were determined by both exogenous and endogenous factors. Surprisingly, during the acute phase of the neglect in which the cat showed no behavioral reaction to stimuli pre-

sented in the contralesional visual hemifield, no such signature was observed for neglected stimuli. These results suggest that although the characteristic signature is initially triggered by the stimulus, it is nevertheless predominantly of endogenous origin (recurrent feedback) and supports the idea that recurrent feedback plays a major role in conscious processing of sensory information.

Another important finding is the observation that stimuli which occurred in the unaffected visual hemifield induced an exceedingly strong representation not only in the intact, but also in the impaired hemisphere. In addition to this bilateral neural representation of a unilateral visual stimulus, ongoing stimulus-independent oscillations increased bilaterally in the frequency range above 30 Hz. These results are very remarkable because they stand in contrast to the hypothesis set out by Payne and Rushmore (2004) which states that in the normal brain the two hemispheres are under mutual inhibitory influence. In their neglect model, a unilateral lesion leads to a fundamental interhemispheric imbalance of neuronal activity. This imbalance indicates a push-pull pattern in which disinhibition of the intact hemisphere is coupled to a pathological inhibition of the impaired hemisphere. The results of this dissertations, however, suggest that neglect-specific interhemispheric interactions are more complex than the mere push-pull pattern of activity levels suggested by Payne and Rushmore. The notion that changes in interhemispheric communication may play a larger role in visual neglect is however supported by the results from the analysis of coherent ongoing oscillations between the two hemispheres. When compared to the intact system, a significant increase in coherent oscillations was observed in the low frequency range up to 14 Hz during the acute phase of neglect.

An examination of the recovery period revealed neither a restoration of interhemispheric activity balance as bilateral behavioral orienting returned, nor was a within hemisphere return to prelesional activity levels observed.

In summary, the results strongly indicate that visual neglect constitutes an impairment in the integration of endogenous and exogenous signals rather than resulting from interhemispheric activity imbalance. This idea is consistent with the hypothesis of Ptak and Fellrath (2013) who suggested that neglect can be understood as a failure to calculate an attentional priority map. The widespread concept of the attentional priority map views the parietal cortex, which also includes the pMS sulcus, as a central component of the attention network where, by integrating internal and external signals, an abstract spatial representation of the environment is computed. This priority map then serves as the basis for attentional selection. In such a priority map, locations or objects are represented with neuronal activity that is proportional to their attentional priority. The characteristic neuronal response signature that was found in this study could represent a neuronal correlate of such an abstract representation. A deficient unilateral integration, as would be the case

in visual neglect, would have the effect that stimuli appearing in the impaired visual hemifield would not be given the required priority, in the form of neuronal activity, to be consciously perceived. Possibly, this insufficient priority is reflected by the observed absence of the characteristic response signature for neglected stimuli.

ZUSAMMENFASSUNG

Selektive Aufmerksamkeit ist das grundlegende kognitive Vermögen, irrelevante sensorische Informationen zugunsten relevanter Informationen heraus zu filtern. Um dies zu ermöglichen, ist eine Integration von exogenen, reizabhängigen und endogenen, vom Verhaltenskontext abhängigen Aufmerksamkeitsfaktoren notwendig. Die anatomische Basis für diese Integration bildet ein hochkomplexes Netzwerk aus kortikalen Vorwärts- (*feedforward*) und Rückprojektionen (*feedback*). Läsionen in spezifischen kortikalen Bereichen dieses Aufmerksamkeitsnetzwerkes führen zum Krankheitsbild des visuellen Hemineglekts, bei dem der Ausfall einer Komponente des Netzwerkes in der Vernachlässigung des kontralateral zur Läsion liegenden Gesichtsfeldes resultiert. Sowohl beim Menschen als auch im Tiermodell kann häufig nach einiger Zeit eine schrittweise Verbesserung bis hin zu einer vollständigen Wiederherstellung der Verhaltensleistung beobachtet werden. Basierend auf Erkenntnissen aus tierexperimentellen Verhaltensstudien wurde die Vermutung aufgestellt, dass dem Neglekt Imbalance neuronaler Aktivität zwischen den beiden Hemisphären und eine daraus resultierende Ungleichverteilung von begrenzten Aufmerksamkeitskapazitäten zugrunde liegen könnten. Eine Restitution würde in diesem Modell mit einer Wiederherstellung des Aktivitätsgleichgewichts zwischen den beiden Hemisphären einhergehen.

Aktuelle Modelle der dem Neglekt zugrundeliegenden Mechanismen basieren hauptsächlich auf Ergebnissen aus Verhaltensexperimenten oder auf Daten, die im anästhesierten Tier erhoben wurden. Bis heute existieren keine neurophysiologischen Untersuchungen am wachen Tier, die das Neglekt-Syndrom und die Regeneration im Verhaltenskontext betrachten. Ziel der vorliegenden Studie war es, zum einen diese Lücke zu schließen und zum anderen eine detaillierte Charakterisierung der feedback-vermittelten Aufmerksamkeitssignale auf frühe kortikale Verarbeitungszentren, wie z.B. den primären visuellen Kortex, zu liefern.

Dazu wurden bilaterale elektrophysiologische Ableitungen im primären visuellen Kortex der Katze während einer aktiven Verhaltensaufgabe durchgeführt. Nach einiger Zeit wurde dann mittels einer Läsion im posteromedialen suprasylvanischen (pMS) Kortex ein visueller Hemineglekt induziert und die Ableitungen bis zum Abschluss der Restitutionsphase fortgeführt.

Die anschließenden Analysen der präläsionalen Aktivitätsmuster zeigten in Reaktion auf wahrgenommene Stimuli eine charakteristische Signatur, die durch eine deutli-

che, in Bezug auf den Zeitpunkt der Stimuluspräsentation relativ spät einsetzende, bilaterale Zunahme von oszillatorischer Aktivität im Theta- und Alpha- Frequenzband gekennzeichnet war. Zusätzlich konnten Modulationen der Latenz bei der Signatur beobachtet werden, die sowohl von exogenen als auch von endogenen Faktoren bestimmt wurden. Während der akuten Phase des Neglekts hingegen, in der die Katze keine Verhaltensreaktion auf kontralateral zur Läsion präsentierte Stimuli zeigte, war keine solche Signatur als Reaktion auf Stimuli in der betroffenen Gesichtsfeldhälfte zu verzeichnen. Diese Ergebnisse lassen den Schluss zu, dass die gefundene charakteristische Signatur zwar durch den Stimulus initiiert wird, aber dennoch überwiegend endogenen Ursprungs ist (*recurrent feedback*) und eine wichtige Rolle bei der bewussten Verarbeitung von Reizen spielen könnte.

Einen weiteren wichtigen Befund stellt die Beobachtung dar, dass Stimuli, die in der nicht betroffenen Gesichtsfeldhälfte lagen, nicht nur in der intakten Hemisphäre, sondern auch in der beeinträchtigten Hemisphäre übermäßig stark repräsentiert wurden. Auch die Analyse der Spontanaktivität zeigte einen Anstieg im Frequenzbereich ab 30 Hz, der ebenfalls auf beiden Hemisphären zu beobachten war. Diese Ergebnisse sind sehr bemerkenswert, da sie im Widerspruch zu der von Payne und Rushmore (2004) aufgestellten Hypothese stehen, dass die beiden Hemisphären unter einem wechselseitigen inhibitorischen Einfluss stehen. Eine unilaterale Läsion würde in diesem Modell ein grundsätzliches interhemisphärisches Ungleichgewicht an neuronaler Aktivität verursachen, bei der eine Disinhibition der intakten Hemisphäre an eine pathologische Inhibition der beeinträchtigten Hemisphäre gekoppelt wäre. Die hier gewonnenen Resultate lassen aber auf neglekt-spezifische interhemisphärische Interaktionen schließen, die komplexer sind als eine reine Asymmetrie der Aktivitätsniveaus. Dass beim Krankheitsbild des visuellen Neglekts auch Veränderungen in der interhemisphärischen Kommunikation eine große Rolle spielen, wird zusätzlich durch die Ergebnisse gestützt, die bei einer Analyse von kohärenten spontanen Oszillationen zwischen den beiden Hemisphären gewonnen wurden. Im Vergleich mit dem intakten System fiel eine signifikante Zunahme von kohärenten Oszillationen im niedrigen Frequenzbereich bis 14 Hz während der akuten Phase des Neglekts auf.

Bei der Untersuchung der Restitutionsphase konnte weder im Vergleich der beiden Hemisphären ein unmittelbarer Zusammenhang zwischen einer Regeneration der Verhaltensleistung und einer Wiederherstellung des Aktivitätsgleichgewichts festgestellt werden, noch konnte innerhalb einer Hemisphäre eine Rückkehr der spontanen Oszillationen auf präläsionales Niveau beobachtet werden.

Zusammenfassend lassen die Ergebnisse eher darauf schließen, dass es beim visuellen Neglekt zu einer Beeinträchtigung bei der Integration von endogenen und exogenen

Signalen kommt. Dies deckt sich auch mit der von Ptak und Fellrath (2013) aufgestellten Hypothese, dass für den Neglekt ein Scheitern bei der Berechnung einer *‚attentional priority map‘* verantwortlich ist. Das weit verbreitete Konzept der *‚attentional priority map‘* sieht den Parietalkortex, zu dem auch der pMS-Sulkus gehört, als eine zentrale Komponente des Aufmerksamkeitsnetzwerkes, in dem durch die Integration von internen und externen Signalen eine abstrakte räumliche Repräsentation der Umwelt gebildet wird, die als Grundlage für die aufmerksamkeitsgesteuerte Selektion dient. In einer solchen *‚priority map‘* werden Orte oder Objekte mit neuronaler Aktivität repräsentiert, die proportional zu ihrer Aufmerksamkeitspriorität ist. Die in dieser Studie gefundene charakteristische neuronale Antwortsignatur könnte ein neuronales Korrelat zu solch einer abstrakten Repräsentation darstellen. Eine fehlerhafte unilaterale Integration, wie es beim visuellen Neglekt der Fall wäre, würde zur Folge haben, dass Stimuli, die in der beeinträchtigten Gesichtsfeldhälfte auftauchen, nicht die nötige Priorität - in Form von neuronaler Aktivität - erhalten würden, um bewusst wahrgenommen werden zu können. Das Fehlen der charakteristischen Signatur welches während der akuten Phase des Neglekts für kontraläsionale Stimuli beobachtet werden konnte, könnte einen solchen defizitären Mechanismus wiederspiegeln.

TABLE OF CONTENTS

LIST OF FIGURES

LIST OF TABLES

List of Abbreviations

AMLS	anteromedial lateral suprasylvian area
aMS cortex	anterior middle suprasylvian cortex
aVP cortex	anterior visuo-parietal cortex
dlPFC	dorso-lateral prefrontal cortex
ERP	event related potential
FFT	fast Fourier transform
FMA	floating microelectrode array
LED	light emitting diode
LFP	local field potential
LGN	lateral geniculate nucleus
LHF	left hemifield
LPl	lateral division of lateral posterior nucleus
LPm	medial division of lateral posterior nucleus
LP-Pulvinar	lateral posterior-pulvinar complex
LVHF	left visual hemifield
MS cortex	middle suprasylvian cortex
MUA	multi unit activity
PLLS	posterolateral lateral suprasylvian area
PMLS	posteromedial lateral suprasylvian area
pMS cortex	posterior middle suprasylvian cortex
PSTH	peri-stimulus time histogram
RF	receptive field
RHF	right hemifield
RVHF	right visual hemifield
SC	superior colliculus
SD	standard deviation
SEM	standard error of the mean
TF-plot	time-frequency plot
TOP junction	temporo-occipito-parietal junction
U	Mann-Whitney U-test
VEP	visual evoked potential
VP cortex	visuo-parietal cortex
WSR	Wilcoxon signed rank test

INTRODUCTION

1.1 VISUAL PERCEPTION & OSCILLATIONS

Mainly influenced by the pioneering studies of Hubel and Wiesel, the classical view is that perception progresses along a hierarchy of multiple, functionally distinct visual areas that are organized into an ascending serial processing stream (Hubel & Wiesel, 1962, 1965). The complexity of processed stimulus features increases at each level as one moves up the hierarchy (Livingstone & Hubel, 1988; Felleman & Van Essen, 1991). In this framework, neuronal activity is mainly generated as a reaction to external stimuli.

Today's view is that perception is a dynamic, integrative, adaptive and highly, but not exclusively parallel process. Therefore, visual perception is a result of externally evoked activity (retinal input), referred to by the term: bottom-up or feedforward processing, and internally generated, context-depending activity such as expectancy, memory, attention, intention, etc. referred to as top-down or feedback processing (Figure 0.1) (Engel *et al.*, 2001; Gilbert & Sigman, 2007; McMains & Kastner, 2011; Gilbert & Li, 2013). Moreover, the integration of information is further supported by intrinsic horizontal signals, exerting contextual modulation at the same processing level (Lamme & Roelfsema, 2000).

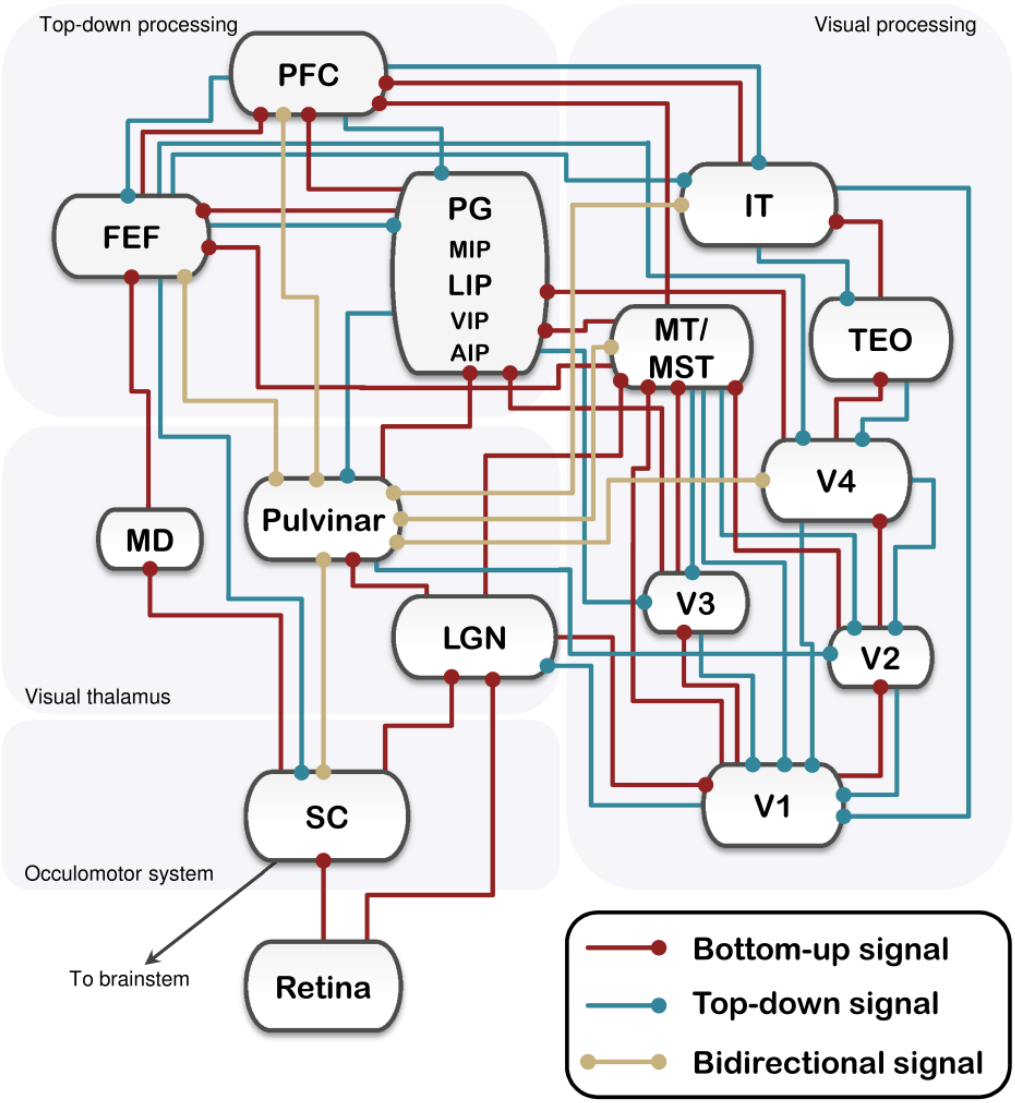

Figure 0.1 Schematic overview of feedforward, feedback and bidirectional signals in the primate visual system. The incoming signals are transmitted from the retina via multiple thalamic bottom-up pathways (red lines) to visual areas. Additionally, the extensive feedback connectivity pattern (blue lines) provides top-down influences on almost every processing level. Abbreviations: AIP, anterior intraparietal area; FEF, frontal eye field; IT, inferior temporal area; LGN, lateral geniculate nucleus; LIP, lateral intraparietal area; MD, mediodorsal thalamus; MIP, medial intraparietal area; MST, medial superior temporal area; MT, medial temporal area; PG, parietal gyrus; PFC, prefrontal cortex; SC, superior colliculus; TEO, posterior inferior temporal area; VIP, ventral intraparietal area.
Figure reproduced and modified from Baluch and Itti (2011), additional data obtained from Gilbert and Li (2013).

In the past decades, neuroscientists have become concerned with the central question of how visual information is integrated, on the functional level, with other sensory signals and internal representations to generate an adequate behavioral output. Based on the finding that synchronized inputs can drive a neuron more effectively than asynchronous inputs, it has been proposed that synchronous oscillatory activity may serve as a possible mechanism for feature binding and integration and that this neuronal synchrony is subject to bottom-up and top-down influences equally. In this context, distinct representational patterns would be formed by the synchronized discharges

of anatomically distributed groups of neurons (assemblies) that encode information about the same object. Internal (top-down) factors such as attention, motivation and experience could modulate these coherent oscillatory (bottom-up) patterns, thereby effectively enhancing or attenuating their impact onto target assemblies (Singer & Gray, 1995; Singer, 1999; Tallon-Baudry & Bertrand, 1999a; von Stein *et al.*, 2000; Engel & Singer, 2001). Moreover, it has been proposed that different scales of bottom-up and top-down integration are mediated by neuronal synchrony in different frequency ranges (von Stein & Sarnthein, 2000; Bastos *et al.*, 2015). In particular, high-frequency oscillations in the gamma range (>30 Hz) have been associated to local interactions and lower frequency oscillations, in the theta (4-8 Hz), alpha (9-14 Hz) and beta (15-30 Hz) range have been related to long-range interactions due to their higher robustness to long conduction delays (Kopell *et al.*, 2000; von Stein & Sarnthein, 2000; Donner & Siegel, 2011).

1.2 FEEDBACK PROJECTIONS & VISUAL SPATIAL ATTENTION

Anatomical studies on corticocortical connectivity in the visual system have revealed a highly complex, reciprocal pattern of intercortical connections among visual areas (Symonds & Rosenquist, 1984a; Felleman & Van Essen, 1991; Scannell *et al.*, 1995). According to the distribution of a neuron's laminar position and termination, these connections can be principally classified into three different types: feedforward, lateral and feedback connections. Feedforward projections originate in the supragranular layers and predominantly terminate in layer IV of hierarchically higher cortical areas whereas feedback connections typically project from the infragranular layers of higher-order areas and terminate outside of layer IV in the lower-order area (Felleman & Van Essen, 1991; Salin & Bullier, 1995). With only a few exceptions, corticocortical feedforward and feedback connections are formed by the axon terminals of pyramidal cells and are therefore excitatory (Salin & Bullier, 1995). Lateral projections interconnect areas at the same hierarchical level and their termination fields spread throughout all layers in a columnar fashion (Felleman & Van Essen, 1991).

1.2.1 FUNCTIONAL ROLES OF FEEDBACK PROJECTIONS

Studies in anaesthetized animals on the functional role of feedback projections reveal that feedback exerts a modulatory rather than a driving effect on the responses of neurons in lower-order areas (Sandell & Schiller, 1982; Mignard & Malpeli, 1991; Hupé *et al.*, 1998). This conclusion is further supported by the observation, that without converging feedforward input, feedback projections are unable to drive a neuron (Vanduffel *et al.*, 1997; Hupé *et al.*, 1998). In general, feedback signals seem to enhance the responses of lower-order neurons, although inactivation of a higher-order area does not always lead to a decrease and sometimes even increases the responses of individual neurons. This response enhancement seems to depend upon two factors: (i) the location of the receptive field (RF) within the center-surround RF of the higher-order neuron and (ii) the stimulus salience, and provides some evidence that cortical feedback may contribute to figure-ground segregation (Hupé *et al.*, 1998; Bullier *et al.*, 2001). In addition to the facilitating effects on neural activity, feedback projections also modulate the tuning properties of neurons. In anaesthetized cats it was shown that feedback signals strongly sharpen the selectivity of orientation tuned neurons and contribute to a large extent to the formation of direction maps in the primary visual cortex (Galuske *et al.*, 2002).

1.2.2 TOP-DOWN ATTENTIONAL SELECTION VIA FEEDBACK PROJECTIONS

Visual selective attention is known to be the fundamental cognitive capacity to filter out irrelevant sensory information for the benefit of behaviorally relevant information. A striking feature of attention is the immense degree of flexibility. It can be directed to a certain location (spatial attention), to a certain object (object-based attention) or to a single feature (feature-based attention) (Posner, 1980; Duncan, 1984; Desimone & Duncan, 1995). Furthermore, spatial attention can be allocated overtly by moving the eyes and the head towards the attended location or covertly without movement of the eyes.

In the past 25 years, there has been growing interest in the neuronal mechanisms of attention and the most prominent attentional effect that has been found on the single-neuron level is a modulation of response strength. The firing rate in response to an attended stimulus lying in the RF of a neuron is increased compared to an unattended stimulus in the same location (Moran & Desimone, 1985). Moreover, the activity of neurons that are either not tuned for the stimulus or that have their RFs in non-attended locations, is often suppressed (Duncan, 1984; Chelazzi *et al.*, 1993; Reynolds *et*

al., 1999). Taken together, these findings, that have been observed at multiple subcortical and cortical levels of the visual information processing stream, provide an efficient strategy to improve the signal quality (signal-to-noise ratio) by selectively enhancing relevant representations and suppressing less relevant representations of visual stimuli (McAdams & Maunsell, 1999; Ignashchenkova *et al.*, 2004; Buschman & Miller, 2007; McAlonan *et al.*, 2008a). Single-unit recordings have additionally shown that top-down attention modulates the position and size of the RFs towards and around attended stimuli (Connor *et al.*, 1997; Womelsdorf *et al.*, 2006).

On the level of neuronal populations, there is growing evidence that top-down attention amplifies information transmission and facilitates signal integration in lower visual areas by synchronizing the oscillatory activity among groups of neurons that encode the currently relevant stimulus (Salinas & Sejnowski, 2001; Tiesinga *et al.*, 2004). Experimentally, such an attention-dependent modulation of neuronal synchronization has mainly been demonstrated for the gamma frequency range (30 – 100 Hz) (Fries *et al.*, 2008; Bosman *et al.*, 2012) but has also been reported for the low-frequency domain (Lakatos *et al.*, 2008).

Other reported mechanisms of top-down attention are the reduction of response variance at the single-cell level to increase the encoding reliability and the de-correlation of response variability at the population level to improve the signal-to-noise ratio (Mitchell *et al.*, 2007; Cohen & Maunsell, 2009).

Although these described attentional modulations can occur concurrently, these effects are relatively weak at lower stages and increase, together with RF size, along each stage of the visual processing hierarchy (Noudoost *et al.*, 2010). Likewise, neurons at different stages are progressively selective to more and more complex stimulus features (Kastner & Ungerleider, 2000).

1.2.3 Origin of top-down Attention

Neurophysiological and neuroimaging studies in humans and monkeys have identified a cortical network, involving prefrontal and parietal areas, to be the possible source of attentional control signals. In particular, the frontal eye field (FEF) in the prefrontal region and the lateral intraparietal area (LIP) in the parietal region are thought to play a key role in guiding the allocation of visual attention (Moore & Fallah, 2004; Wardak *et al.*, 2004). Both areas are interconnected with each other as well as with cortical and subcortical visual structures and microstimulation of these regions evoke increased firing rates in visual areas and an enhancement of behavioral performance (Cutrell & Marrocco, 2002; Moore & Armstrong, 2003). Studies comparing the latencies

of top-down signals revealed that these signals appear first in the FEF, followed by the dorso-lateral prefrontal cortex (dlPFC) region and then in the LIP, suggesting that top-down attention acts via a descending cascade (Buschman & Miller, 2007; Ibos *et al.*, 2013). In addition to the frontoparietal network, a contribution of the superior colliculus (SC) and the thalamus to the guiding and control of attention has also been suggested (Petersen *et al.*, 1987; Müller *et al.*, 2005; McAlonan *et al.*, 2008b).

1.2.4 The Attentional priority map hypothesis

In the past few years the idea of multiple priority maps located in the FEF, LIP and SC has been increasingly emphasized (Thompson & Bichot, 2005; Bisley & Goldberg, 2010; Krauzlis *et al.*, 2013). A priority map is defined as an abstract topographic representation of the visual space in which attentional priority is proportionally encoded by neuronal activity (Serences & Yantis, 2006; Bisley, 2011). Accordingly, attention would be allocated to the object or location that is represented by the highest neuronal activity on the priority map. Various internal and external factors contribute to the formation of attentional priority (Figure 0.2 A). Beside the physical salience of stimuli, current goals, expectations and predictions based on prior knowledge and experience are used to compute a feature- and modality-independent priority map (Bisley & Goldberg, 2010; Awh *et al.*, 2012). Under this view, the final attentional selection is eventually realized on the basis of a winner-take-all mechanism to direct attention to the item or location with the highest priority (Figure 0.2 B) (Zénon *et al.*, 2009; Zelinsky & Bisley, 2015).

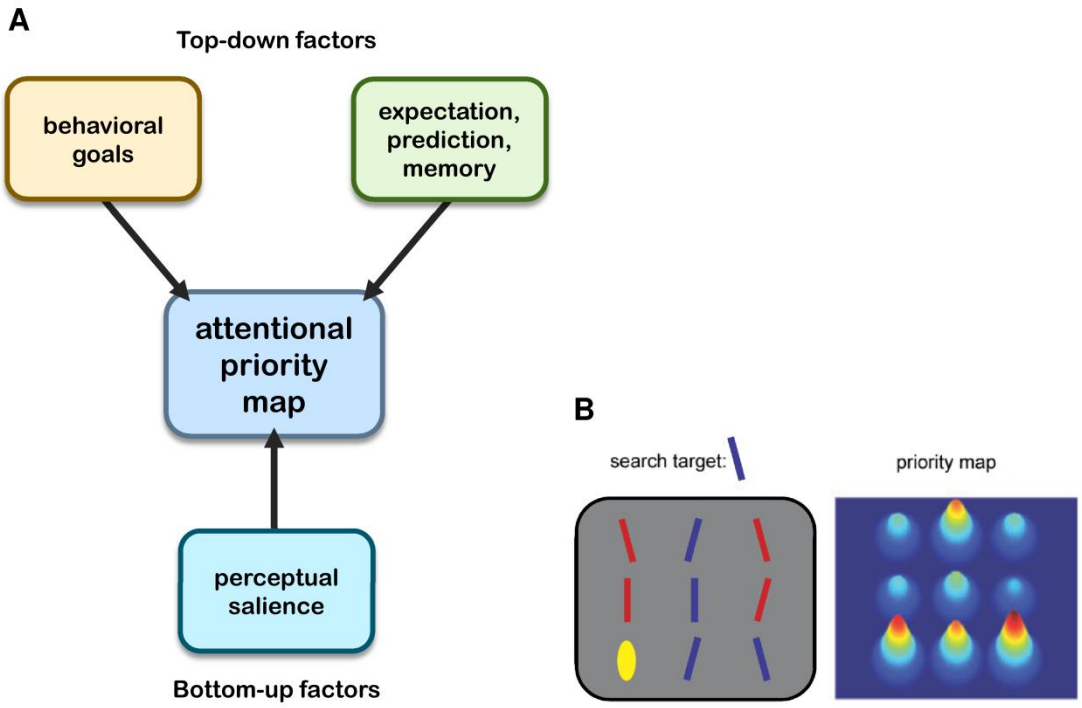

Figure 0.2 The concept of attentional priority maps. (A) External and internal factors that contribute to the attentional priority map. **(B)** The left panel shows a hypothetical search task, the right panel shows the respective theoretical priority map. Red bars evoke representations with lower activity than blue bars and bars that have the same orientation like the target elicit representations with higher activity. The yellow stimulus has a high salience and is therefore represented with increased activity. Modified from Bisley (2011).

1.3 SPATIAL HEMINEGLECT

Unilateral lesions in specific cortical areas of the attention network lead to the complex clinical syndrome of visual hemineglect. In neglect, the failure of one network component results in the inability to attend to or be aware of the entire contralateral visual hemifield (Mesulam, 1981; Rafal, 1994). Spatial hemineglect in humans results most frequently from damage to the right hemisphere. In daily life, patients with neglect shave, comb or dress only the ipsilesional side of their body and when asked to copy a drawing, the contralesional side of the figure is omitted.

Apart from the conspicuous unilateral bias, a number of further deficits contribute to the neglect pathology. A generally decreased arousal, slower visual processing speeds and often a lack of awareness for the disorder (anosognosia) are frequently associated with neglect (Rafal, 1994; Bartolomeo & Chokron, 2002). It is commonly believed that hemineglect does not arise as a result of damage to the visual processing pathway but rather is a disruption of the endogenous processes that are responsible for the allocation of attention (Mesulam, 1999; Bartolomeo & Chokron, 2002; Rastelli *et*

al., 2008). One experimental setup that provides strong support to this idea is the 'line bisection task', a conventional detection test for the presence of neglect in humans. Normal subjects place the bisection mark at the approximate center of the line whereas neglect patients exhibit a substantial rightward error. Moreover, the extent of the deviation from the center is proportional to the total length of the line, indicating, on some level, a processing of the entire line (Mozer *et al.*, 1997; Mesulam, 1999).

The neglect phenomenon can also affect mental imagery and memory performance. Such a representational neglect was first described by Bisiach and Luzzatti (1978) who asked two neglect patients to recall prominent features along the Piazza del Duomo in Milan from their mental imagery. Depending on the patient's imagined vantage point, i.e. facing towards or away from the cathedral, the patients were only able to recall details located to their right whereas left-sided features were largely neglected. Thus, the neglect patients failed to normally access internally generated representations although knowledge of details from both side was stored in the patients' memory. It should be noted, however, that not every patient with perceptual neglect also shows representational neglect (Bartolomeo, 2007). Importantly, the neglect syndrome is not restricted to the visual domain but can also affect auditory or somatosensory modalities and the execution of movements (Kerkhoff & Schenk, 2012).

Frequent cortical lesion sites that lead to spatial hemineglect are the temporo-occipito-parietal (TOP) junction including the posterior and inferior parietal cortex, the cingulate fields, and the frontal eye fields (FEF) (Figure 0.3) (Mesulam, 1999; Driver & Vuilleumier, 2001; Mort *et al.*, 2003).

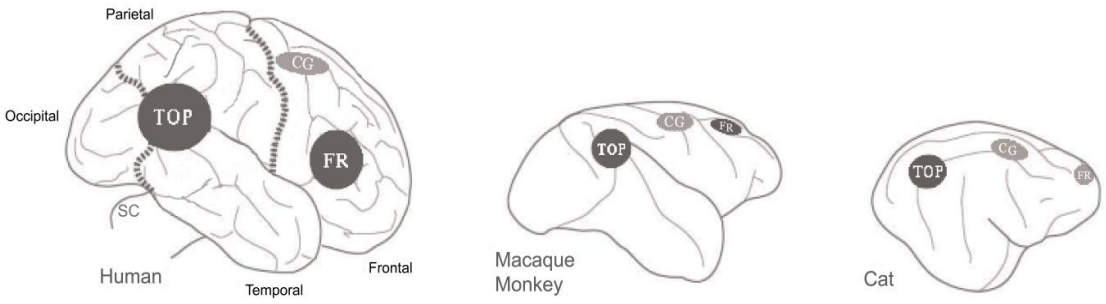

Figure 0.3 Lateral views of a human, a monkey and a cat brain with the positions of the most frequent cortical lesion sites that induce visual hemineglect. Light grey spots indicate that the region is partly buried within a sulcus. Abbreviations: TOP, temporo-occipito-parietal region; CG, cingulate field; FR, frontal region with FEF. Modified from Payne & Rushmore (2003).

1.3.1 Possible mechanisms underlying spatial hemineglect

According to the opponent-processor model postulated by Kinsbourne (1970a) each hemisphere is directing attention towards the contralateral hemispace, thereby exerting mutual inhibition on its opponent. With neglect, damage to one hemisphere would evoke a disinhibition of the intact hemisphere that results in a robust attentional bias towards the ipsilesional side. Support for this hypothesis is provided by the observation that neglect patients show a strong tendency to orient their gaze and attention towards ipsilesionally located objects (Marshall & Halligan, 1989; Làdavas *et al.*, 1990). More recently, further support to the opponent-processor model was provided by the results from a functional magnetic resonance imaging (fMRI) study (Corbetta *et al.*, 2005). The authors observed a functional interhemispheric imbalance of the structurally intact superior parietal lobules, the intraparietal sulcus and the dlPFC, that was demonstrated by a relative hyperactivation of the intact hemisphere and a relative hypoactivation of the impaired side. A similar hypothesis of interhemispheric imbalance was also proposed in the cat model of neglect by Payne and Rushmore (2004). According to their model, a disruption of cortical or corticocollicular circuits and a concomitant hyperactivation of the intact hemisphere stimulates additional inhibitory mechanisms in the affected hemisphere, thereby strengthening the imbalance of neural activity. As a consequence, a bias in the orientation system towards the ipsilesional hemifield is implemented (Figure 0.4). In agreement with the idea of an interhemispheric imbalance, studies in animal models of neglect showed that the orienting deficit could be cancelled by an additional contralateral lesion or deactivation of either homotopic cortical regions or the superior colliculus (Sprague, 1966; Lomber & Payne, 1996; Payne *et al.*, 1996). The explanation provided for the paradoxical restoration of function was that the second lesion serves to rebalance the activity levels between the two hemispheres and reduces the pathological level of inhibition exerted on the impaired side (Payne & Rushmore, 2003, 2004).

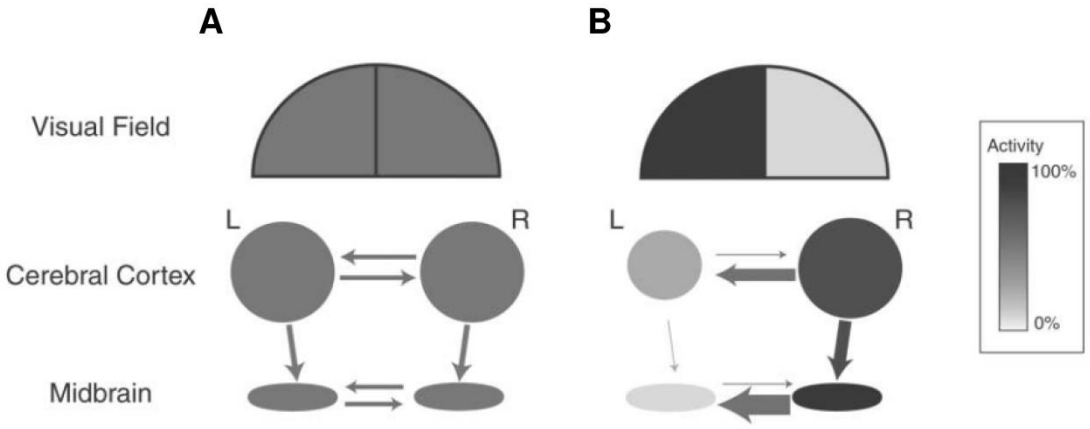

Figure 0.4 Diagrams of activity levels and inhibitory interactions between the two hemispheres and midbrain structures in the intact brain (A) and the impaired brain (B). (A) As a result of a mutual inhibitory influence (horizontal arrows) the activity levels between the two sides in the intact brain are balanced. **(B)** Damage to one hemisphere (smaller circle) induces a functional imbalance of activity through the implementation of a pathological level of inhibition exerted on the impaired side. As a consequence, activity generated by contralesional stimuli is insufficient to surpass the threshold that is set by the strong contralateral suppression of activity. Adapted from Payne and Rushmore (2003).

More recently, Ptak and Fellrath (2013) suggested the hypothesis that hemineglect may result from damage to the attentional priority map. Specifically, damage to the parietal region or any other region that computes an integrated priority map, induces a deficit in the attentional selection mechanisms and subsequently leads to a biased locus of selection. In this context, ipsilesional stimuli would have competitive advantages due to an increased priority of ipsilesional relative to contralesional field representations and therefore are more likely to be selected by the winner-take-all mechanism.

1.3.2 FUNCTIONAL RECOVERY FROM VISUAL HEMINEGLECT

Typically, a partial restitution of behavioral deficits may be observed in neglect patients after a few weeks or months (Hier *et al.*, 1983). In the course of behavioral recovery, neglect patients frequently exhibit a permanent attentional deficit that is referred to as visual extinction. When two stimuli are presented simultaneously in both visual hemifields, patients fail to report the contralesional stimulus. Similarly, a spontaneous functional recovery and extinction phenomenon is commonly observed in the cat model of spatial neglect although with a comparatively shorter time course (Payne & Rushmore, 2004). Moreover, the comparable characteristics of a functional restitution provide important possibilities not only for comprehensive studies of acute spatial neglect but also for the research on a subsequent restoration of function in this animal model. This is particularly noteworthy, since only little is known about the underlying

neural principles. It is widely believed that there are at least three basic mechanisms involved in the recovery of function (Nudo, 2011). First, compensation for the impaired functions by recruitment of intact homologous cortical and subcortical structures or the remaining perilesional regions. Second, reversal or resolution of diaschisis (the loss or change of function in brain areas distant to the lesion site) and, finally, physiological and neuroanatomical reorganization and neurogenesis (Kleim, 2011; Nudo, 2011; Carrera & Tononi, 2014).

Imaging studies in neglect patients during the acute phase have shown decreased activity levels in those ipsilesional regions that belong to the attention network. Furthermore, activity in homologous regions in the intact hemisphere was enhanced (Corbetta *et al.*, 2005). The authors further reported that in the course of recovery, a behavioral improvement was correlated with a reversal of the imbalance in activity levels. Thus, recovery from neglect might be partially related to a restoration of physiological activity patterns.

1.3.3 THE CAT AS AN ANIMAL MODEL FOR HEMINEGLECT

In the past 50 years, the visual system and more recently, also the neglect syndrome have been extensively studied in cats, thereby revealing an immensely high degree of similarity between anatomical and functional characteristics of the human and feline visual and attention system. In both humans and cats visual hemineglect is induced by damage to the posterior and inferior portion of the parietal lobe or the SC (Payne & Rushmore, 2004). It should be noted, however, that unlike humans, there is no right hemispheric dominance for neglect in cats.

1.3.3.1 *General mechanisms of neglect and its recovery in cats*

Payne and Rushmore (2004) suggested the presence of mutual inhibition between the two hemispheres and between the superior colliculi that is mediated by transcallosal and intercollicular connections, respectively. Without visual stimulation, these functionally inhibitory circuits are balanced. According to their model, a stimulus in one hemifield would then induce a left-right asymmetry in the activity patterns caused by a stimulus-locked neural response in only one hemisphere (Figure 0.5). In the neglect condition, damage to or deactivation of the visuoparietal (VP) cortex at the TOP junction would result in a nontransient decrease of activity levels on the impaired side, which cannot be surpassed by visual stimulation (Figure 0.6 A). It was further suggested that the anterior visuoparietal (aVP) cortex might play a critical role in mediating a functional compensation for the orienting deficit. In two experiments carried out by

Lomber et al. (2006) it was shown that the additional deactivation of aVP following a functional recovery from neglect was sufficient to reintroduce the visual orienting deficit. Importantly, a lesion in the aVP alone caused no spatial hemineglect. Moreover, as revealed by the second experiment, an irreversible inactivation of both regions, the VP and aVP cortex, resulted in a permanent deficit in visual orienting behavior. These results suggest that the aVP cortex contributes strongly to compensatory mechanisms in the course of recovery from neglect (Figure 0.6 B).

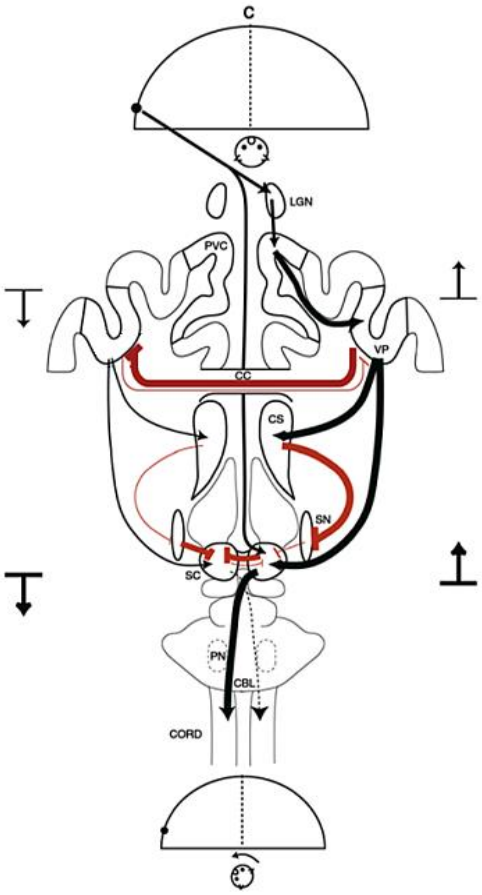

Figure 0.5 Circuits that mediate the orienting behavior in the cat. Excitatory and inhibitory pathways are denoted by black (→) and red lines (|), respectively. A stimulus in the left visual hemifield increases activity levels in the right hemisphere and superior colliculus (↑) and decreases activity on the left side (↓). The suppression of activity is mediated via callosal fibers and via the intercollicular commissure. Eventually, crossed brainstem spinal pathways are activated to evoke head and gaze orienting towards the stimulus. Abbreviations: aVP, anterior visuoparietal cortex; CORD, cervical spinal cord; CBL cerebellum; CC, corpus callosum; CS, corpus striatum (caudate nucleus and putamen); LGN, lateral geniculate nucleus; PN, pontine nuclei; PVC, primary visual cortex (areas 17 and 18); SC, superior colliculus; SN, substantia nigra; VP, visuoparietal cortex. Adapted from Payne and Rushmore (2004)

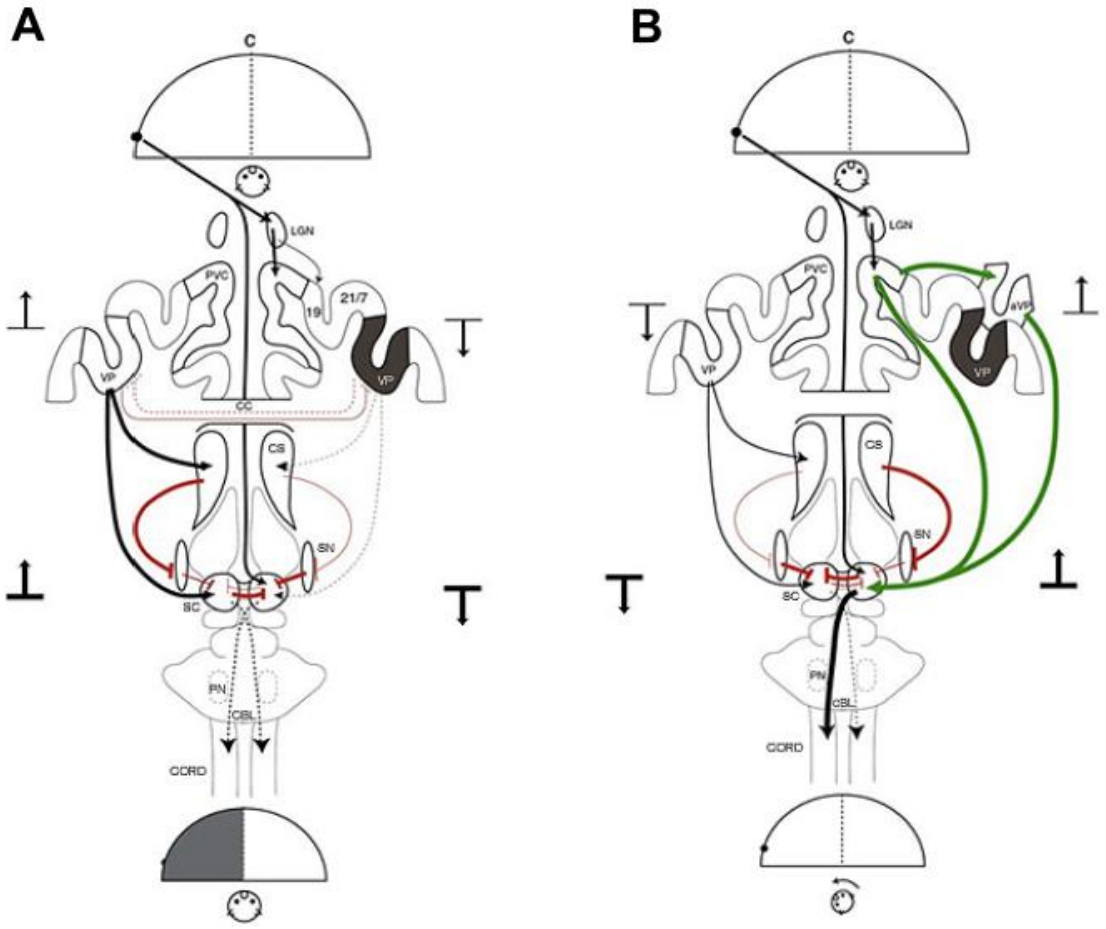

Figure 0.6 (A) A lesion in the VP region (gray) **decreases activity levels on the impaired side and diminishes inhibitory forces acting upon the contralateral counterpart.** The intact side is released from inhibition and, in turn, further reduces activity levels in the impaired hemisphere. The result is a profound neglect for contralesional visual stimuli **(B)** Compensatory pathways (green) presumably involved in the restoration of orienting behavior. The information from the primary visual cortex is directly and indirectly, via the aVP cortex, rerouted to the SC to re-establish adequate orienting behavior. Conventions and abbreviations as in Figure 1.5. Adapted from Payne and Rushmore (2004)

1.4 ANATOMY OF THE CAT VISUAL SYSTEM

Visual information processing starts in the retina, where light impulses are transformed into electrical impulses. Already at this early stage, the incoming signal is subjected to further preparation. On one hand, lateral interconnections of different retinal cell classes provide a contrast enhancement and, on the other hand, a differentiated signal processing is performed at different luminance levels. The retinal output to higher visual processing stages is then transmitted via ganglion cells, whose axons form the optic nerve. Due to their different response properties, the cat retinal ganglion cells are grouped into three functional classes that are referred to X-, Y- and W-cells (Cleland *et al.*, 1971a; Stone & Hoffmann, 1972a). X-cells, also known as brisk-sustained cells, show sustained responses and linear spatial summations across their narrow receptive fields and, therefore, are used for high acuity vision. Y-cells, also referred to as brisk-

transient cells, have wide receptive fields, transient responses and do not show a linear spatial summation. It is believed that Y-cells process temporal aspects of vision (e.g. motion) (Cleland *et al.*, 1971b; Fukada & Saito, 1971). Compared to the X-cells, the Y-cells have faster axonal conduction velocities. The third class of cells, the W-cells, are also known as sluggish-sustained and sluggish-transient cells. W-cells exhibit both, sustained and transient responses and have the slowest axonal conduction velocities within the groups of retinal ganglion cells (Stone & Hoffmann, 1972b).

In the further process, the nasal fibers of the optic nerve undergo a decussation at the optic chiasm so that the left visual hemifield is projected to the right hemisphere and vice versa. From the optic chiasm, the retinal ganglion cell axons project to six locations in the brain each of which is involved in the regulation of a different function. The fibers terminate in the lateral geniculate nucleus (LGN) in the thalamus, the SC in the tectum, the pretectum, the pregeniculate nucleus, the suprachiasmatic nucleus of the hypothalamus, and the accessory optic system (Mather, 2006). The two pathways, that are essential for visual processing, since they direct the information from the retina to the visual cortex, are the retinogeniculocortical pathway via the LGN and the retinotectal pathway via the SC.

1.4.1 THE RETINOGENICULOCORTICAL PATHWAY

The majority of the retinal ganglion cells project to the dorsal part of the lateral geniculate nucleus (LGN). The LGN is composed of four main layers with three dorsal magnocellular layers, named A, A1 and C_M and the ventral parvocellular layer, referred to as C_P (Payne & Peters, 2001). Adjacent to the dorsal LGN is the medial interlaminar nucleus (MIN), a three-layered structure, which also receives retinal fibers and to some degree parallels the morphology of the dorsal LGN (Payne & Peters, 2001). Each layer of both structures is retinotopically organized (Sanderson, 1971; Illing & Wässle, 1981). The X-cells terminate mainly in the dorsal layers A and A1 whereas Y-cells innervate layers A, A1 or C_M and MIN layers 1 or 2. The parvocellular layer C_P and MIN layer 3 receive input from the W- cells (Figure 0.7) (Illing & Wässle, 1981; Bowling & Michael, 1984).

The LGN neurons project via the optic radiation to cortical areas 17, 18, and 19 in the occipital lobe. In the optic radiation the orderly point-to-point representations that have been established by the termination patterns of retinal axons, is preserved. Thus, each of the cortical areas contain a retinotopically organized representation of the contralateral visual hemifield (Tusa *et al.*, 1978, 1979; Payne & Peters, 2001). Because

both areas, 17 and 18, receive significant direct input from the LGN they have been referred to as the primary visual cortex (Payne & Peters, 2001). The geniculate fibers arising from the X-, Y-, and W-stream have different sites of termination within the primary visual cortex. While the X-cells project exclusively to area 17, the Y- and W-cells terminate in both areas 17 and 18 (Dreher *et al.*, 1980).

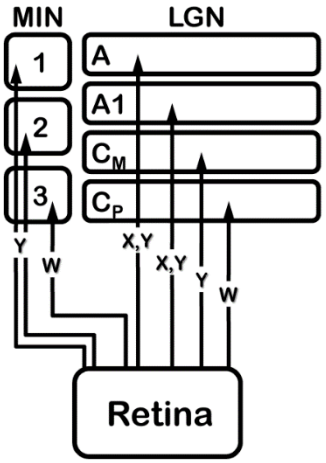

Figure 0.7 Termination pattern of retinal ganglion fibers in the lateral geniculate nucleus (LGN) and the medial interlaminar nucleus (MIN). Data obtained from Payne and Peters (2001)

1.4.2 THE RETINOTECTAL PATHWAY

The second pathway leading from the retina is mainly formed by fibers of the Y- and W-cell type, which project to the superior colliculi (SC) in the tectum (Wässle & Illing, 1980). Each SC is composed of seven layers. The three superficial layers receive direct visual input from the retina and primary visual cortex, which is arranged to form a retinotopic representation of the contralateral visual field. The deeper layers receive information from the auditory, somatosensory, and motor systems. Likewise, these incoming signals are used to build tonotopic and somatotopic representations, respectively (Meredith & Stein, 1986). The different sensory maps are combined to create a single multisensory map with the optical axis as its primary reference (Stein *et al.*, 2013). The SC is thought to play a central role in the control of saccades and orienting responses toward an object or a location of interest (Stein *et al.*, 2013). Anatomically, the SC sends ascending projections to the visual thalamic nuclei, including the LGN and Pulvinar, to the caudal and rostral intralaminar thalamic nuclei and to the suprageniculate nucleus. The descending projections terminate in brainstem structures and the spinal cord to exert control over motor responses in orienting behavior. In addition to these ascending and descending pathways the SC is heavily interconnected with the basal ganglia and substantia nigra (Krout *et al.*, 2001; McHaffie *et al.*, 2005; Hoshino *et al.*, 2010; Stein *et al.*, 2013). Because of its important role in orienting responses and the ability to integrate multimodal signals the SC is believed to be part of the attention network (Krauzlis *et al.*, 2013).

From the SC the tectopulvinar projections lead to the lateral posterior-pulvinar complex (LP-Pulvinar), a group of thalamic nuclei. The LP-Pulvinar is commonly subdivided into three main sections that are referred to as the lateral (LPl) or striate-recipient zone, the medial (LPm) or tecto-recipient zone, and the pulvinar nucleus (LP-Pul) or retino-recipient zone (Graybiel & Berson, 1980; Updyke, 1983; Abramson & Chalupa, 1988). Each of the three regions contains a coarse retinotopic representation of the contralateral visual hemifield and exhibits a unique pattern of reciprocal projections to the cortex (Raczkowski & Rosenquist, 1981). The LPl projects to the primary visual cortex, to the visuotemporal cortex (areas 20a, 20b, 21a and 21b) and to areas in the medial bank of the suprasylvian sulcus. The LPm projects to the posteromedial and posterior suprasylvian areas. Finally, the LP-Pul projects to the visuotemporal cortex, areas 5 and 7, to the splenial visual area, and to the cingulate gyrus (Figure 0.8) (Symonds *et al.*, 1981; Raczkowski & Rosenquist, 1983; Abramson & Chalupa, 1985).

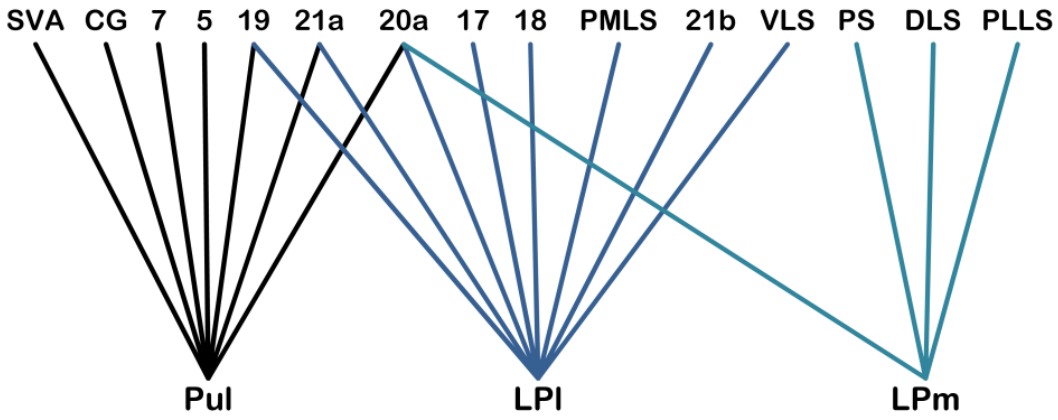

Figure 0.8 Projections from the LP-Pulvinar complex to visual cortical areas. Each subdivision of the LP-Pulvinar complex has an exclusive pattern of reciprocal projections to the visual cortex. Abbreviations: PLLS, PMLS, posterolateral-, posteromedial- , lateral suprasylvian area; CG, cingulate gyrus area; DLS, dorsal lateral suprasylvian area; VLS, ventral lateral suprasylvian area; LP, lateral posterior; LPI, lateral division of lateral posterior nucleus; LPm, medial division of lateral posterior nucleus; Pul, pulvinar nucleus; PS, posterior suprasylvian area; SVA, splenial visual area. Reproduced from Symonds et al. (Symonds *et al.*, 1981)

On a functional level, the LP-Pulvinar complex is involved in higher-level motion processing, visuo-motor transformations and attentional selection of targets (Dumbrava *et al.*, 2001; Arend *et al.*, 2008; Grieve *et al.*, 2009).

1.4.3 VISUAL CORTICAL AREAS OF THE CAT

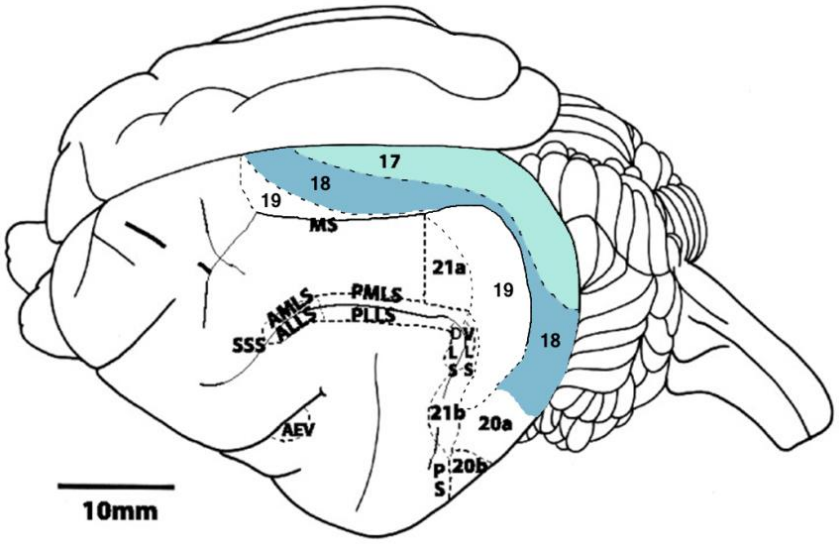

Figure 0.9 Dorsolateral view of the cat brain. Indicated are the visual cortical areas in the left cerebral hemisphere. Each of them is retinotopically organized. The primary visual cortex (areas 17 and 18) is highlighted in blue. Abbreviations: AEV, anterior ectosylvian area; ALLS, AMLS, PLLS, PMLS, anterolateral-, anteromedial-, posterolateral-, posteromedial-, lateral suprasylvian area; DLS, dorsal lateral suprasylvian area; VLS, ventral lateral suprasylvian area; PS, posterior suprasylvian area; MS, marginal sulcus; SSS, superior suprasylvian sulcus. Modified from Romo et al. (2011)

1.4.3.1 *Primary visual areas*

In contrast to the neurons of the subcortical structures, neurons in the primary visual cortex display orientation and direction selectivity (Hubel & Wiesel, 1962). Moreover, the distribution of orientation preference shows a gradual, monotonic change across the cortical surface. These so-called cortical maps are formed by vertical columns and all cells within a column show similar preferences for target orientation and direction of movement (Albus, 1979; Braitenberg & Braitenberg, 1979). Besides these common features, however, there are also functional differences between the two primary visual areas 17 and 18. The neurons in area 18 have larger receptive fields than those in area 17. Furthermore, both areas have a distinct topographic representation of the visual field (Hubel & Wiesel, 1965; Tusa *et al.*, 1981a; Payne & Peters, 2001).

Electrophysiological mapping techniques allow for a reconstruction of visual field representations in relation to the corresponding positions on the cortical surface. This is accomplished by recording and subsequently plotting the receptive fields of many neurons in different locations and was first described by Hubel and Wiesel (1962). Thus, consecutive mapping studies on the retinotopic organization of the cat visual cortex revealed the existence of multiple visual maps.

It was found that area 17 contains a single point-to-point (first order) representation of the complete contralateral hemifield ranging from 60° in the lower to 60° in the upper visual quadrant and up to 90° along the horizontal meridian (Figure 0.10 A) (Tusa *et al.*, 1978). By contrast, area 18 has a representation with a discontinuity in the visual field transformation referred to as second order representation. Here the upper and lower field representation is split along the horizontal meridian. The result is an asymmetric representation of the upper and lower visual field and large receptive fields covering the periphery (Figure 0.10 B) (Tusa *et al.*, 1979; Albus & Beckmann, 1980). On top of the topographical organization, the central visual field is magnified in both areas. Therefore it has been suggested, that the primary visual cortex is specialized for central vision (Tusa *et al.*, 1981b).

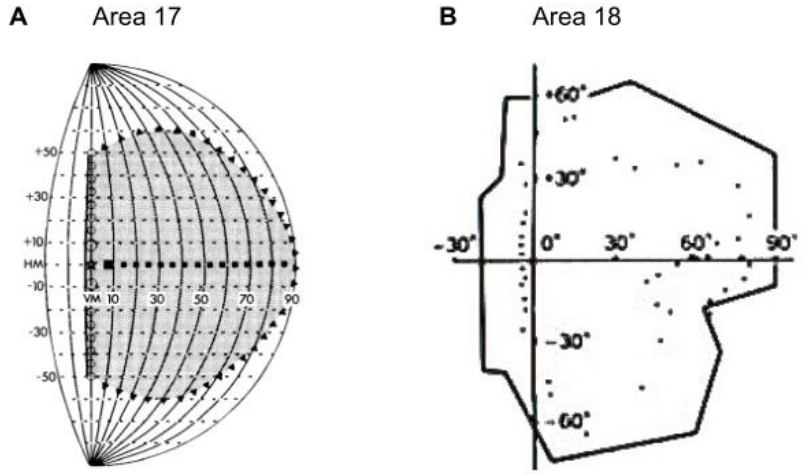

Figure 0.10 Extent of visual field representations of the primary visual cortex. (A) The extent of the visual field represented in area 17 is shown in a perimeter chart. Area 17 contains a complete representation of the contralateral visual hemifield. Abbreviations: HM, horizontal meridian; VM, vertical meridian. Adapted from Tusa et al. (1978). **(B)** The extent of the visual field representation of area 18. The continuous line marks the outer borders of the most peripheral receptive fields (RF), the dots mark the RF centers. In area 18 is also the central part of the ipsilateral visual hemifield represented. Adapted from Albus and Beckmann (1980).

A special case holds for the interhemispheric connections between the cerebral hemispheres. The majority of callosal projections in area 17 and 18 arise from the 17/18 transition zone, a cortical region that contains a representation of the vertical meridian including the area centralis (Sanides, 1978).

1.4.3.2 *The lateral suprasylvian areas*

From the primary visual cortex visual information is further transmitted to higher-order areas in the lateral suprasylvian sulcus (LS), the visuotemporal areas, the splenial visual area (SVA) and to the anterior ectosylvian visual area (AEV) (Symonds & Rosenquist, 1984b; Scannell *et al.*, 1995). The region of the lateral suprasylvian sulcus has been further subdivided into six separate areas, each of them containing a retinotopic representation of the contralateral visual hemifield (Palmer *et al.*, 1978). The two rostral areas within the LS have been designated anteromedial and anterolateral lateral suprasylvian areas (AMLS and ALLS respectively), the four caudal areas within the LS have been termed posteromedial, posterolateral, dorsal and ventral lateral suprasylvian areas (PMLS, PLLS, DLS and VLS respectively) (Palmer *et al.*, 1978).

In cats, similar to visual processing in primates, information about form and spatial aspects is processed by two distinct pathways. The dorsal motion processing stream is routed via area PMLS and the ventral form processing stream via area 21a. Based on analogous anatomical and functional characteristics, both areas have been considered as the equivalent to primate areas MT and V4, respectively (Figure 0.11) (Payne, 1993; Dreher *et al.*, 2006).

Studies on the functional role of the LS region have found that each of the six areas is concerned with the analysis of motion signals but only the posterior middle suprasylvian (pMS) region, with areas PMLS and PLLS, and the posterior suprasylvian cortex, including areas DLS and VLS, are critical for orienting behavior. Damage to these areas along the LS sulcus have been shown to induce a profound neglect (Lomber *et al.*, 1996; Lomber & Payne, 2004). In the present work, the focus was on the functional interaction between the pMS region and area 18. Therefore, the two areas within the pMS cortex will be described in more detail below.

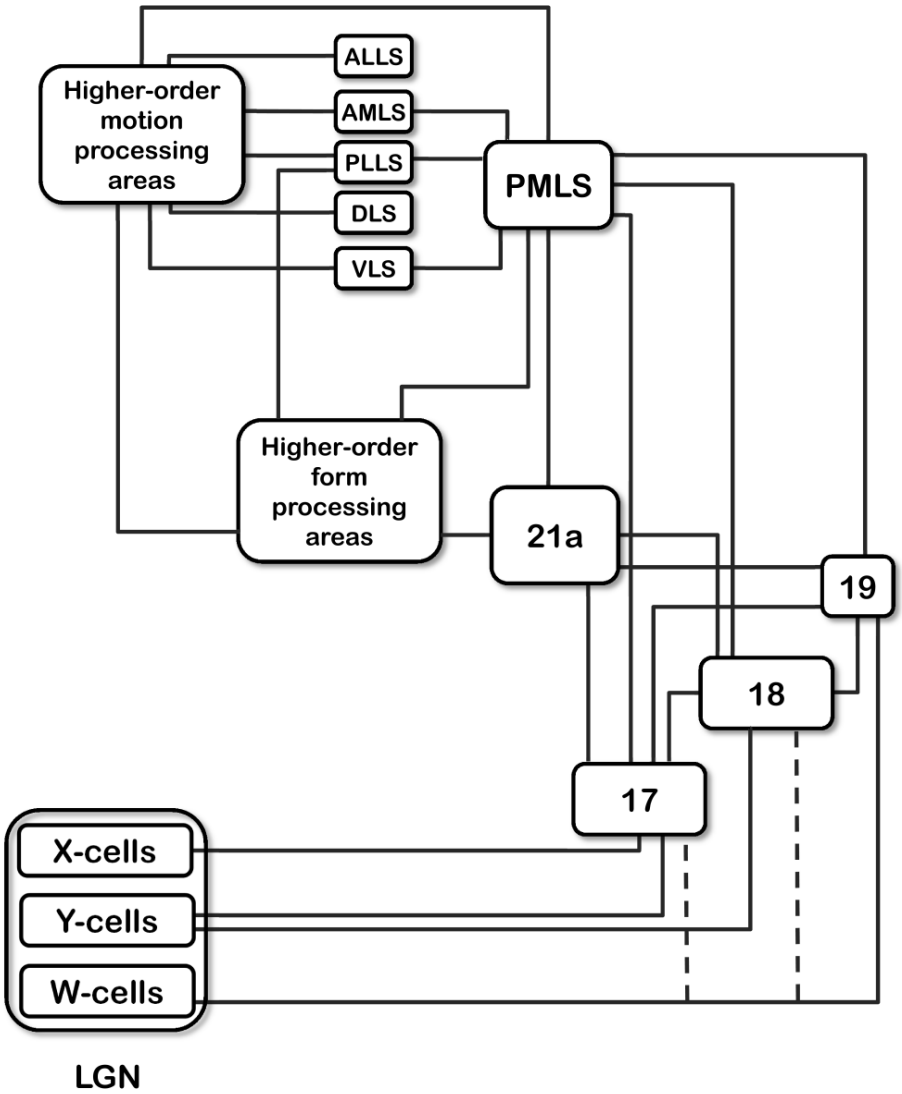

Figure 0.11 Simplified schemata of the cortical visual pathways in the cat. In contrast to the separated organization of X-, Y-, and W-cell fibers, that originates in the retina and is maintained in the LGN, the primary visual cortex already receives convergent information. Despite the generally high degree of interconnectivity, areas PMLS and 21a may be regarded, respectively, as gateways to a primarily motion- and form- processing pathway. Abbreviations: ALLS, AMLS, PLLS, PMLS, anterolateral-, anteromedial-, posterolateral-, posteromedial- , lateral suprasylvian area; DLS, dorsal lateral suprasylvian area; VLS, ventral lateral suprasylvian area; LGN, lateral geniculate nucleus. Reproduced and modified from Dreher et al. (1996)

Several studies on the anatomical and functional properties of areas PMLS and PLLS have not only revealed differences in the physiological organization but also in the connectivity pattern between these two areas. It was shown that in area PMLS the receptive fields are relatively smaller than in area PLLS. Moreover, in area PMLS the retinotopic representation contains mainly the lower visual field close to the horizontal meridian whereas in area PLLS the upper and lower visual field is represented equally. In addition, in area PLLS but not in area PMLS it was found that a central part of the ipsilateral visual hemifield is also represented (Figure 0.12) (Zumbroich *et al.*, 1986; Grant & Shipp, 1991).

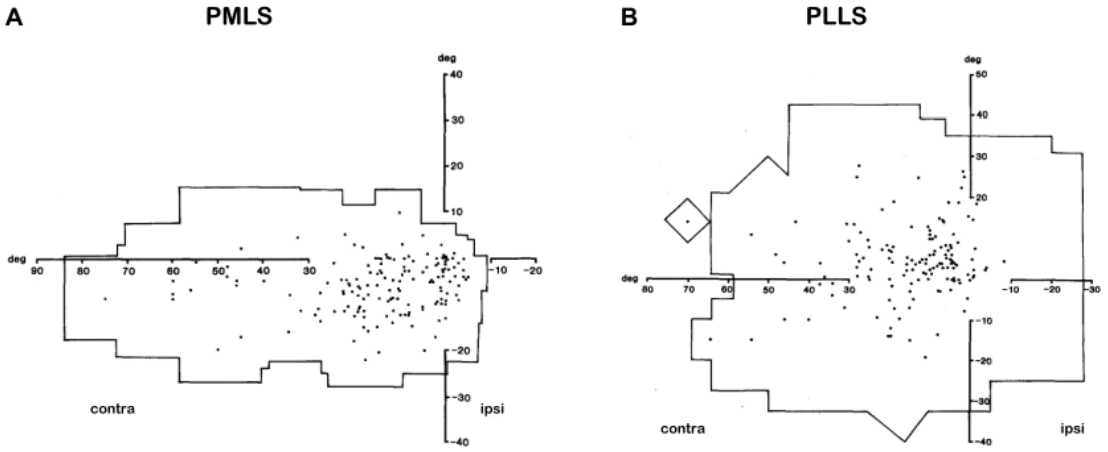

Figure 0.12 Extent of visual field representations of areas PMLS (A) and PLLS (B). The total extent is marked by the outer lines, the dots present the centers of the receptive fields (RF). In area PMLS mainly the lower quadrant of the contralateral visual field and a small portion of the ipsilateral visual field is represented. In comparison, the visual field representation in area PLLS stretches further in the upper and lower contralateral field as well as in a considerable part of the ipsilateral hemifield. Abbreviations: PLLS, PMLS, posterolateral-, posteromedial- , lateral suprasylvian area. Adapted from Zumbroich et al. (1986).

Several neuroanatomical studies have also revealed a segregation of thalamo-cortical and cortico-cortical projections that both areas receive. It was shown that area PMLS receives reciprocal thalamo-cortical input from the LPl, the pulvinar, the LPm and the LGN whereas area PLLS receives input only from the LPm, the C layer of LGN and from the thalamic intralaminar nuclei (Sherman & Spear, 1982a; Tong *et al.*, 1982; Raczkowski & Rosenquist, 1983; Rosenquist, 1985). A comparison of cortico-cortical input has revealed strong reciprocal input from the primary visual cortex of both hemispheres to area PMLS and weak or absent input to from these areas to area PLLS (Sherman & Spear, 1982b; Symonds & Rosenquist, 1984a).

1.4.3.3 *Feedback pathways from the posterior middle suprasylvian cortex*

In addition to the geniculate and extrageniculate feedforward pathways to the pMS cortex, it has been shown that a massive feedback projection emerges from this region to terminate in areas 17, 18 and 19. Moreover, a modest feedback projection to the primary visual cortex of the contralateral hemisphere was additionally identified (Payne & Lomber, 2003). Besides cortico-cortical feedback, pMS cortex is the source of a wide range of cortico-thalamic and cortico-tectal connections. Feedback signals that originate in pMS cortex were found to terminate in the SC, in all layers of the LGN, MIN and geniculate wing, and in the LP-pulvinar complex, with major projections to LPl (Figure 0.13) (Updyke, 1981; Sherman & Spear, 1982a; Segal & Beckstead, 1984; Abramson & Chalupa, 1985; Payne & Lomber, 2003).

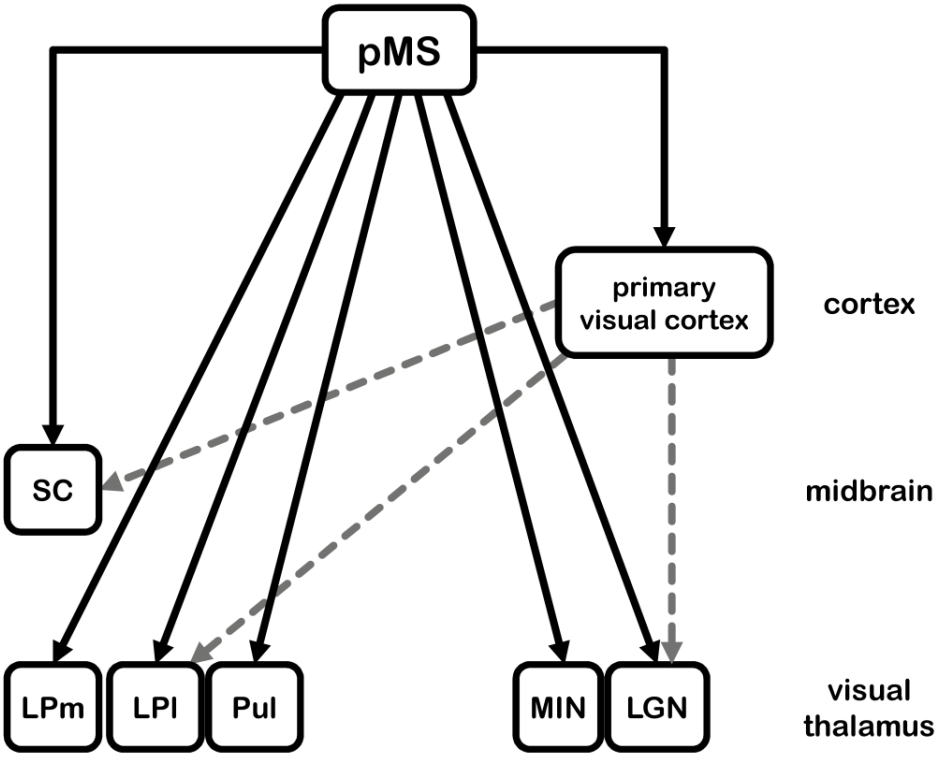

Figure 0.13 Feedback projections from the pMS cortex. Direct feedback projections from the pMS region (black lines) terminate in the primary visual cortex, the SC and in all structures of the visual thalamus. By contrast, the primary visual cortex sends feedback signals (grey dashed lines) only to the SC, the LGN and the LPl. Abbreviations: LGN, lateral geniculate nucleus; MIN, medial interlaminar nucleus; LPI, lateral division of lateral posterior nucleus; LPm, medial division of lateral posterior nucleus; pMS, posterior middle suprasylvian cortex (areas PMLS and PLLS); Pul, pulvinar nucleus; SC, superior colliculus. Data obtained from Payne and Lomber (2003), Sherman and Spear (1982a), Abramson and Chalupa (1985), Updyke (1981) and Segal and Beckstead (1984).

1.5 Aim of the Study

The current lesion study comprises a detailed analysis of electrophysiological data obtained from the primary visual cortex of the cat during an active orienting task. In this context, the neural activity patterns of the intact system were compared with the activity profiles of the acute neglect condition and a subsequent restoration of function. The central questions to be answered with this project were: (i) What are the effects of a lesion in the visuoparietal region and the resulting loss of feedback signals to the neuronal dynamics in the primary visual cortex? (ii) Which activity patterns, if any, in the early visual cortex are associated with a recovery from neglect?

2 MATERIAL AND METHODS

This study was performed with three male cats aged between 18 and 24 months. The animals originated from the cat colony of the Max-Planck-Institute for Brain Research in Frankfurt. All experimental procedures have been approved by the local authorities and were performed in accordance with the German Animal Welfare Act and the global guidelines for animal research of the Society for Neuroscience.

2.1 VISUAL PERIMETRY TASK

For the visual perimetry task a tabletop arena with a radius of 66 cm was used. Red LED lights (3 mm red LED 264-7SURC/S530-A2, Everlight Electronics Co., Ltd., Taiwan) were fixed above the holes at the base of the semicircular wall covering the whole visual field from left 90° to right 90° spaced in 15 degree intervals. Before each session the background illumination was markedly reduced to increase the salience of the stimuli.

At the beginning of each trial the cat was placed by a human handler in the center of the arena with the head directed towards the central position. First, an LED light (fixation LED) lit up at the central (0°) position, which the cat was previously trained to fixate. Second, a peripheral target LED lit up 1.85 s later (Fig, 2.1). The target LED locations were selected in a pseudorandomized manner with hemifields and eccentricities equally balanced across blocks with 28 trials each.

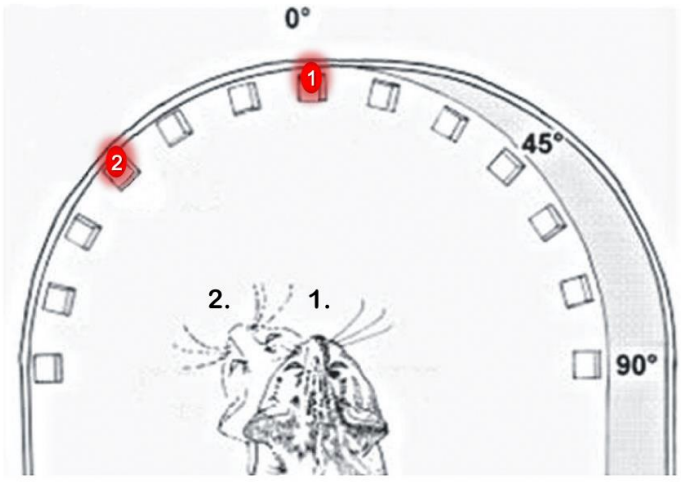

Figure 2.1: Visual perimetry task. Fixation LED (1.) and target LED (2.) are colored in red. A rapid and correct orientation towards the target LED was rewarded with a high incentive food reward, which the cat collected through the holes at the base of the semicircular wall. The locations of the target LED were selected in a pseudorandomized order. Modified from Payne & Lomber (2003).

A rapid response with fast head orienting towards the target LED was rewarded with a high incentive food reward provided through the hole at the corresponding eccentricity. These trials were marked as a correct response. If the cat moved to the central position after target LED onset, the trial was marked as an incorrect response or if the stimulus appeared in the contralesional hemifield and the cat did not approach the corresponding hole, as a neglected target. In these cases, the cat collected a low incentive food reward. Catch trials, in which the target LED was absent, were interspersed and served as controls.

In order to ensure that all three cats had normal vision in preparation for the electrophysiological recordings, all cats were initially trained on the Perimetry task until their behavioral performance had reached a consistent level. To obtain an adequate number of trials for each possible behavioral outcome, individual sessions were combined according to the similarity in daily behavioral performance, into a single pre-lesion period and several post-lesion periods for each cat. Polar plots were used to visualize the summarized behavioral performance within a period as percentages (Figure 2.2).

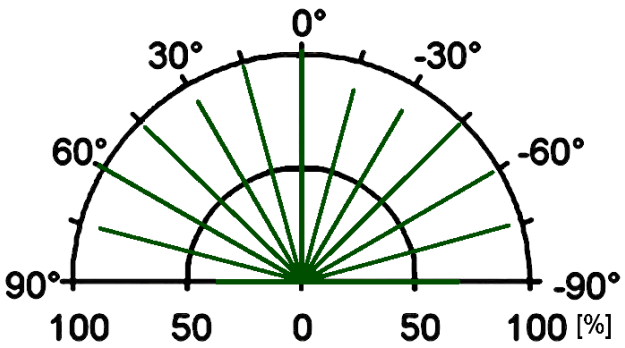

Figure 2.2 The outline of the polar plot represents each stimulus location in 15° increments throughout the visual field. The length of the green lines indicates the number of correct responses for the corresponding stimulus location as a percentage. The inner semicircle represents a behavioral performance of 50 % correct.

2.1.1 Definition of behavioral Conditions

The classification for the ipsilateral and contralateral hemispheres during the pre-lesion recording period was done relative to the respective visual hemifield in which the stimulus was presented (Figure 2.3).

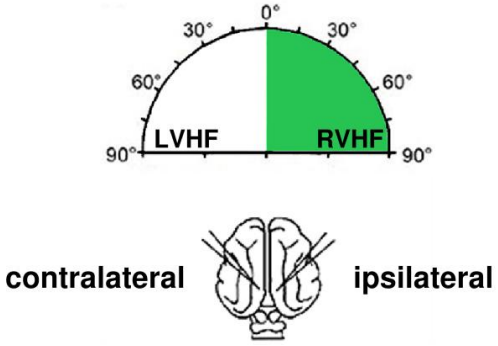

Figure 2.3 In the pre-lesion recording phase, the ipsi- and contralateral hemispheres were defined with respect to the visual hemifield in which the stimuli occurred (quadrant with green background). The two electrode icons in the cat brain schematic indicate the recording sites. Abbreviations: LVHF, left visual hemifield; RVHF, right visual hemifield.

The post-lesion recording period had three different behavioral conditions that were defined relative to the hemisphere with the pMS-lesion (Figure 2.4).

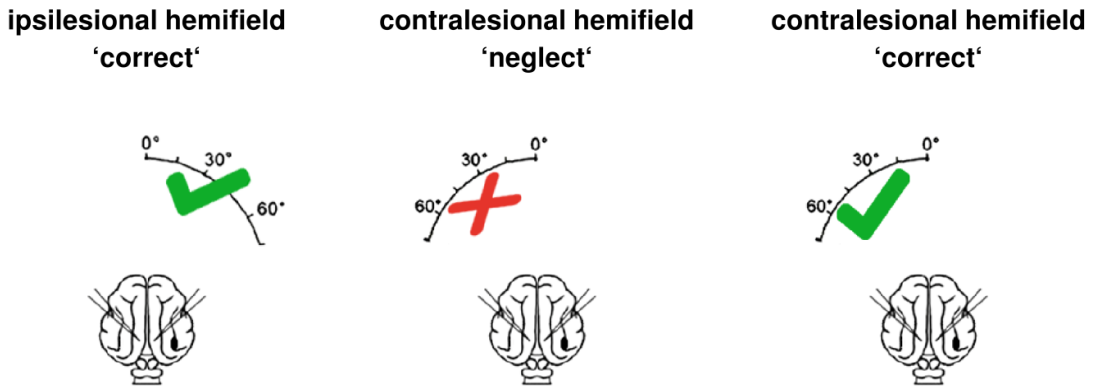

Figure 2.4 shows the three behavioral conditions that were analyzed in this study. The lesion in the pMS region is depicted in black on the cat brain schematic. The green check mark indicates that the cat correctly attended to stimuli in the respective visual hemifield (left and right diagram). The middle diagram shows the neglect condition in which the cat had neglected contralesional targets, as indicated by the red X. Over the course of functional recovery, the cat regained the ability to detect and localize targets in the visual hemifield that was previously neglected (right diagram). Other conventions as in figure 2.3.

2.2 Electrode Design

For electrophysiological recordings Plextrode® Floating Microelectrode Arrays (FMAs) (Plexon Inc. Dallas, Texas, USA) were used. The FMAs are comprised of 14 platinum–iridium microelectrodes embedded in a ceramic substrate 2 mm^2 in size (Figure 2.5). Each array included one reference, one ground and twelve recording electrodes with alternating lengths of either 1 mm or 1.5 mm and an equidistant inter-electrode spacing of 400 μm. The impedance specification was 1 MΩ for the recording electrodes and 5 kΩ for the reference electrode. A flexible set of coated gold lead wires with a length of 2.5 cm connected the array to a Plexon Omnetics® connector and allowed the FMA to float within the moving neural tissue.

Figure 2.5: Sample illustration of a Plextrode® Floating Microelectrode Array (FMA). The electrodes are fixed onto a ceramic array that is connected with a flexible bundle of gold wires to a connector.
source: http://www.plexoninc.com/products/electrodes/fma.html

2.3 SURGERIES

In an initial surgery FMAs were bilaterally implanted into area 18 and a stainless steel base ring with a removable Plexiglas® cover plate was set into the resulting circular craniotomy. This allowed for early recognition of infections emerging in the area around the FMAs and a respective surgical intervention. During this surgery, a head holder was also implanted and bilateral craniotomies over both pMS sulci were made. One craniotomy was done in preparation for the subsequent lesion and the other craniotomy provided for the insertion of a small silver plate electrode for reference in the contralateral pMS sulcus. Following a roughly fourteen-day period of collecting pre-lesional reference data a second surgery was performed where a unilateral pMS cortex lesion with ibotenic acid was induced.

2.3.1 PRELIMINARY PROCEDURES AND INDUCTION OF ANESTHESIA

The cats were not fed for at least 12h prior to surgery and the evening before received a dose of 0.1 mg/kg bodyweight dexamethasone (Voren®, Boehringer-Ingelheim) to reduce cerebral swelling.

Anesthesia was induced by intramuscular injection of a 1:2 mixture of 1 mg/kg xylazinhydrochloride (Rompun®, Bayer) and 10 mg/kg ketaminhydrochloride (Ketanest® S, Pfizer). To prevent cardiac depression 0.1 mg/kg atropine sulfate (Atropinsulfat, B. Braun) was additionally administered. After anesthesia induction, the cat was swiftly intubated.

2.3.2 MAINTENANCE OF ANESTHESIA AND SURGICAL PREPARATIONS

During the surgery, anesthesia was maintained with an inhalant containing a mixture of halothane (1%), N_2O (70%) and O_2 (30%) and was provided by a ventilation pump (model 665/683, Harvard Apparatus). The pump was set to a volume of 50 – 60 ml per respiration cycle and adjusted to the ventilation frequency that yielded a desired end-tidal CO_2 concentration of ~3% (~15 cycles/min). Electrocardiography, end-tidal CO_2, concentration of supplied gases and respiration pressure was continuously monitored (DASH 3000, GE Healthcare).

The cat was placed in a Horsley-Clarke stereotaxic instrument and the head was fixed. Body temperature was maintained at 38°C through a heating pad that was controlled via a rectal thermocouple. Two subcutaneous electrodes were fixed on either side of the thorax to monitor the electrocardiogram. To prevent dehydration physiologi-

cal saline solution (NaCl 0.9%, B. Braun) was continuously administered with an infusion pump (Perfusor®, B. Braun) through a venous catheter in the front leg. During the surgery several doses of glucose (10%, B. Braun) and isotonic, electrolytic saline solution (NaCl, B. Braun) were also applied. The top of the head was shaved and cleaned with an iodine solution (Braunol®, B. Braun). After disinfection surgery was performed under sterile conditions.

2.3.3 Post surgery procedures

Prior to recovery a 0.1 ml/kg dose of the long-acting wide-spectrum antibiotic cefovecin (Convenia®, Pfizer) and of the analgesic carprofen (Rimadyl®, Pfizer) was administered by subcutaneous injection.

The animals were given daily injections of carprofen and dexamethasone for two days post-surgery. The wound margin around the implant and the area along the sutures were carefully cleaned with hydrogen peroxide (3%, P.W. Beyvers GmbH) three times a week or as needed. After 7 – 10 days the sutures were removed.

2.3.4 Bilateral implantation of floating-microelectrode arrays

A sagittal incision along the midline was made and both, skin and muscle were folded back laterally to expose the skull. The location of the subsequent craniotomies over both pMS sulci (Horsley-Clarke HC coordinates: A9 to P3; L10 – L16) and the desired outline of the base ring (inner ø 20mm; centered around HC coordinate A3) were marked on the skull (Figure 2.6).

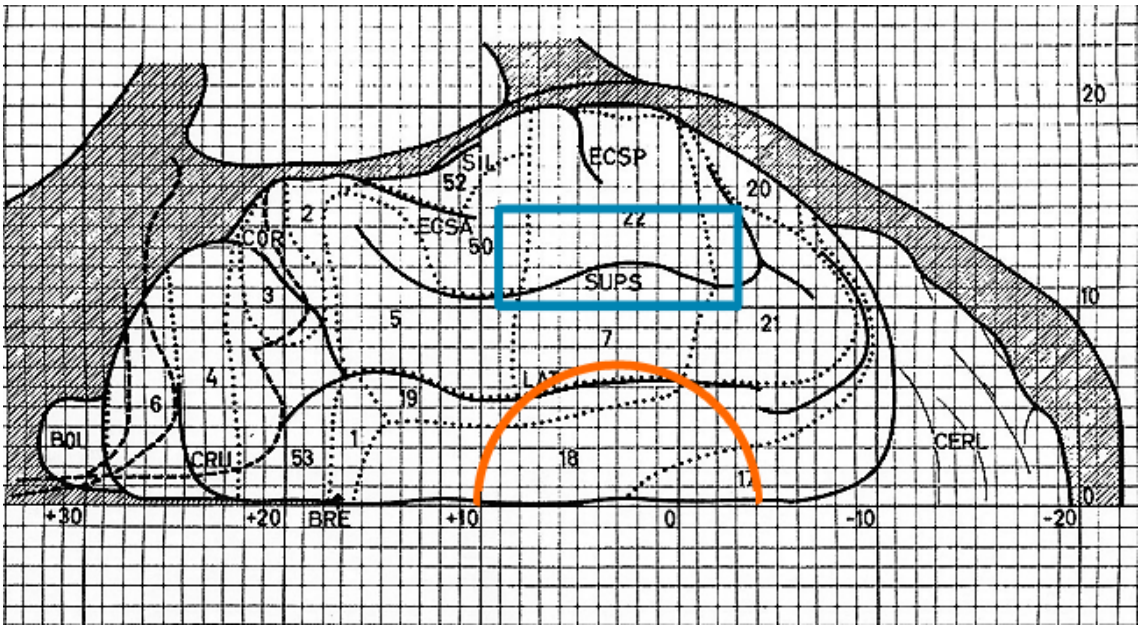

Figure 2.6 Dorsal view of the right hemisphere of the cat. The craniotomy for the ibotenic acid injections (blue rectangle) was made above the suprasylvian sulcus (SUPS). The craniotomy for the recording chamber (orange circle) was located above area 18. Modified from Reinoso-Suarez (1961).

A circular craniotomy was made over the primary visual cortex region using a hand-held Dremel tool and the bone was removed. The edge of the craniotomy was smoothed and afterwards treated with bone wax to control for bone bleeding. Subsequently a craniotomy over each pMS sulcus was performed. To prevent dehydration and contamination the exposed dura was rinsed with physiological saline solution and covered with Spongostan™ (Ethicon Inc.). The titanium base ring for the recording chamber was set in place and fixed with dental acrylic (Paladur®, Heraeus Kulzer) and titanium screws.

After the dura mater over the primary visual cortex was carefully removed, a vacuum holder (Plexon) attached to a micromanipulator was used to position the FMA over the desired implantation site with electrodes oriented perpendicular to the cortical surface. Prior to array insertion small titanium skull screws were tightened posterior to the chamber and the metal casing with the FMA connector (omnetics®) inside was fixed with dental acrylic onto the skull.

Upon FMA insertion, a small amount of tissue glue (Histoacryl®, B. Braun) was applied to hold the array in place and the part of the gold cable running outside of the chamber was covered with a thin layer of dental acrylic to prevent strain.

Once both FMAs were implanted, a small silver plate for electrical grounding was placed under the dura in the pMS sulcus contralateral to the future lesion site. The silver plate was connected via a thin wire to a gold plug that allowed for connection to the pre-amplifier (Headstage, Plexon).

After cleaning, the chamber was then filled with the antibiotic chloramphenicol (Kemicetine®, Pfizer) and clear agar and tightly sealed with a clear custom-made cover. If needed, a small screw in the center of the cover could be opened at any time to administer antibiotics and reduce pressure in case of an infection. Before closing the surgery a headholder was implanted above the frontal sinus. For this, small titanium screws were mounted on the skull and the headholder was fixed using dental acrylic. The entire implant was reinforced with dental acrylic before skin and muscles were sutured (ETHIBOND® EXCEL, Ethicon) snug around the pedestal (Figure 2.7).

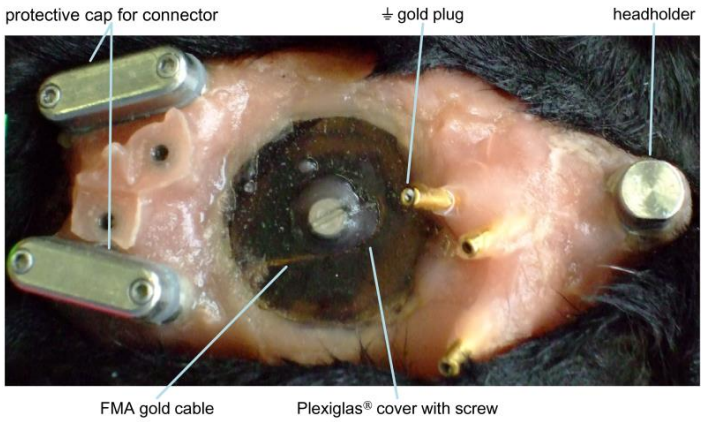

Figure 2.7 Dorsal view of an implant. The FMA connectors were located posterior, the headholder was placed anterior above the frontal sinus. The recording chamber with the Plexiglas® cover was located in the central region.

2.3.5 Unilateral Ibotenic acid lesion of pMS cortex

Ibotenic acid

Ibotenic acid (2-amino-2-(3-oxo-1,2-oxazol-5-yl)acetic acid) is an excitatory neurotoxic α-amino acid, derived from mushrooms of the *Amanita* genus and is structurally related to the neurotransmitter glutamate. Ibotenic acid induces increased activity at *N*-methyl-*d*-aspartate (NMDA) and metabotropic glutamate receptors causing local hyperactivity and subsequent neuronal cell death through excessive accumulation of intracellular Ca^{2+}.

Excitotoxins such as ibotenic acid are known to selectively destroy neurons within a distinct radius while sparing fibers of passage when injected intracerebrally (Schwarcz *et al.*, 1979; Guldin & Markowitsch, 1982). The cortical regions damaged by the ibotenic acid are characterized by a pronounced loss of neurons and the development of a glial scar (Eysel & Schweigart, 1999).

Lesion of pMS cortex

Anesthesia was induced by intramuscular injection of 0.04 mg/kg dexmedetomidine hydrochloride (Dexdomitor®, Orion Pharma) and 0.1 mg/kg atropine sulfate (Atropinsulfat, B. Braun) and surgical preparations were performed as described in section 2.3.2. Before the dental acrylic covering the pMS craniotomy was drilled away, receptive fields of the recorded neuron population in area 18 were mapped by flashing oriented light bars at various positions along the receptive field. After the pMS sulcus on the desired hemisphere was exposed, the dura mater was reflected and a Hamilton® syringe (10μl, model 801, Hamilton Co.) attached to a micromanipulator was positioned over the sulcus in the respective angle. Twenty to twenty-two injections of 1μl of sterile ibotenic acid (10μg/μl, 95%, Sigma) were made into the medial and lateral bank starting posterior at the bend of sulcus and moving anterior in 2 mm increments (see Table 2.1 for details). The horizontal distance from the middle of the sulcus was 8 mm for

both, medial and lateral injection sites and ibotenic acid was equally injected 2 mm and 5 mm in depth at each site. After each penetration the tissue was allowed to settle for 10 minutes.

Table 2.1 Summary of ibotenic acid lesions

			Number of injection sites	
Cat	Hemisphere	Injection angle (°)	medial (PMLS)	lateral (PLLS)
R1	Right	45	6	5
L1	Left	40	5	5
L2	Left	45	6	4

Abbreviations: PMLS, posteromedial lateral suprasylvian cortex; PLLS, posterolateral lateral suprasylvian cortex

After completion of the injections the exposed cortical surface was covered with Spongostan™ and the craniotomy was re-sealed with dental acrylic. Surgical closing and post-surgery procedures were performed as described in section 2.3.3.

Electrophysiological recordings during the perimetry task started 1-2 days after the lesions.

2.4 Neural Recording and Data acquisition

During recording sessions a head stage (Plexon®) was attached to the FMA output connector pre-amplifying the neural signal 20x (Figure 2.8). For a more secure connection the head stage was modified so that it could be screwed to the implant. A head stage cable (Plexon®) with a length of 1.8 m connected each head stage to the main amplifier (MCP-Plus, Alpha Omega Engineering). Here, the signals from the microelectrodes were again amplified 100x and then filtered separately for spikes [800-5000 Hz] by the MCP Plus and for the local field potential (LFP) [0-800 Hz] by a custom-built filter (Max Planck Institute for Brain Research). LFPs were then digitized at 2 kHz through a Power1401 (Cambridge Electronic Design Limited) analog-to-digital converter and monitored with the data acquisition software Spike2 (version 4.01, Cambridge Electronic Design Limited). Neural spiking activity was sampled at 22 kHz through a Power1401 mkII (Cambridge Electronic Design Limited) and monitored in the same way.

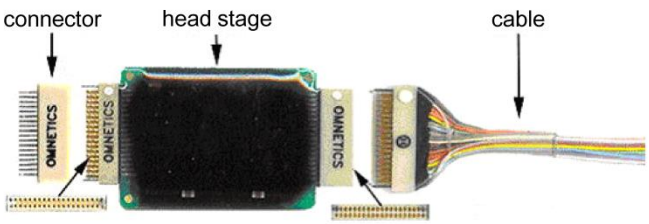

Figure 2.8 Plexon headstage. The connector was fixed to the implant. The signal was pre-amplified in the head stage (20x) and then transmitted via the cable to the main amplifier.
source:http://www.plexoninc.com/products/headstage/headstages.html

Trial recording was started by pressing a button on the manually controlled stimulus box (Max Planck Institute for Brain Research) for the perimetry task. The trigger also sent the stimulus label and information about the stimulus location to the data acquisition software. Within a trial, each lasting 8 seconds, two event labels marked the onset of the fixation LED and the target LED. The behavioral outcome (correct/neglect etc.) was encoded by manually set labels after each trial.

2.5 Receptive Field Mapping

Size and orientation of the receptive fields from the recorded neuron population were mapped onto a large sheet of paper fixed to a screen. The distance of the screen from the eyes was 57 cm. The projections of the optic disk were also drawn on the paper sheet after they were determined by using an ophthalmoscope. The location of the *area centralis* (center of gaze) and the visual axis was then inferred from the position of the optic disk (Bishop *et al.*, 1962). Eccentricities of the receptive fields relative to the area centralis were mapped into a spherical polar coordinate system. This system uses the two angles, azimuth and elevation to describe the visual direction relative to the center of gaze.

2.6 Data analysis

The orienting response evoked large movement artifacts that could easily be distinguished by eye from the neural activity. For that reason, the total trial duration was reduced to 3.2 s to exclude these artifacts from further analysis.

All computations for analysis were performed using custom code written in MATLAB (MathWorks).

2.6.1 Spiking Activity

For each recording period the raw data traces of each channel that belonged to one stimulus location and condition (e.g. left visual hemifield, 15° position, correct) were concatenated. The action potentials (spikes) were detected by setting an amplitude threshold on the concatenated raw signal traces and stored as discrete timestamps. The threshold was automatically set and for the estimate of the noise level a median-based approach was chosen (Quiroga *et al.*, 2004). Changes in the trial-averaged multi-unit activity in response to both stimuli were then assessed by calculating the peri-stimulus time histograms (PSTH) with a bin width of 1ms. In a PSTH the trial averaged spike rate is represented as a function of time and defined as spikes per second.

2.6.2 ANALYSIS OF LOCAL FIELD POTENTIALS

The local field potential (LFP) is a low-frequency (< 300Hz) extracellular electrical potential in which excitatory and inhibitory synaptic processes are integrated at the neural population level (Mazzoni *et al.*, 2012). It carries information about the cortical network state and reflects contributions of several neural processing pathways such as top-down and bottom up pathways.

To account for changes in the oscillatory activity due to an altered cortical state, trial data was divided into four 350 ms analysis windows centered around the first and second LED onsets (Figure 2.9). The figure below shows the stimulus time course and the four analysis windows (AW).

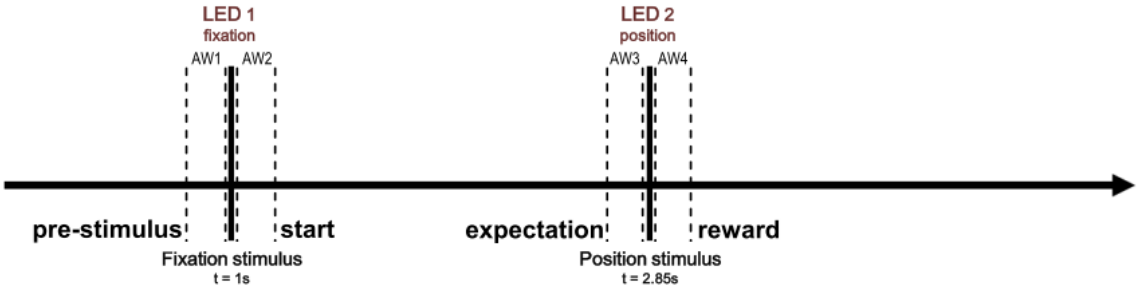

Figure 2.9: Stimulus time course and analysis windows (AWs). Each AW has a length of 350ms. The pre-stimulus analysis window AW1 started 350 ms before the onset of the fixation stimulus (1st LED). AW2 marked the start of a trial and was the 350 ms right after the onset of the 1st LED. The expectation analysis window (AW3) immediately preceded the onset of the target LED (2nd LED) and was followed by the reward analysis window (AW4). In AW4 the distinction between 'correct', and 'neglect' was made. Additionally, as a control, 'catch' trials without the target stimulus (2nd LED) were recorded.

2.6.2.1 *Event-related potentials*

To evaluate peak latency differences in response to the fixation and target stimuli, event-related potentials (ERPs) were calculated for all eccentricities in the visual field. Therefore, the signal average over all electrodes within one electrode array was taken and, as a next step, all correct responses to a single stimulus position were averaged to increase the signal-to-noise ratio (SNR). The signal was baseline corrected relative to a pre-LED onset period of 200 ms. The duration of every ERP analysis window was 350 ms, starting at the onset of either the fixation cue (first LED) or the position stimulus (second LED). For the computation of ERPs the Matlab toolbox FieldTrip (http://www.ru.nl/fcdonders/fieldtrip/) was used.

For a second comparison, the pre- and post-lesion peak latency differences were analyzed by subtracting the pre-lesion peak latencies from the respective post-lesion peak latencies.

2.6.2.2 *Time-frequency analysis*

The power spectra were estimated by using a multi-taper algorithm implemented in the Chronux toolbox (http://www.chronux.org)(Bokil *et al.*, 2010).The first five tapers of the discrete prolate spheroidal sequence (DPSS) were applied on an analysis window starting 200 ms prior to target LED onset and ending 250 ms post target LED onset. The sliding window duration for the underlying fast Fourier transform (FFT) was 200 ms with an overlap of 10 ms each and in order to obtain more accurate amplitude estimates, zero padding was applied.

After averaging the signal over all electrodes from on FMA, further averaging was done in two ways. For the induced activity, the FFT was calculated for each trial belonging to a certain condition and then averaging was done over all single trial spectra. Consequently, the induced activity contains time-locked and non time-locked oscillations (Tallon-Baudry & Bertrand, 1999b). For the evoked activity averaging over all trials from the same experimental condition was done before the FFT was calculated on the averaged waveform. In the evoked activity non time-locked activity is attenuated and stimulus-locked activity is more pronounced.

The normalization for the spectra was done by subtraction of 'catch' trials (trials without the second LED signal). Only the stimulus positions where the cat showed a behavioral performance of more than 75% prior to the lesion were marked in the post-lesional analysis as 'neglected'.

2.6.2.3 *Frequency band analysis*

By applying a FFT, the induced LFP signal power in the frequency range of 4 to 99 Hz was computed and separated into the following five different frequency bands:

Table 2.2 Frequency bands with their frequency ranges

Frequency band	Symbol	Frequency range [Hz]
theta	θ	4-8
alpha	α	8-14
beta	β	14-30
gamma1 (low)	γ1	30-48
gamma2 (high)	γ2	52-99

The power of each frequency band was calculated for the four different analysis windows AW1 to AW4. Normalization with the pre-stimulus AW1 and calculation of change in percent was performed in the following way:

$$\%\, change = \frac{(AWx - AW1)}{AW1} * 100 \qquad AWx = AW2,\ AW3,\ AW4$$

The results must be interpreted as changes in power relative to the power in each frequency band during the pre-stimulus analysis window (AW1). If the resulting value was smaller than zero (negative value), the resulting power was less than the pre-stimulus power. If the value was greater than zero, the resulting power was increased relative to the pre-stimulus power. The amount of the power increase/decrease relative to the pre-stimulus power was expressed as the percentage change.

AW baseline

For the analysis of ongoing neural activity an analysis window of 1s duration was chosen. The baseline analysis window started 500 ms after the onset of the fixation LED and ended 350 ms before the onset of the of the target LED (Figure 2.10).

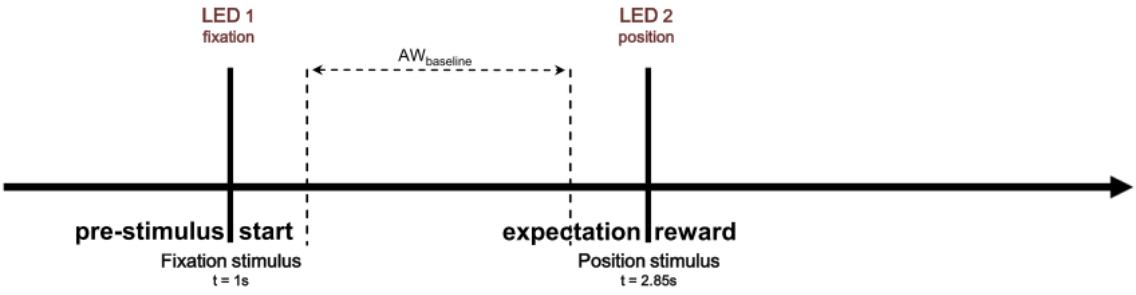

Figure 2.10 Trial course and location of the baseline analysis window ($AW_{baseline}$)

The resulting trials were first averaged over all electrodes from one FMA and then averaged within each recording period (pre, pl1…pl_{end}). The frequency band power was calculated as described above and power in the delta range (1-4 Hz) was included in the calculation. Lesion-induced modulation of endogenous oscillatory power was quantified by computing a modulation index (MI) for each frequency band as follows:

$$MI \in [-1,1]$$

$$MI = \frac{FB_{pln} - FB_{pre}}{FB_{pln} + FB_{pre}}$$

pln = post-lesion period 1 - end
pre = pre-lesion period

The results are a ratio between the frequency band power in $AW_{baseline}$ from a single post-lesional recording period and the respective frequency band power in $AW_{baseline}$ from the prelesion recording period. A MI below zero indicates a power decrease relative to the pre-lesion period, a MI greater than zero indicates a power increase with respect to the pre-lesion period.

2.6.2.4 *Analysis of interhemispheric coherence*

One methodological approach to measure functional connectivity in the form of synchronous oscillations between different brain areas is to compute the spectral coherence. In particular, spectral coherence quantifies the similarity of two recorded neural signals in the frequency domain. It is a non-directed connectivity metric, i.e. it does not determine the direction of interaction.

As a first step in the analysis of LFP-LFP coherence between areas 18 of the two hemispheres a re-referencing of the electrode signals was performed. In LFP recordings, spurious functional connectivity estimates can result from volume conduction and the usage of a common reference channel. To remove these signal components that are common to all recording sites, the average signal from all electrodes of one FMA was subtracted from the signal recorded from each electrode of the contralateral FMA.

The coherence spectra between all possible electrode pairings (x and y) in four different frequency ranges were calculated by using the following formula

$$coh_{xy}(\omega) = \frac{|S_{xy}(\omega)|}{\sqrt{S_{xx}(\omega)S_{yy}(\omega)}}$$

where $S_{xx}(\omega)$, and $S_{yy}(\omega)$ represent the power spectra and $S_{xy}(\omega)$ the cross-spectrum of the two signals x and y at frequency ω averaged across all trials belonging to a recording period. The coherence ranges between 0 and 1, in which 0 indicates no coherence, and 1 indicates perfect coherence between the two signals x and y at frequency ω. Coherence was computed within the $AW_{baseline}$ and to calculate the power and cross-spectra the multi-taper method implemented in the Chronux toolbox (http://www.chronux.org) with five DPSS tapers. The resulting values were then averaged to obtain one value per specified frequency range.

Lesion-induced alterations of coherence for each post-lesion period in the respective frequency range were quantified by calculating percent change with respect to the pre-lesion recording period.

2.6.3 Statistical Analysis

The data from each comparative analysis were tested for normality by performing a Kolmogorov-Smirnov test. In most of the analysis, the normal distribution hypothesis had to be rejected at the 5% level or the sample size did not allow a Gaussian distribution as in the case of the ERP peak latency comparison (section 3.1.2). Therefore, the non-parametric Wilcoxon rank sum test (WRS) was used for independent samples to test whether the distribution medians were equal. For paired samples, the Wilcoxon signed rank test (WSR) was used. Statistical significance was defined as a two-tailed p-value < 0.05. The Wilcoxon rank sum test is equivalent to the Mann-Whitney U-test (U).

2.7 Perfusion and Histology

At the end of electrophysiological studies, the cats were sedated with ketamine and euthanized with an intraperitoneal lethal dose (100 mg/kg) of sodium pentobarbital (Narcoren®, Merial GmbH). Animals were then transcardially perfused with saline phosphate buffer solution (0.9% NaCl in 0.1 M phosphate buffer, PB; pH 7.4), followed by 4% paraformaldehyde in 0.1 M phosphate buffer (PB; pH 7.4). The brains were removed and cryoprotected in 4% paraformaldehyde/30% sucrose in PB for ~24 h, then kept in 30% sucrose in PB for ~14 d before they were sectioned. Coronal sections were cut at a thickness of 60 μm on a freezing microtome (RM2235, Leica). Every fifth section was mounted onto poly-L-lysine coated slides and alternately stained with cresyl-violet for Nissl substance and cell bodies or by using the Gallyas silver impregnation method to reveal myelinated axons. Sections were then dehydrated in an ascending alcohol series, dried and covered with glass slips.

Via microscopy the locations of all relevant areas and lesion sites were determined. The identification was based on area positions relative to sulcal landmarks and cytoarchitectonic differences following previously published anatomical data (Hubel & Wiesel, 1969a; Palmer *et al.*, 1978; Tusa *et al.*, 1978, 1979, 1981b; Symonds & Rosenquist, 1984b; Sherk, 1986). The digital reconstruction was performed with a Neurolucida (MBF Bioscience) system.

Table 2.3 Nissl stain protocol

Procedural step		Time (minutes)
1	wash with water	2
2	70% ethyl alcohol	5
3	96% ethyl alcohol	5
4	70% ethyl alcohol	2
5	distilled water	2
6	50% potassium disulfide solution	12-15
7	wash with distilled water	2 x 1
8	1.5% cresyl violet solution	1
9	0.2M acetate buffer	2
10	70% ethyl alcohol	2
11	96% ethyl alcohol	2
12	isopropanol	2
13	wash with xylene (2 times)	2 x 5

Table 2.4 Gallyas silver stain protocol

Procedural step		Time (minutes)
1	wash with water	1
2	acetic acid anhydride/pyridine solution	30
3	wash with water	2 x 5
4	alkali silver nitrate solution	45
5	0.5% acetic acid	3 x 5
6	physical developer solution	18-20
7	1% acetic acid	1
8	0.2% potassium hexacyanoferrate-III	10
9	distilled water	1
10	0.5% sodium thiosulfate	2 x 3
11	wash with distilled water	3 x 4
12	70% ethyl alcohol	2
13	96% ethyl alcohol	2
14	isopropanol	2
15	wash with xylene (2 times)	3

3 RESULTS

To date there are no comparable neurophysiologic lesion studies that investigate the neuronal dynamics in the primary visual cortex of the cat during the Perimetry task. For this reason, this thesis will provide at first an overview of how the stimulus is represented in the intact V1 (section 3.1). This section is followed by the behavioral results of all three cats over the duration of the entire experiment (section 0) and the results of the histological examinations (section 3.3). The results of the post-lesion period are subdivided into an analysis of the neglect situation (section 3.4.1), a comparative analysis of stimulus-dependent changes in neural activity (section 3.4.2) for ipsilesionally presented stimuli and an analysis of stimulus-independent ongoing activity over the time course of the experiment (section 3.4.3).

3.1 EVALUATION OF THE PRE-LESION RECORDING PERIOD

3.1.1 STIMULUS-INDUCED CHANGES OF LOCAL FIELD POTENTIALS

For each cat the rasterized LFP traces were calculated for two time periods: 1) the period following the fixation stimulus and 2) the time period following the target stimulus for all correct responses. Signals recorded on the same electrode array were averaged and each trial was converted to color coded lines indicating high or low signal amplitude.

In all three cats, the fixation and the target stimulus evoked a similar change in LFP amplitude. In cat R1 (Figure 3.1 A) the response profile for the fixation stimulus showed a negative peak at ca. 175 ms after LED onset in all trials and on both electrode arrays. The negative peak, in response to the target LED, showed a higher temporal variability, but generally occurred within 80-130 ms after stimulus onset (Figure 3.1 B). Additionally, recordings of the left hemisphere indicated an increase of LFP amplitude at 250 ms (Figure 3.1 B lower plot). Compared to cat R1, cat L1's negative peak in response to the fixation stimulus also appeared around 175 ms but showed a high inter-trial latency variability (Figure 3.1 C). The second LED evoked no clear response profile in this cat. At 250 ms however, a transient change in amplitude could be observed for the majority of trials on both electrode arrays (Figure 3.1 D). The response profiles of cat L2 to both stimuli were comparable to those of cat R1 (Figure 3.1 E, F).

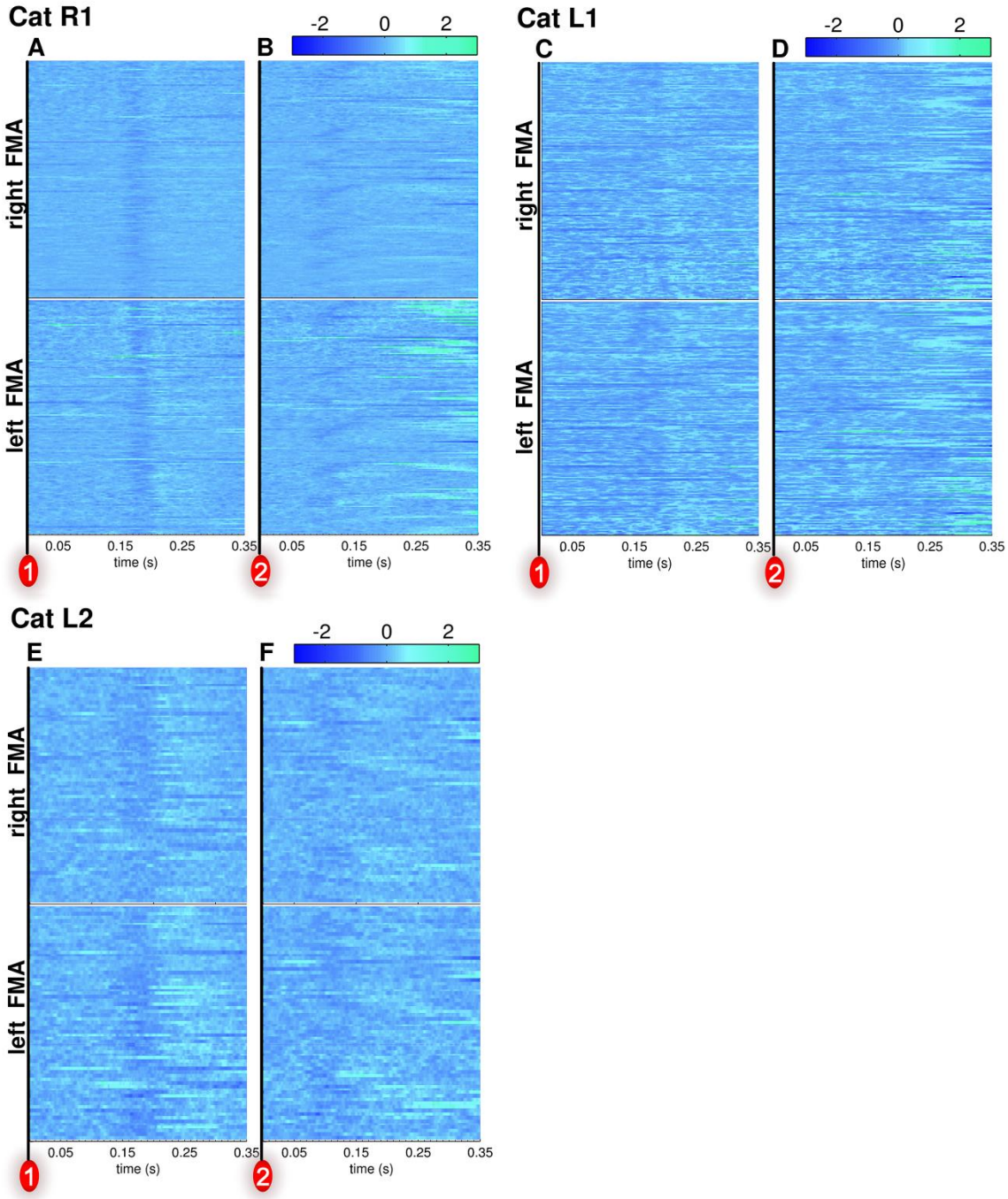

Figure 3.1 Rasterized stimulus-evoked LFP changes. The voltage trace from all electrodes within one floating microelectrode array (FMA) was averaged and a conversion of each trial to color coded lines was done. Trials recorded on the right FMA are shown in the upper row of each panel and trials recorded on the left FMA are shown in the lower row of each panel. The line color indicates a high (light blue to green) or a low (dark blue to light blue) signal amplitude in volt. All trials are stacked and aligned from stimulus onset up to 350 ms. The left plot of each panel (A, C, E) indicates a 350 ms long time window after fixation LED (1st LED) onset, the right plot of each panel (B, D, F) indicates a 350 ms long time window after onset of the target LED (2nd LED). (A) Rasterized LFP changes from cat R1 in response to the fixation stimulus. The 1st LED evoked a trough at around 175 ms in the LFP. (B) The negative peak in response to the target LED showed a higher temporal variability and shorter peak latencies of 80-130 ms after stimulus onset. (C, D) The response profiles of cat L1 to the 1st LED as well as to the 2nd LED were markedly less pronounced than in the two other cats. Nevertheless, the time course corresponded approximately to that of cat R1 and L2. (E, F) In cat L2 the LFP amplitude changes in response to the fixation LED and the target LED showed strong similarities with those of cat R1. number of trials: R1 n = 149; L1 n = 178; L2 n = 68

3.1.2 ANALYSIS OF EVENT RELATED POTENTIALS

To evaluate the latency differences in response to the fixation and target stimuli, event-related potentials (ERPs) were calculated for all eccentricities in the visual field. This involved taking the average voltage trace of all correct responses to a single stimulus over all electrodes within one electrode array. The length of every ERP analysis window was 350 ms, starting at the onset of either the fixation cue (1st LED) or the target stimulus (2nd LED). In general, a distinct ERP could be measured only for eccentricities in that hemifield, which lay contralateral to the silver reference plate. As a representative example, the ERP waveforms of cat R1 are shown in figure 3.2 and the precise peak latencies are reported in Table 3.1. The focus of the following evaluation rests on the three ERP components; N1, P1 and P2, as they were consistent across all three cats.

The analysis of event-related potentials revealed two main findings. First, there is a general difference between the ERP elicited by the fixation stimulus and the ERPs evoked by the various target stimuli. Second, the latencies of the main ERP components are related to the stimulus location in the visual hemifield.

Both the fixation cue and the target stimuli elicited a distinct negative peak (N1) in the primary visual cortex. Although the fixation cue and the central stimulus (0°) had the same location in the visual field, the N1 component in response to the target stimulus appeared with a peak latency around 90 ms earlier than the N1 component evoked by the fixation stimulus (Fig.3.2 A, B). The peak latency in the latter case was ~180 ms on both recorded hemispheres. The temporal occurrence of the N1 component evoked by the stimulus at 15° was similar to the N1 peak latency that was evoked by the central (0°) post-fixation stimulus (Fig.3.2 C, B). For the peripheral stimulus locations, a steadily increasing latency delay of the N1 peak was observed. The delay started at the 30° target position and increased up to the 75° position in the right visual hemifield (Fig.3.2 D-G). The stimuli at the 30°, 45°, 60° and 75° location elicited a N1 component with a peak latency of circa 100 ms, 110 ms, 115 ms and 130 ms respectively. Frequently, a positive peak (P1) immediately followed the negative peak. P1 was considerably more pronounced in the ERP that was recorded from the left primary visual cortex. The fixation cue merely elicited a P1 component on the left primary visual cortex with a peak latency of ~215 ms while the central stimulus (0°) evoked a P1 component with a peak latency of circa 150 ms (Fig.3.2 A, B). Apart from the two central stimuli, the P1 component only occurred when one of the two near-center stimuli was shown at either 15° or 30° in the right visual hemifield (Fig.3.2 C, D). The P1 peak latency was ~130 ms and ~160 ms, respectively. A second positive peak, the P2 component, was exclusively

evoked by non-central stimuli (Fig.3.2 C-G). Furthermore, analysis of P2 revealed an opposing peak latency pattern, when compared to the N1 component, with gradually decreasing latencies for increasingly peripheral target locations. A P2 component with a peak latency of ~350 ms was elicited by a stimulus at 15° (Fig.3.2 C), whereas a stimulus at the 30° position evoked a P2 component with a peak latency of ~325 ms (Fig.3.2 D). When the stimulus occurred at the 45° location, a P2 peak latency of circa 300 ms was observed (Fig.3.2 E). If the stimulus was located either at the eccentricity of 60° or 75° in the right visual hemifield, the P2 peak latency was around 280 ms and 260 ms (Fig.3.2 F, G).

Table 3.1: Precise peak latency values of the three main ERP components obtained from cat R1. The earliest peak latency for each component is highlighted on both hemispheres.

Stimulus position	peak latency						Number of trials
	Right (ipsilateral) FMA			Left (contralateral) FMA			
	N1	P1	P2	N1	P1	P2	
	ms						
fixation cue	176	-	-	182	215	-	137
center 0°	95	149	-	**91**	156	-	13
RHF 15°	**87**	**128**	349	95	**130**	349	11
RHF 30°	97	158	323	107	156	329	5
RHF 45°	106	-	292	110	-	308	10
RHF 60°	111	-	281	116	-	285	13
RHF 75°	128	-	**255**	129	-	**257**	11

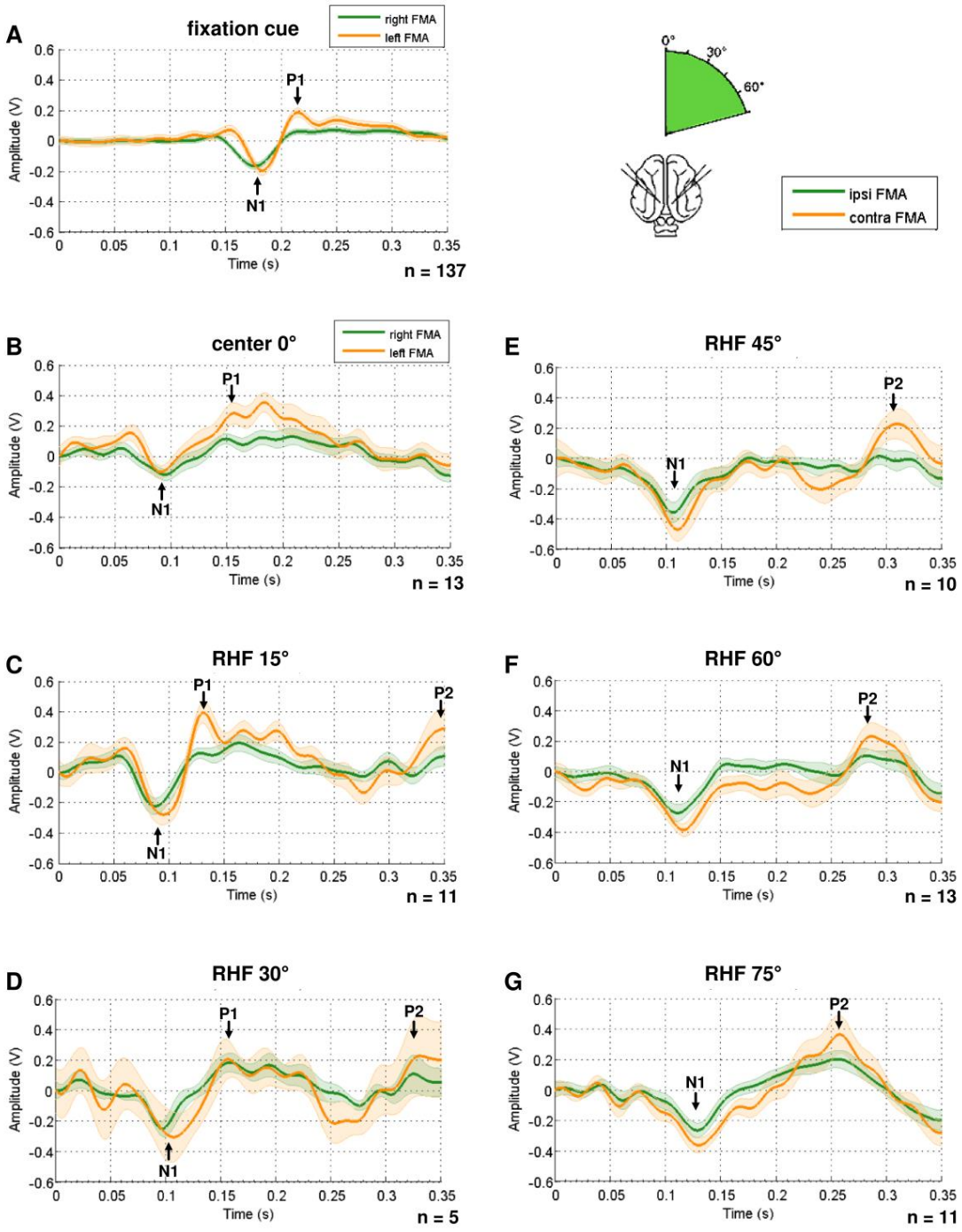

Figure 3.2 Pre-lesional ERP results of cat R1 during the arena task. Shown are the bilaterally recorded ERP traces in response to stimuli that were presented at a single position in the cat's central or right visual hemifield (as indicated by the icon on the right side). The first negative component is marked as N1, the first and the second positive component is denoted by P1 and P2, respectively. **(A)** ERP evoked by the fixation cue (1st LED). P1 occurred solely within the ERP of the left V1. **(B)** ERP evoked by the target stimulus (2nd LED) at the central position (0°). Note the earlier occurrence of the N1 and P1 component compared to the peak latencies in response to the fixation cue. **(C)** ERP evoked by the target stimulus at the center-near 15° position. Note the occurrence of the P2 peak at ~350 ms after stimulus onset **(D)** ERP in response to the center-near 30° stimulus. **(E)** ERP evoked by the target stimulus at the 45° position. The P1 component was absent. A distinct P2 component could only be observed on the contralateral hemisphere (orange line). **(F)** ERP in response to the peripheral 60° stimulus. **(G)** The ERP evoked by the peripheral 75° stimulus showed the lowest P2 peak latency. n = number of trials; Abbreviations: FMA: floating-microelectrode array; RHF: right visual hemifield; ipsi: ipsilateral; contra: contralateral; Shaded area shows SEM.

Summary

The response pattern for ERP components elicited by the target stimulus (2nd LED) displayed an increasingly later occurrence of the N1 component, the more peripheral the target LED was located. This finding also applied for the P1 component, although this component was exclusively elicited by central (0°) or center-near (15° and 30°) stimuli. An opposing peak latency pattern was observed for the P2 component, which occurred latest in response to the stimulus at the 15° position and at earliest in response to the 75° targets.

Surprisingly, a comparison between the N1 and P1 components evoked by the fixation cue (1st LED) and the same components evoked by the central target (2nd LED), revealed substantial peak latency differences. In all three cats, the central 0° target elicited shorter N1 and P1 peak latencies than the fixation cue, although both stimuli occupied the same position in the visual field. Moreover, the N1 (and P1) component generally displayed a more rapid onset in response to the target LED than to the fixation LED. Possibly this effect is associated with a different internal evaluation of the two stimuli.

3.1.3 RECEPTIVE FIELDS

The receptive field (RF) positions of the recorded neurons in area 18 were assessed and subsequently mapped onto a spherical polar coordinate system to illustrate the distribution of the RFs over the visual field. In this coordinate system, the visual direction relative to the area centralis is expressed by two angles, azimuth and elevation.

In all three cats, the RFs of the recorded units were located in the lower contralateral visual field. With only few exceptions, the recorded cells had overlapping fields that were clustered around the 30-degree eccentricity.

In cat R1, the visual field portion that was covered by the receptive fields of the neurons recorded in the right primary visual cortex ranged from an azimuth of -22 to -41 degrees and an elevation of -21 to -29 degrees (Figure 3.2, upper panel). The receptive fields of cells recorded on the left hemisphere covered an area of the visual field that stretched across an azimuth of 18 to 32 degrees and an elevation of -19 to -32 degrees (Figure 3.2, lower panel).

By comparison, the receptive fields recorded in cat L1 were generally located closer to the horizontal midline extending over an elevation of -11 to -18 degrees for cells recorded in the right hemisphere (Figure 3.3, upper panel) and -11 to -23 degrees for units recorded on the left side (Figure 3.3, lower panel). In the right hemisphere, the peripheral extension ran from -25 to -33 degrees whereas in the left hemisphere the area stretched horizontally from 24 to 33 degrees.

In cat L2 the receptive fields of cells recorded in the right primary visual cortex covered an area of the visual field that ranged from -18 to -29 degrees along the vertical axis and from -22 to -32 degrees along the horizontal axis (Figure 3.4, upper panel). The receptive fields recorded on the left side covered a total area of -17 to -26 degrees elevation and 15 to 26 degrees azimuth (Figure 3.4, lower panel).

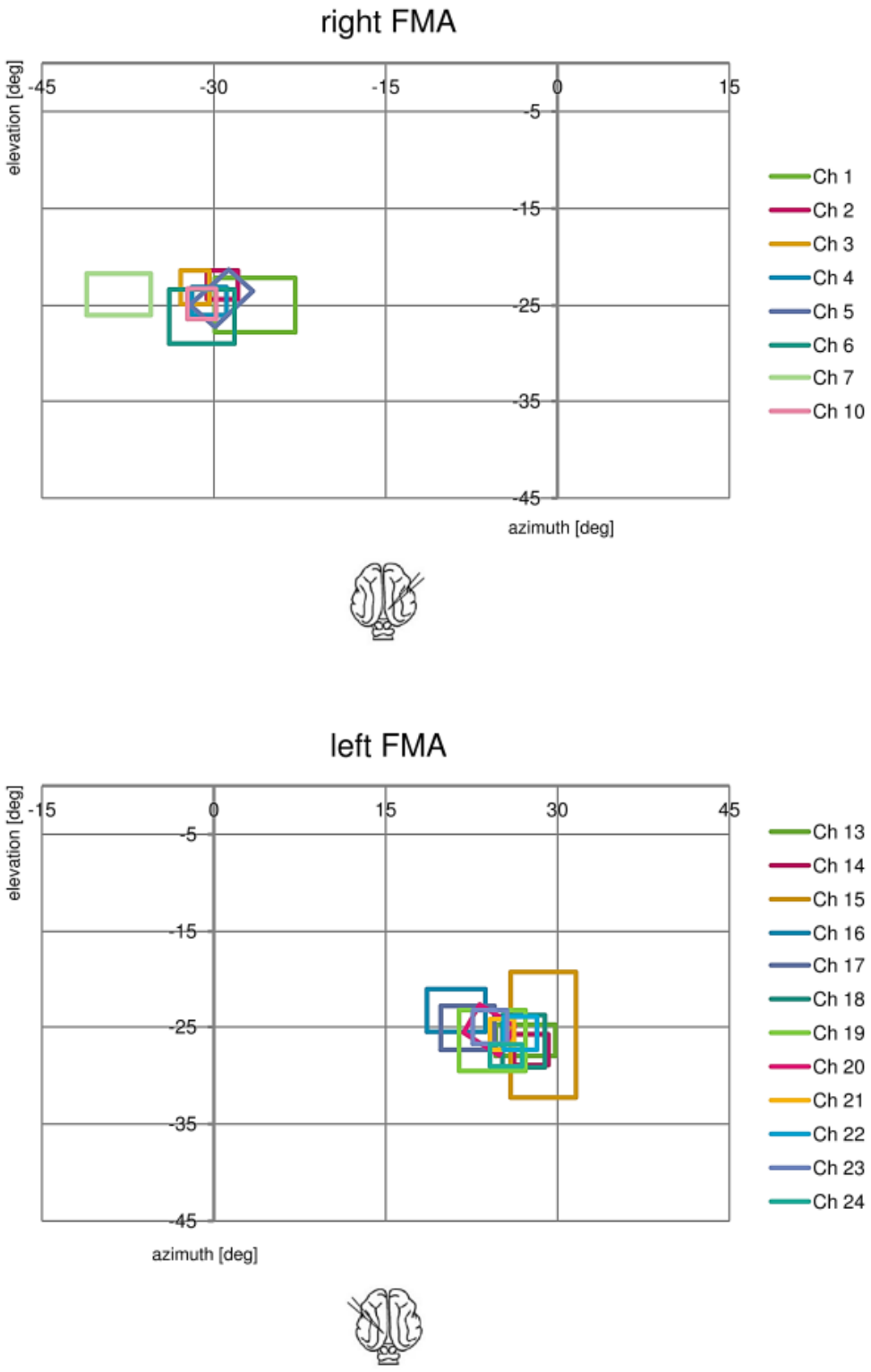

Figure 3.2: Receptive fields (RFs) of neurons recorded in area 18 of the right (upper panel) **and left** (lower panel) **hemisphere of cat R1.** The center of gaze (area centralis) is located at 0°. The orientation, width and length of the fields indicate the most effective stimulus orientation and distance. The RFs from the recorded neurons are all located in the contralateral lower visual field quadrant (elevation ≈ -25°). With one exception (channel 7), the RFs of the cells recorded on the right side show a considerable amount of overlap and cover a visual field area between an azimuth of -20 to -35 degrees. The RF of the neuron recorded on channel 7 is located more peripherally (azimuth = -37 - -41 degrees). The overlapping RFs of the cells recorded on the left hemisphere cover a range between an azimuth of 21 to 30 degrees. The largest RF was recorded on channel 15 (azimuth = 25 - 33°; elevation = -19 - -32°). Abbreviations: FMA, floating micro-electrode array.

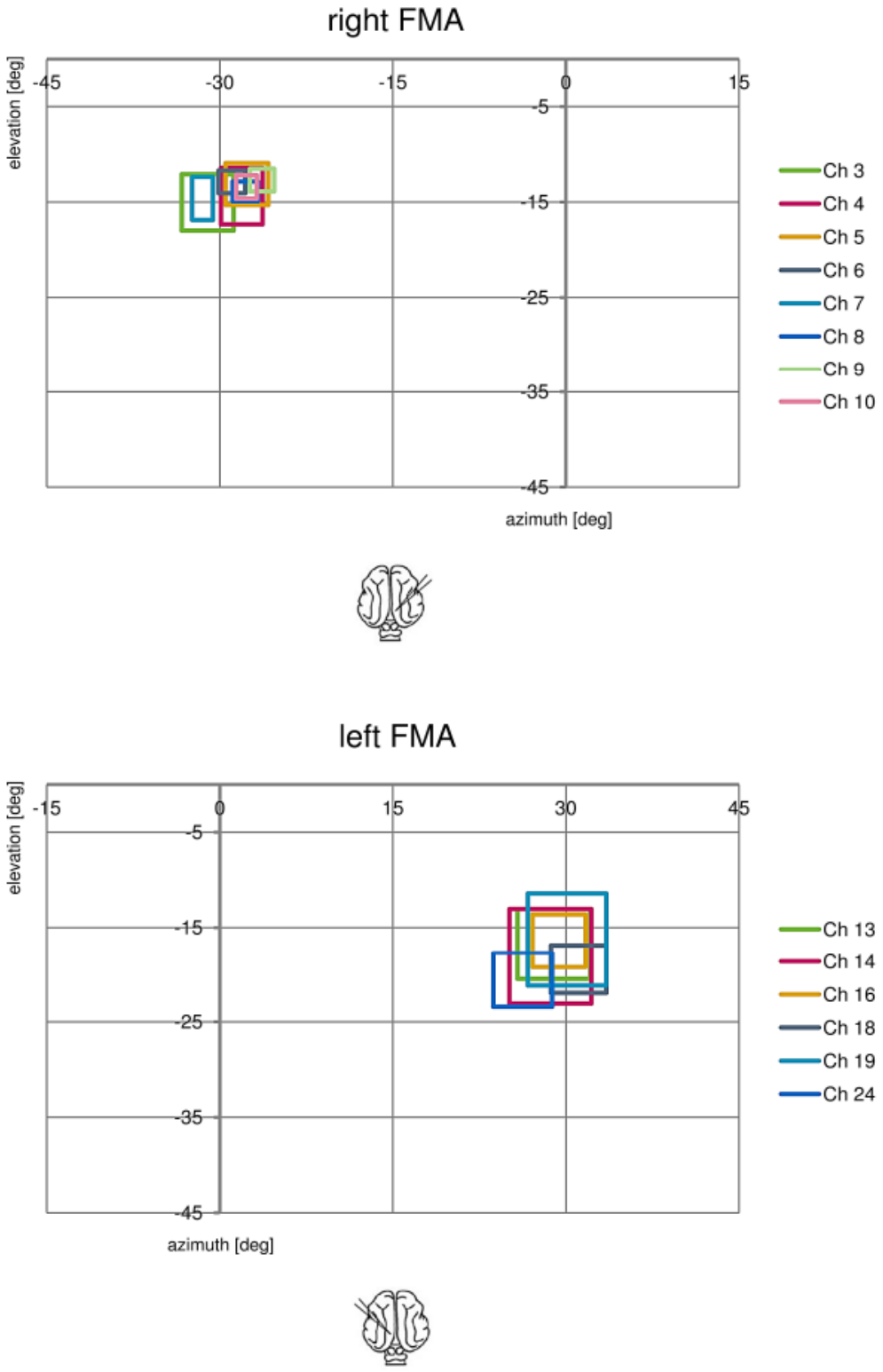

Figure 3.3: Receptive fields of neurons recorded in area 18 of the right (upper panel) **and left** (lower panel) **hemisphere of cat L1.** The center of gaze (area centralis) is located at 0°. The RFs from the recorded neurons in the right hemisphere were clustered around an elevation of -15° and an azimuth of -30°. By contrast, the recorded neuron population in the left primary visual cortex had bigger RFs, which were distributed around an elevation of -18° and an azimuth of 30°. Conventions and abbreviations as in Figure 3.2.

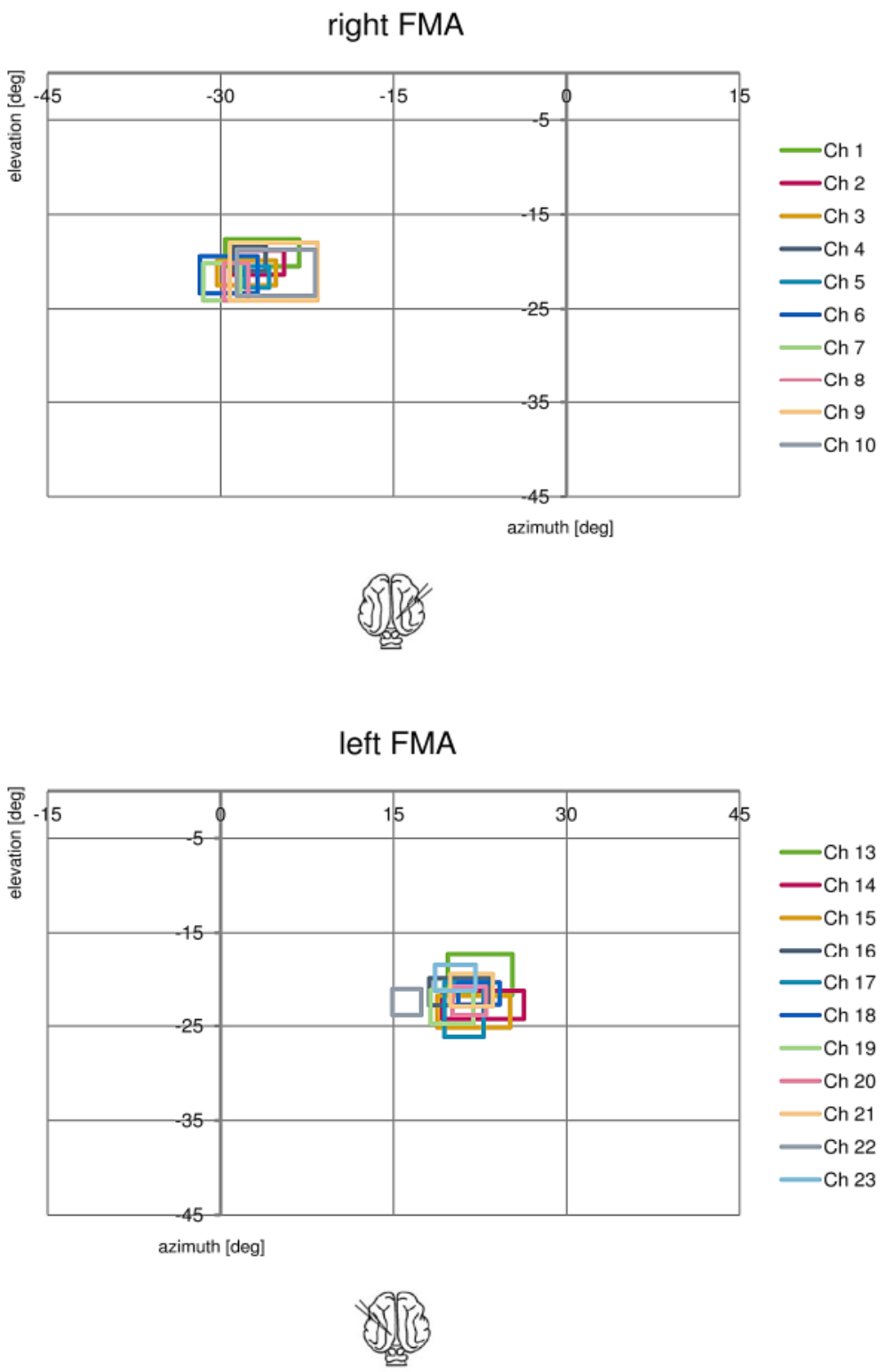

Figure 3.4: Receptive fields of neurons recorded in area 18 of the right (upper panel) **and left** (lower panel) **hemisphere of cat L2.** The center of gaze (area centralis) is located at 0°. The RFs of the cells recorded on the right side covered an area between -18° and -29° along the vertical axis and between -22° and -32° along the horizontal axis. The overlapping RFs of the cells recorded on the left hemisphere covered a range between 18° and 26° azimuth and showed roughly the same range along the vertical axis as the population recorded on the right hemisphere. Conventions and abbreviations as in Figure 3.2

3.1.4 PERI-STIMULUS-TIME HISTOGRAMS

To explore how the multi-unit activity (MUA) in response to both stimuli changed over time, peri-stimulus time histograms (PSTH) were computed. Since the RFs of the recorded neurons were clustered around an eccentricity of 15° to 30° in the contralesional visual hemifield, only spike responses elicited by these two target LED locations were considered.

The temporal pattern of spiking activity in response to both stimuli was not only highly variable within different recording channels but also within recording sessions, stimulus locations and hemispheres. In most cases, however, the onset of either LED induced a rate increase that was usually stronger in response to the target LED than in response to the fixation cue. Another conspicuous feature that frequently occurred on both hemispheres was a peak around 1.35 seconds prior to target LED onset that maybe related to eye movements. The PSTHs and raster plots of a pre-lesion recording session obtained from cat R1 are shown in figure 3.6 as a representative example.

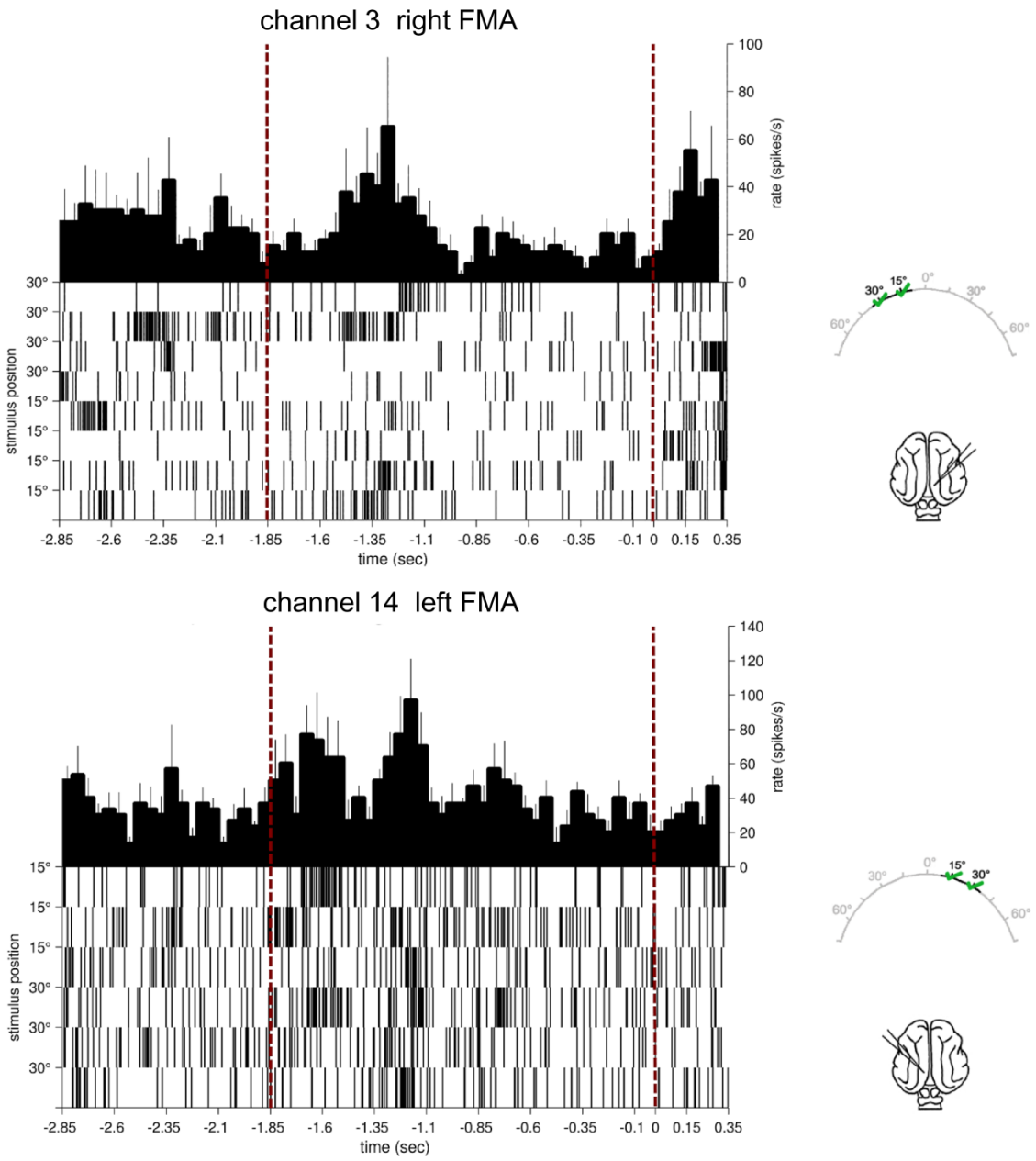

Figure 3.5 Examples of peri-stimulus time histograms (PSTHs) and corresponding single-trial responses of MUA during a pre-lesional recording session of cat R1. The upper panel indicates the spiking activity of neurons recorded on a single channel of the right FMA, the lower panel shows the signal recorded from a single channel of the left FMA (cat brain icon). Each panel indicates the multi-unit response to the presentation of the target LED at either the 15° or 30° location in the contralateral visual hemifield. The bottom portion of each panel shows the raster plots for each single trial and the top portion depicts the PSTH. Zero on the abscissa denotes the onset of the target LED. The first red dashed line marks the onset of the fixation cue, the second dashed line marks the onset of the target LED. The bin size of the PSTH is 1 ms. The upper panel shows a substantial spike rate increase in response to the target LED whereas the lower panel indicates a distinct increase in firing activity only in response to the fixation cue. In both PSTHs the conspicuous peak is visible around t = -1.35 s. Abbreviations: FMA, floating micro-electrode array.

3.2 BEHAVIORAL RESULTS

The behavioral performance of each cat on each recording day formed the basis for pooling the individual recordings sessions together to recording periods. This was mainly done to obtain a sufficient number of trials for each possible condition and was based on the assumption that behavioral changes are closely related to neuronal activity changes. The average performance of each cat during the recording periods is illustrated in Figure 3.6, Figure 3.7, and Figure 3.8. Post-lesion days are given below the recording periods. The lengths of the green lines in each polar plot show the percentage of correctly attended stimulus locations in the perimetry apparatus. The icons of the cat brain below the polar plots indicate the lesion site marked in black. Prior to the lesion, none of the cats reached a performance level above 50% for the 90 degree targets in either visual hemifield. Therefore, this target location was excluded from further analysis.

3.2.1 CAT R1

The cat R1 showed an excellent *pre-lesion* performance for nearly all stimulus locations except for the most peripheral positions at 90° in both visual hemifields (Figure 3.6 a). A unilateral lesion in the right pMS sulcus produced a decrease in performance for targets that lay in the contralesional visual hemifield. One exception was the performance for stimuli presented at the 15° position, which remained unaltered by the lesion (Figure 3.6 b). In the following post-lesion period (post-lesion 2) the cat recovered the ability to respond to stimuli that were located at 30 and 45 degrees in the contralesional hemifield. Simultaneously, the responsiveness to the ipsilesional target at 75° decreased substantially (Figure 3.6 c). In post-lesion 3 a high-level performance for all stimulus locations up to 60 degree in both visual hemifields was observed (Figure 3.6 d). The post-lesion periods 4 - 7 (Figure 3.6 e-h) described a corresponding response pattern with a reduced performance around or below 50% for the ipsilesional 75 degree position. R1 displayed a neglect for contralesional stimulus locations at 60 and 75 degree. Moreover, an increased number of accuracy error trials was observed in which the cat responded to a stimulus in the contralesional visual field, but incorrectly oriented to a target, which was typically displaced by 15°. In post-lesion 8 and 9 (Figure 3.6 i-j) a correct response to the ipsilesional target location at 75 degree was achieved with a performance level above 50%. In addition, the performance for the contralesional 45 degree position increased to 100% while a continuing profound neglect for the eccentricities at 60 and 75 degree in the contralesional hemifield was observed. Within the post-lesion periods 10

and 11 (Figure 3.6 k-l) an improvement in the perception of the contralesional 60 degree location to a performance level of ~ 50% occurred. In addition the responsiveness to the ipsilesional 75 degree position increased to 100% in post-lesion 11. Post-lesion periods 12 - 13 (Figure 3.6 m-o) described a proceeding capacity to respond to the contralesional 60 and 75 degree targets. Within post-lesion periods 15 and 16 (Figure 3.6 p-q) R1 fully recovered the contralesional visual hemifield. In the ipsilesional hemifield a slightly reduced performance for the 75 degree target was observed. In the final post-lesion periods 17 and 18 (Figure 3.6 r-s) the performance level for all eccentricities up to 75 degree in both visual hemifields was 100%.

In summary, R1 displayed a fast recovery within 3 days for the center-near 30 degree position. Although the same time range was needed to recover the 45 degree target the performance level in the early phase of recovery was reduced to 80% when compared to pre-lesion level (100%) . This performance reduction lasted until post-lesion 8. A reliable (>50% in at least 2 consecutive post-lesion periods) detection and localisation of the peripheral 60 degree started on the 34th postlesional day (post-lesion 10). The pre-lesional performance level of 100% was reached in the late post-lesion period 16. A similar pattern of performance but with a later recovery onset was observed for the contralesional 75 degree target. A correct localization above chance (>50%) started in post-lesion 12 and proceeded until post-lesion 16. In post-lesion periods 17 and 18 the performance of 100% exceeded the pre-lesion performance (90%). Surprisingly the performance for the ipsilesional 60 and 75 degree positions decreased after the lesion. This was particularly true for the most peripheral position at 75 degree.

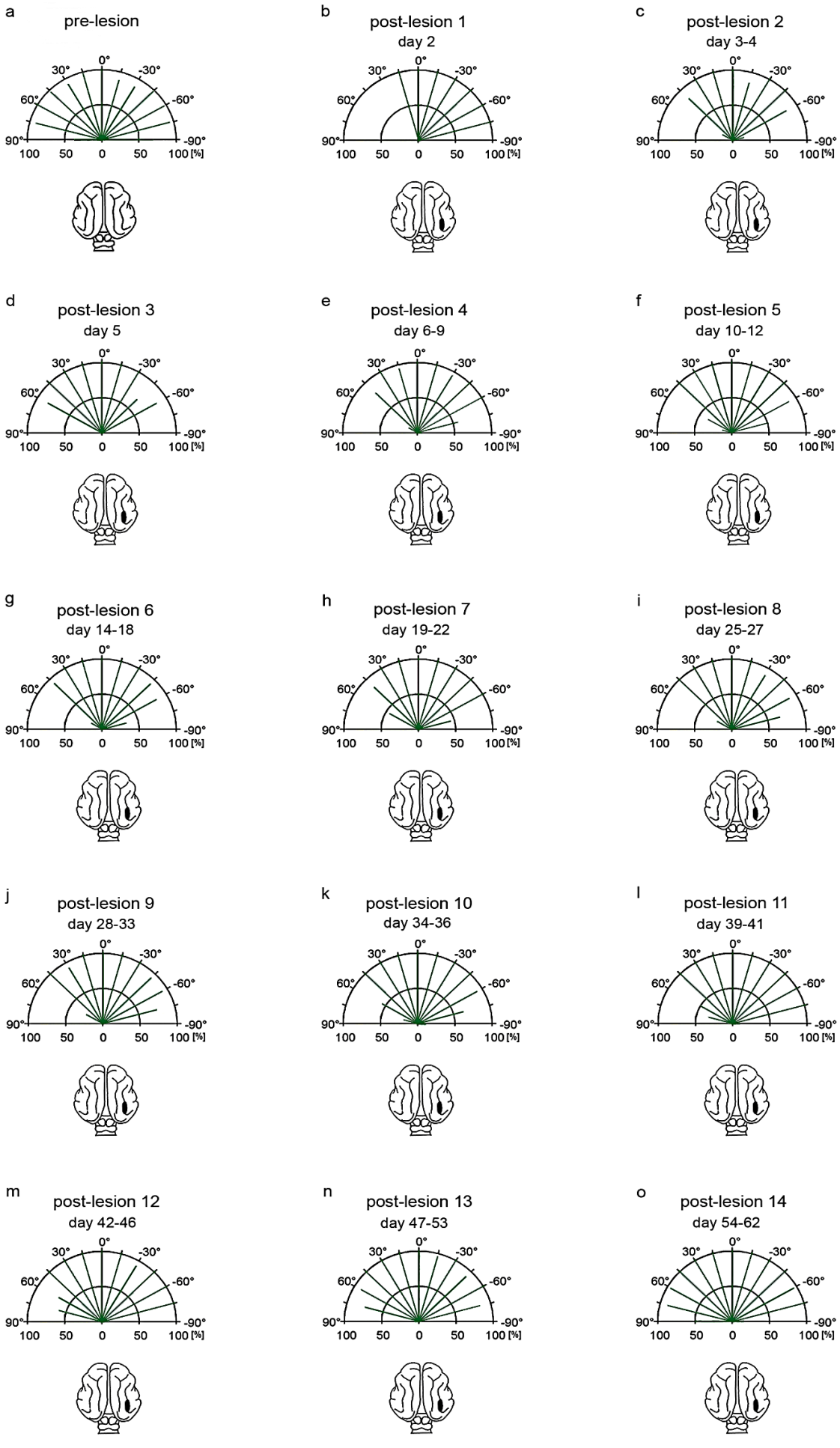
a
pre-lesion
b
post-lesion 1
day 2
c
post-lesion 2
day 3-4
d
post-lesion 3
day 5
e
post-lesion 4
day 6-9
f
post-lesion 5
day 10-12
g
post-lesion 6
day 14-18
h
post-lesion 7
day 19-22
i
post-lesion 8
day 25-27
j
post-lesion 9
day 28-33
k
post-lesion 10
day 34-36
l
post-lesion 11
day 39-41
m
post-lesion 12
day 42-46
n
post-lesion 13
day 47-53
o
post-lesion 14
day 54-62
0°
30°
-30°
60°
-60°
90°
-90°
100 50 0 50 100 [%]

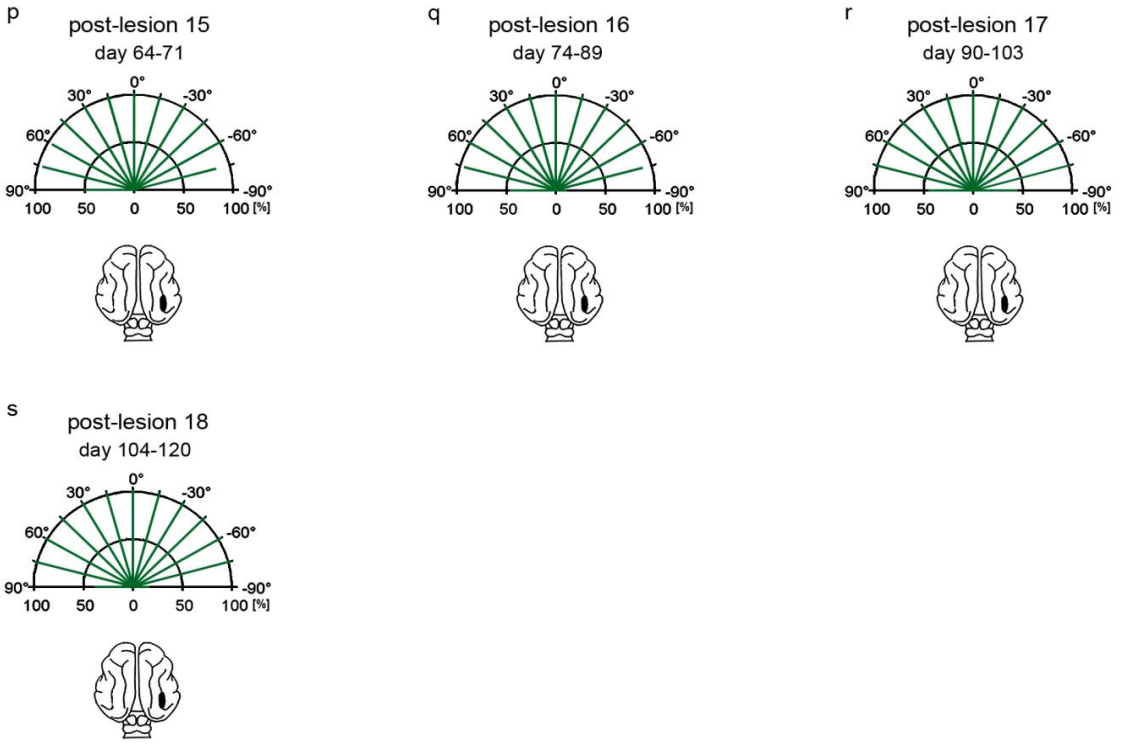

Figure 3.6 Behavioral performance of cat R1 before and after a lesion in the right pMS cortex. Note the long time period that was needed to recover the peripheral positions at 60° and 75°. The length of the green lines indicates the correct responses in percent for each eccentricity in the perimetry apparatus. Specified above each plot are the name of the recording period and the post-lesion days included therein. Below each polar plot is an icon of the cat brain where the lesion site is depicted in black. n = number of trials.
(a) pre-lesion: n = 276 in 7 recording sessions (rs); (b) pl 1: n = 21 in 1 rs; (c) pl 2: n = 78 in 2 rs; (d) pl 3: n = 78 in 1 rs; (e) pl 4: n = 156 in 3 rs; (f) pl 5: n = 105 in 2 rs; (g) pl 6: n = 156 in 3 rs; (h) pl 7: n = 117 in 3 rs; (i) pl 8: n = 118 in 3 rs; (j) pl 9: n = 156 in 3 rs; (k) pl 10: n = 143 in 3 rs; (l) pl 11: n = 156 in 3 rs; (m) pl 12: n = 159 in 3 rs; (n) pl 13: n = 263 in 5 rs; (o) pl 14: n = 261 in 5 rs; (p) pl 15: n = 183 in 5 rs; (q) pl 16: n = 261 in 10 rs; (r) pl 17: n = 221 in 9 rs; (s) pl 18: n = 197 in 9 rs; pl, post-lesion.

3.2.2 CAT L1

In the pre-lesion recording period cat L1 displayed a high-level performance only for near-center stimulus locations (Figure 3.7 a). Both peripheral eccentricities at 60 and 75 degree in both visual hemifields were attended in less than 50% of the trials. In comparison L1 exhibited a slightly better performance for targets that were presented in the right visual hemifield. The lesion in the left pMS-cortex induced a profound neglect for the entire contralesional hemifield (Figure 3.7 b). In addition, the performance for both peripheral and the 45 degree target locations in the ipsilesional hemifield decreased, while the responsiveness to the 15 degree target increased to 100%. In the second post-lesion period a low-level performance (~35%) for the contralesional near-center 15 degree position marked the onset of a restoration of behavior (Figure 3.7 c). In comparison with post-lesion 1, the responsiveness to ipsilesional targets remained almost unchanged. The third post-lesion phase indicated a continued functional restitution of near-center target locations; 15, 30 and 45 degree to a performance level above 50% (Figure 3.7 d). Additionally, the responsiveness to the equivalent stimulus locations in the ipsilesional hemifield was also raised to a level above 50%. In post-lesion 4 L1 displayed a further increase in behavioral performance for the entire visual field with the highest rate of correct trials for the center-near stimulus locations (Figure 3.7 e). In the consecutive post-lesion period (post-lesion 5) the responsiveness to all eccentricities was equal to or greater than 90% (Figure 3.7 f). A similar high-level performance was observed for the post-lesion periods 6 – 8 with the exception of the ipsilesional 75° target where the performance was reduced to ~55% (Figure 3.7 g-i).

The total duration of the lesion-induced neglect of the entire contralesional hemifield amounted to 10 days. During this time, the cat produced a large number of accuracy errors. Additionally, in comparison to the pre-lesion period, the behavioral responsiveness to the ipsilesional 45° target decreased. L1 recovered to pre-lesion performance within 11 to 16 days. Starting with post-lesion period 4, the behavioral performance exceeded the pre-lesion performance in all subsequent periods. A comparison of the two hemifields in the last three post-lesion periods revealed an improved capacity to detect and localize the contralesional 75° target.

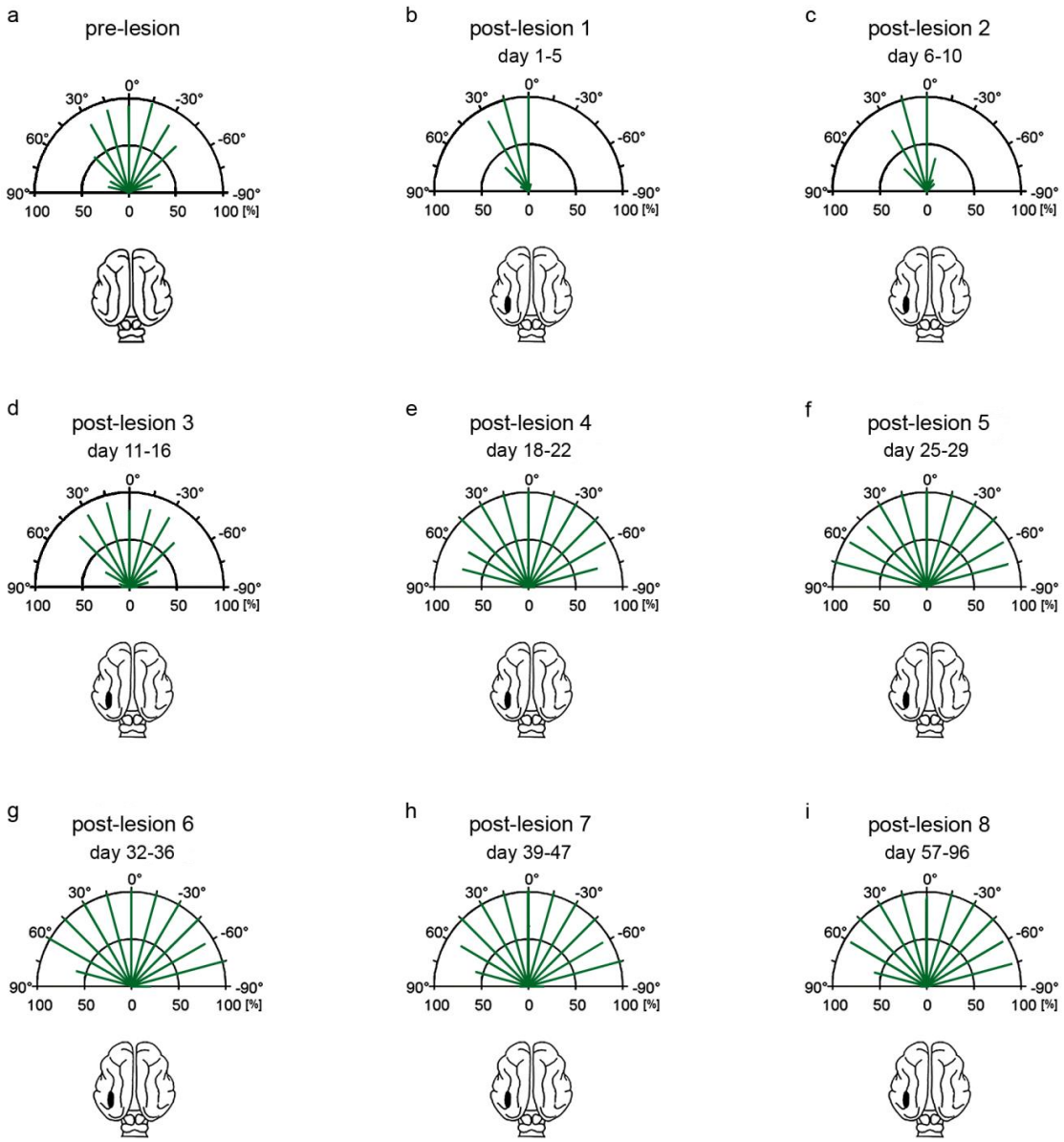

Figure 3.7 Behavioral performance of cat L1 before and after a lesion in the left pMS cortex. Note the performance improvement due to continuous training after the complete restoration of function. Conventions as in Figure 3.6.
(a) pre-lesion: n = 514 in 9 recording sessions (rs); (b) pl 1: n = 260 in 5 rs; (c) pl 2: n = 247 in 5 rs; (d) pl 3: n = 286 in 6 rs; (e) pl 4: n = 183 in 5 rs; (f) pl 5: n = 169 in 5 rs; (g) pl 6: n = 131 in 5 rs; (h) pl 7: n = 162 in 6 rs; (i) pl 8: n = 182 in 7 rs; pl, post-lesion.

3.2.3 CAT L2

Prior to the lesion cat L2 achieved a high-level performance to all eccentricities in the entire visual field (Figure 3.8 a). The responsiveness to targets that were presented in the left visual hemifield was slightly enhanced compared to right visual hemifield responsiveness. A lesion in the left pMS-cortex did produce a lasting incapacity to detect and localize contralesional targets (Figure 3.8 b-i). This long-term impairment applied solely to the responsiveness to static stimuli. When the capacity to respond to moving stimuli was tested with a laser pointer, a recovery of function for the center-near contralesional hemifield was observed after two days. After another two days, L2 recovered the capacity to respond to moving targets in the peripheral contralesional field.

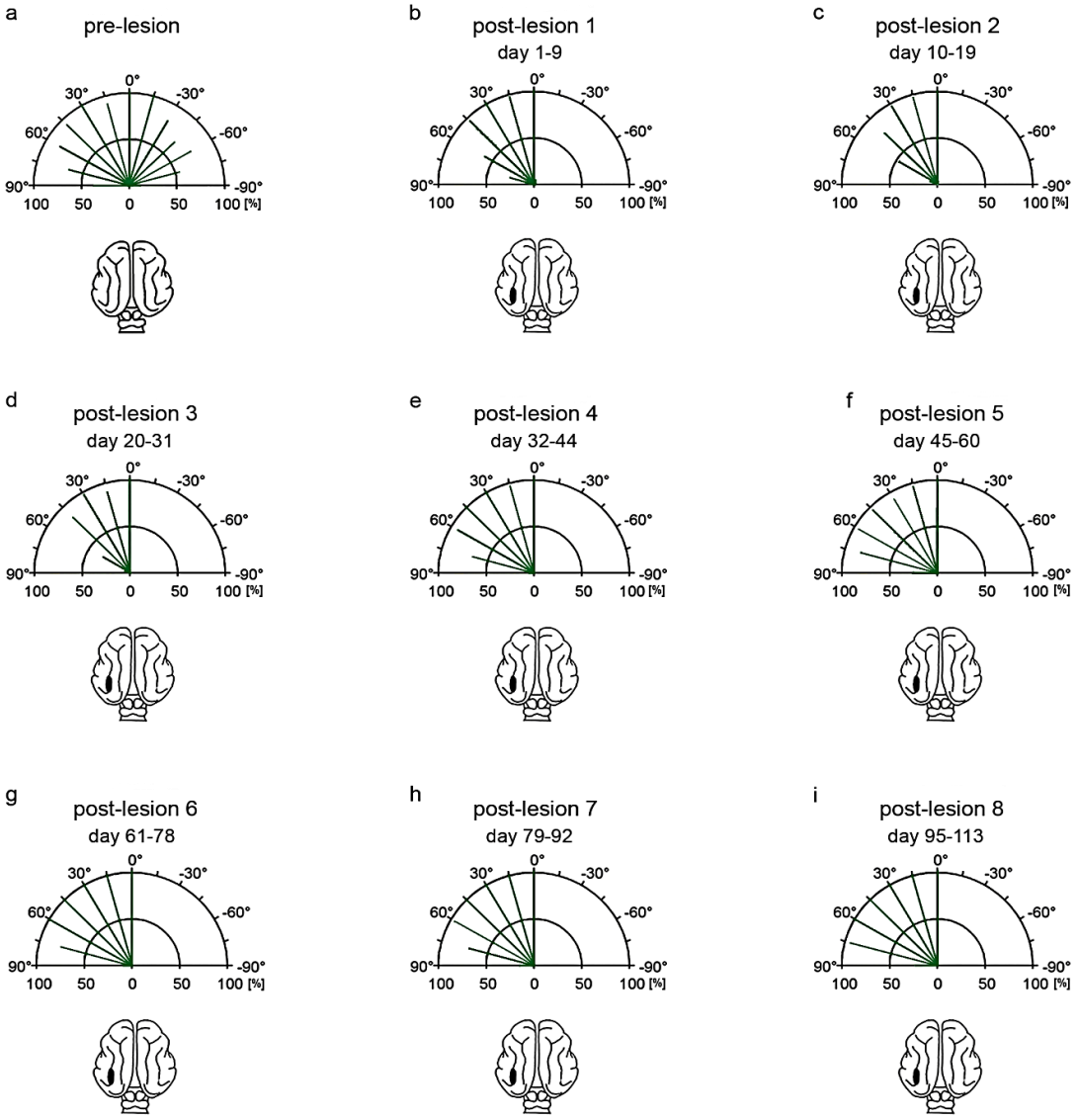

Figure 3.8 Behavioral performance of cat L2 before and after a lesion in the left pMS cortex. The lesion induced a permanent inability to detect and localize static stimuli in the contralesional visual hemifield. Same conventions as in Figure 3.6.
(a) pre-lesion: n = 115 in 7 recording sessions (rs); (b) pl 1: n = 560 in 9 rs; (c) pl 2: n = 468 in 10 rs; (d) pl 3: n = 521 in 10 rs; (e) pl 4: n = 494 in 10 rs; (f) pl 5: n = 313 in 9 rs; (g) pl 6: n = 275 in 10 rs; (h) pl 7: n = 197 in 9 rs; (i) pl 8: n = 184 in 9 rs; pl, post-lesion.

3.3 HISTOLOGY

3.3.1 MORPHOLOGICAL CHANGES

Subsequent to the electrophysiological study, the brains of the three cats were studied histologically. The size, extent and morphology of the lesioned area were evaluated. Furthermore, the primary visual cortex was examined for possible damage, caused by the implantation of the FMAs.

Already at the macroscopic level it was possible to recognize, that the lesioned pMS sulcus was significantly widened compared to the intact pMS sulcus. The Nissl-stained material revealed that degenerated neurons, a generally low neuronal density and an almost complete loss of pyramidal and granular cells (Figure 3.9 A) characterized the lesion site. Often the gray matter appeared perforated and displayed a pronounced gliosis. In the Gallyas myelin stained sections degenerated axons within the lesioned area were clearly visible (Figure 3.10 A). Furthermore, when compared to the intact pMS sulcus, the lesioned region showed differences in the structure and the amount of fibers (Figure 3.10 A, B). Lesion induced changes in the LGN could not be observed in any of the three cats, also area 17, 18 and 19 appeared unaffected by the lesion in pMS cortex.

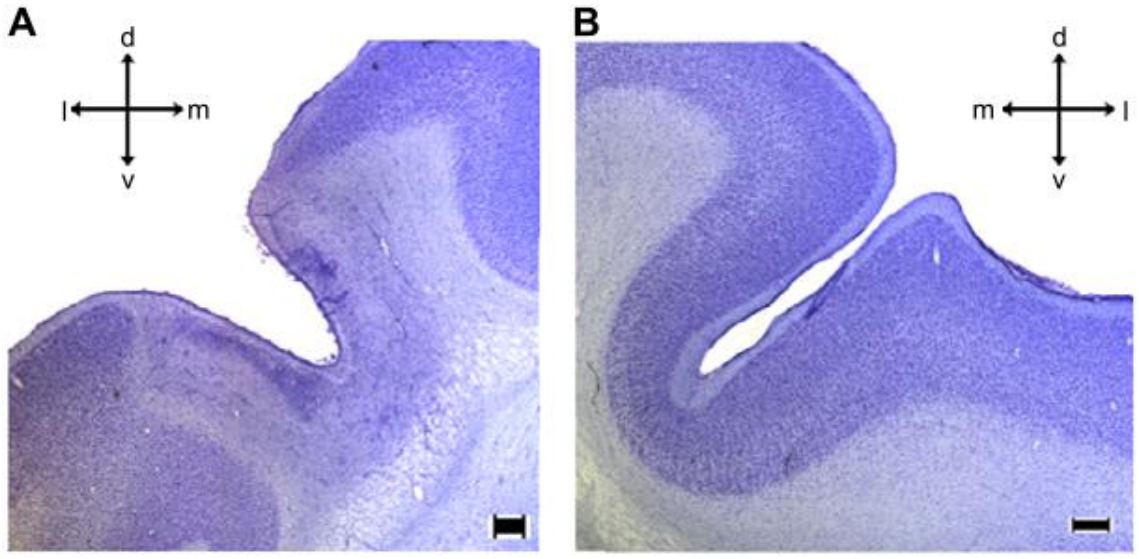

Figure 3.9 Nissl-stained coronal sections of the posterior medial suprasylvian sulcus (pMSS) from cat L2. (A) Left lesioned pMS sulcus from cat L2 (section 150). The ibotenic acid lesion caused significant morphological changes **(B)** Right intact pMS sulcus from cat L2 (section 150). Scale bar: 1mm. Abbreviations: d: dorsal; l: lateral; m: medial; v: ventral;

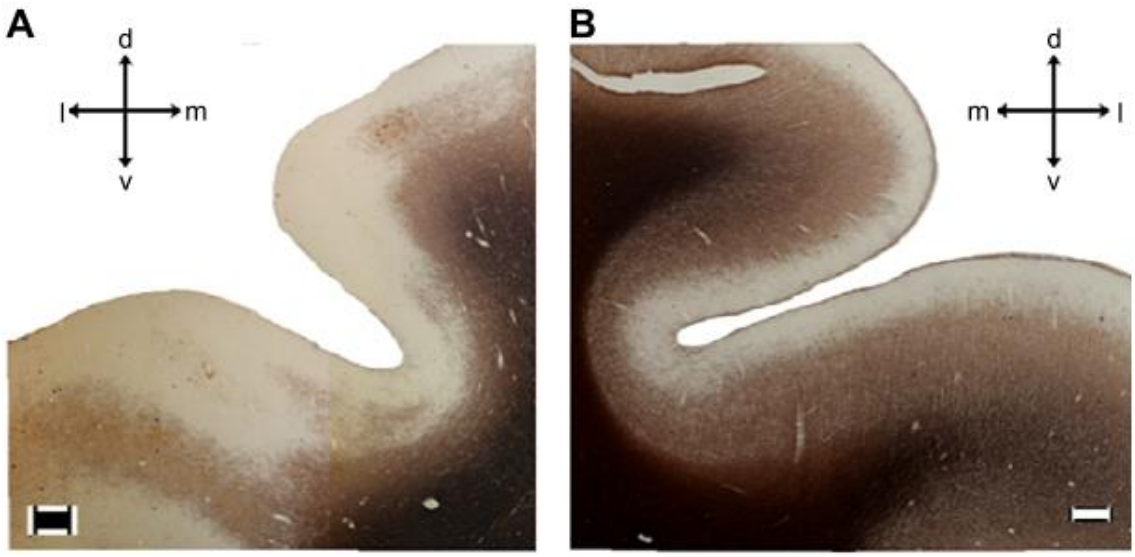

Figure 3.10 Coronal sections of the posterior medial suprasylvian sulcus (pMSS) from cat L1 stained with the Gallyas silver impregnation of myelin. (A) Left lesioned pMS sulcus from cat L1 (section 155). Within the lesioned area, the axons were degenerated. **(B)** Right intact pMS sulcus from cat L1 (section 155). Scale bar: 1mm. Abbreviations: d: dorsal; l: lateral; m: medial; v: ventral;

3.3.2 LESION RECONSTRUCTIONS

By using the NeuroLucida (MBF Bioscience) software, the cortical areas damaged by the ibotenic acid injections were reconstructed from Nissl-stained sections.

The reconstruction of the lesion in cat R1 showed that the damaged area was limited to the middle suprasylvian sulcus of the right hemisphere (Figure 3.11). The ibotenic acid affected no additional brain regions. Based on the section thickness (60 µm) and the number of sections that indicated the lesion, an approximate posterior to anterior lesion length of 9 mm was estimated. In addition, the lesion surface in μm^2 was determined on each section and used to estimate the volume of the lesion. The lesion volume of cat R1 was approximately 73.02 mm^3.

In cat L1, the diffusion of ibotenic acid caused additional damage in parts of the ipsilesional splenial sulcus, the lateral sulcus and the posterior suprasylvian sulcus (Figure 3.12). The estimated lesion length from posterior to anterior was 9.6 mm and the approximate lesion volume was 138.32 mm^3.

In cat L2 the lesion was, as in cat R1, limited to the middle suprasylvian sulcus (Figure 3.13). However, L2 displayed with 10.2 mm the largest posterior to anterior extension. The calculated lesion volume was 63.13 mm^3. Table 3.2 shows the lesion dimensions of all three cats.

Table 3.2 Lesion dimensions of all three cats. The largest posterior to anterior expansion of the lesion and the largest lesion volume are highlighted.

	Cat R1	**Cat L1**	**Cat L2**
Location of lesion	in right pMS cortex	in left pMS cortex	in left pMS cortex
Behavioral outcome	functional recovery	functional recovery	no functional recovery
Length (posterior to anterior)	9.0 mm	9.6 mm	**10.2 mm**
Volume	73.02 mm^3	**138.32 mm^3**	63.13 mm^3

3.3.3 TISSUE DAMAGE CAUSED BY THE ELECTRODE IMPLANTATION

In all three cats, minimal tissue damage through the FMAs was evident. The deterioration was mainly located medial to the lateral sulcus and related to the first cortical layer.

As part of the FMA implantation, a small silver plate was attached to the contralesional suprasylvian sulcus as a reference electrode. In cat L1 the reference silver plate was not applied, as in cats L2 and R1 on the surface of the sulcus, but inserted into it. This resulted in additional damage in the contralesional pMS sulcus of cat L1. However, the damage was limited to the first two cortical layers.

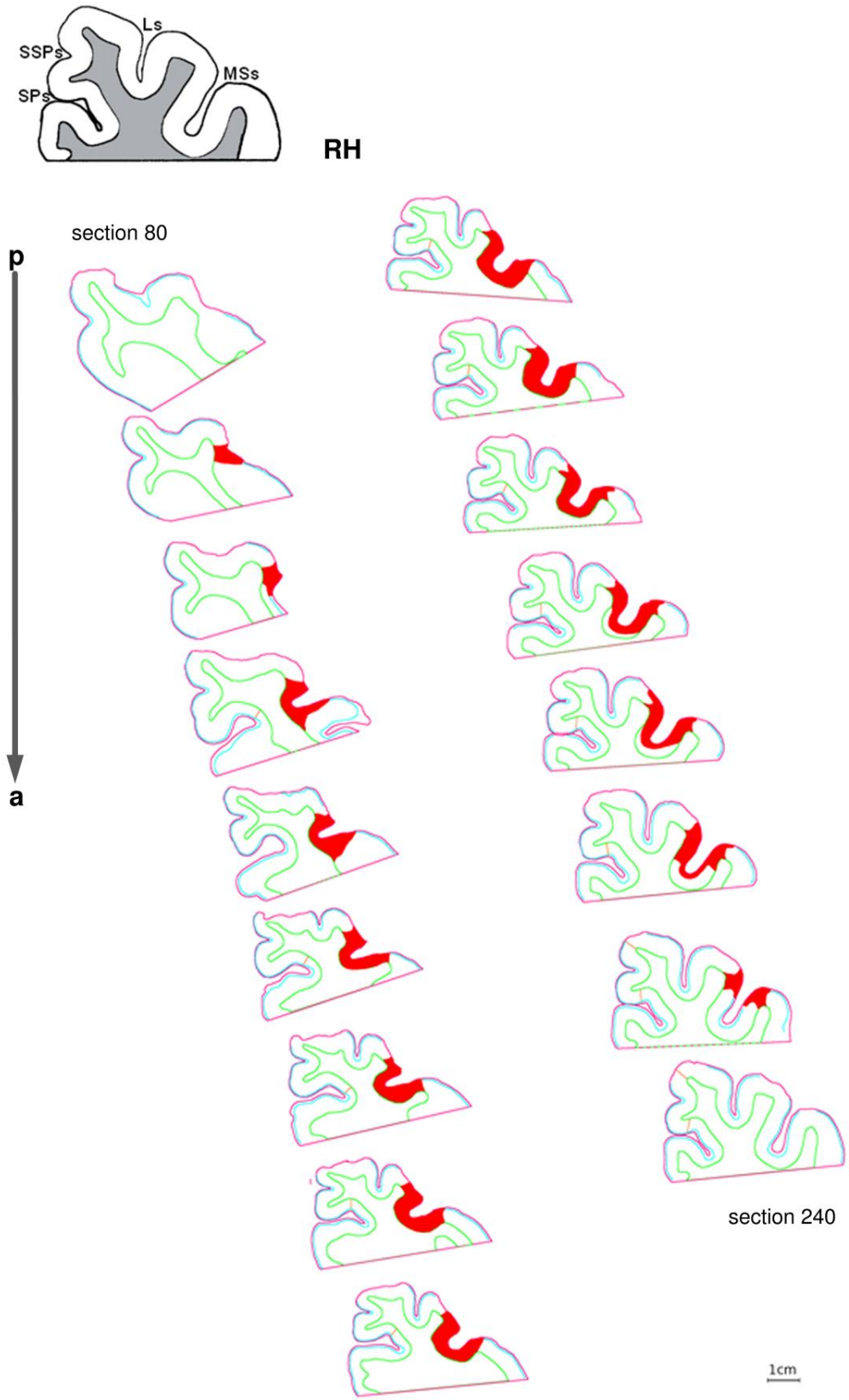

Figure 3.11 Lesion reconstructions of cat R1. With NeuroLucida reconstructed contours of coronal sections 80 to 240 of the right hemisphere with a lesion in the middle suprasylvian sulcus (red shading). In cat R1, the lesion is limited to the MS sulcus, presumably to the areas PMLS and PLLS. The green line defines the boundary between the white and grey matter and the blue line outlines the first cortical layer. Cortical sulci of interest are labeled in the schematic section above. a, anterior; p, posterior; Ls, lateral sulcus; SSPs, suprasplenial sulcus; SPs, splenial sulcus; MSs, middle suprasylvian sulcus; RH, right hemisphere. Scale bar = 1 cm

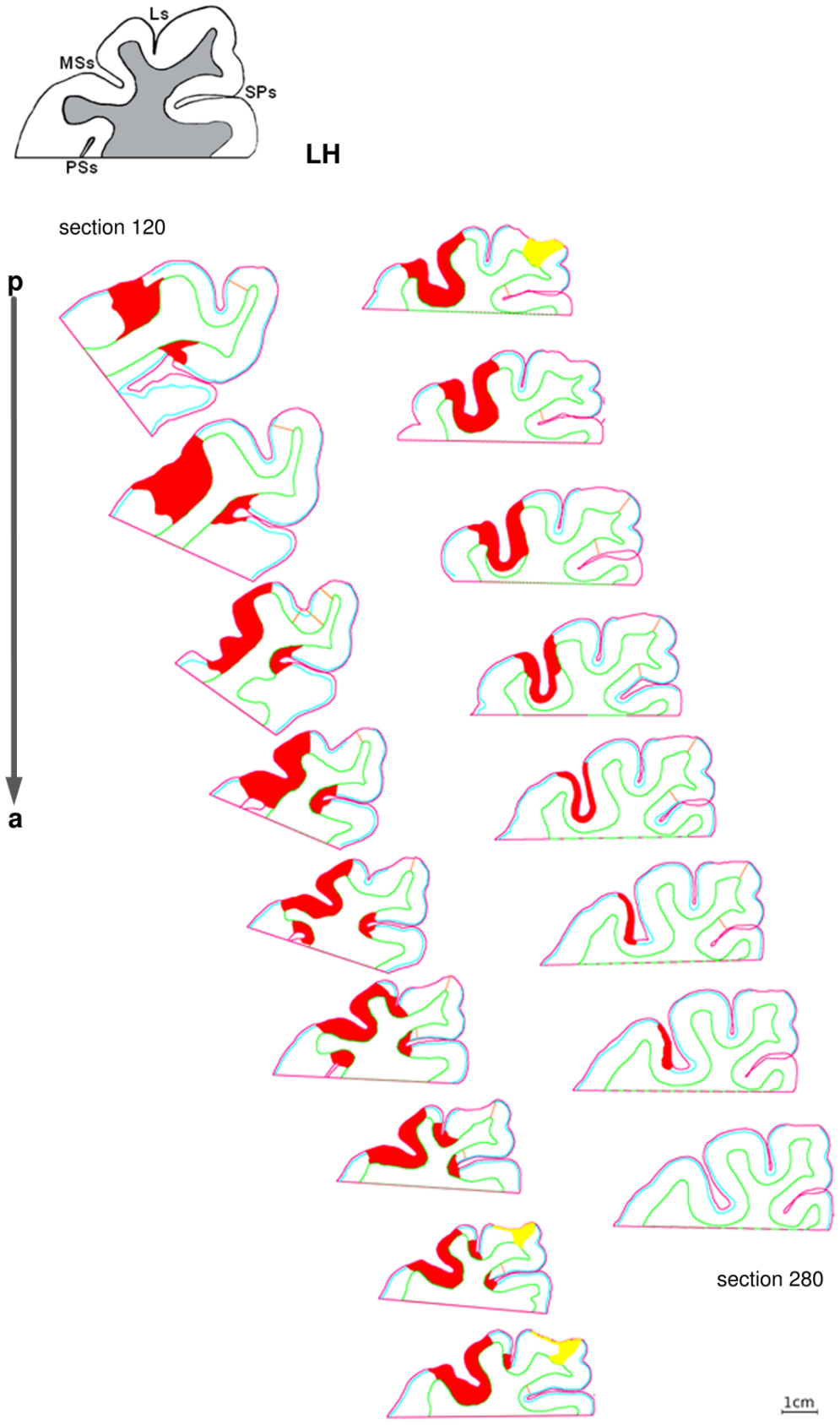

Figure 3.12 Lesion reconstructions of cat L1. Coronal reconstructions of the sections 120 to 280 from the left hemisphere. The red shaded areas indicate zones of cortical damage caused by the ibotenic acid. An encroachment of the lesion into the fundi of the splenial sulcus, the lateral sulcus and the posterior suprasylvian sulcus was observed. The yellow shaded regions mark additional cortical damage that was not caused by the ibotenic acid. Conventions and abbreviations as in Figure 3.11. LH, left hemisphere. Scale bar = 1 cm

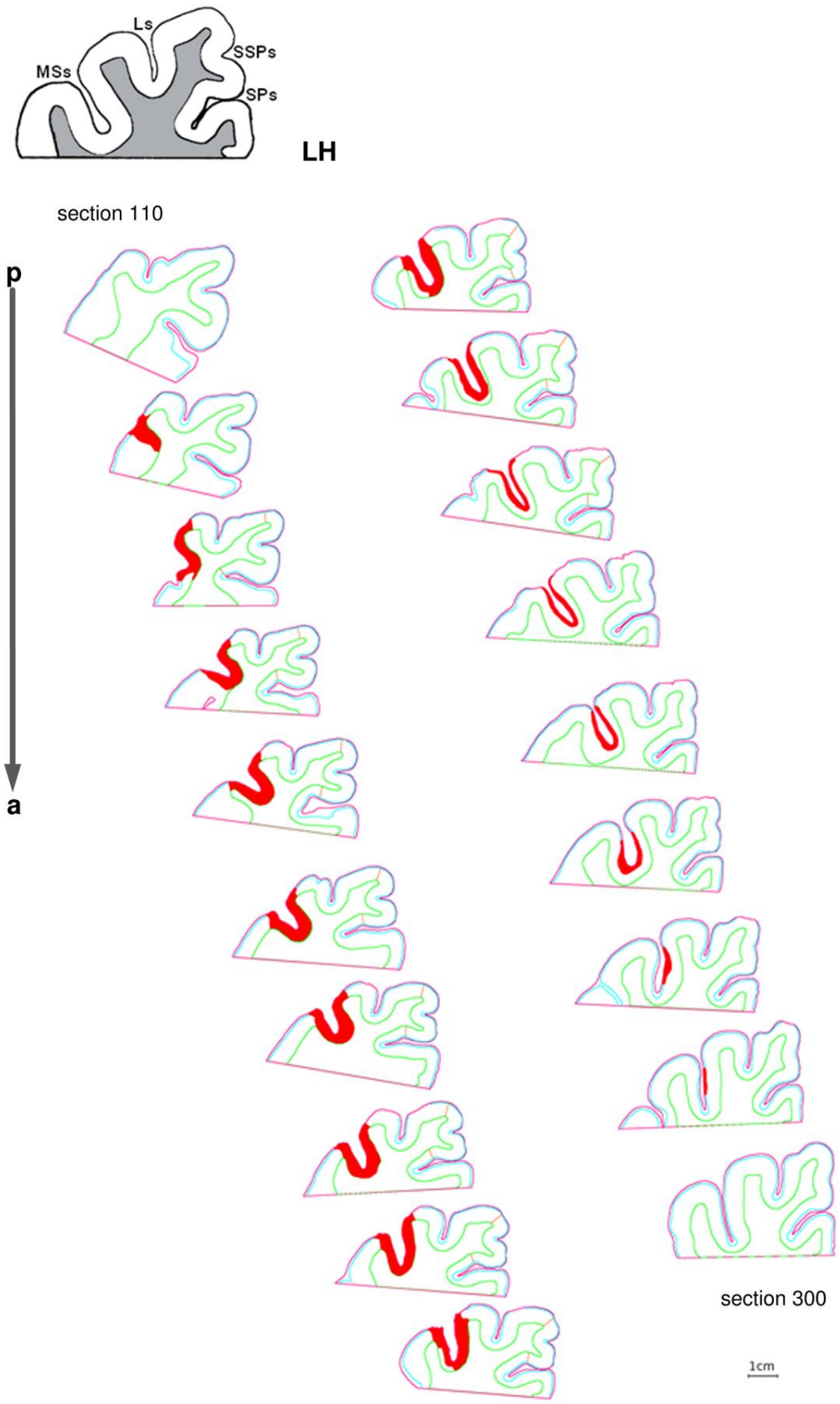

Figure 3.13 Lesion reconstructions of cat L2. Contours of the coronal sections 110 to 300 from the left hemisphere with a lesion in the middle suprasylvian sulcus (red shading). As in cat R1, the extent of the lesion is limited to the MS sulcus. Conventions and abbreviations as in Figure 3.11 andFigure 3.12. Scale bar = 1 cm

3.4 ANALYSIS OF THE NEURONAL ACTIVITY DURING THE POST-LESION PERIOD

3.4.1 THE NEGLECT SITUATION

To gain insight into the neuronal processes that take place when the cat neglects the target stimulus, a detailed analysis of the neglect condition was performed.

The most striking result of this analysis was an explicit and full suppression of a late component of the overall response to the target stimulus, hereafter referred to as the response signature.

3.4.1.1 *Analysis of local field potentials*

A comparison of the rasterized LFP between trials where the target stimulus was (1) attended-to and trials where it was (2) neglected, revealed that the typical change in LFP amplitude in response to the 2nd LED occurred only in correctly performed trials. If the target stimulus was neglected, no changes in LFP amplitude were observed. In both conditions (correct and neglect) the response profile for the fixation stimulus, with a negative peak around 175 ms after LED onset, remained unchanged. Figure 3.14 shows representative examples from cat L2 of the rasterized LFP results for either correctly performed or neglected trials.

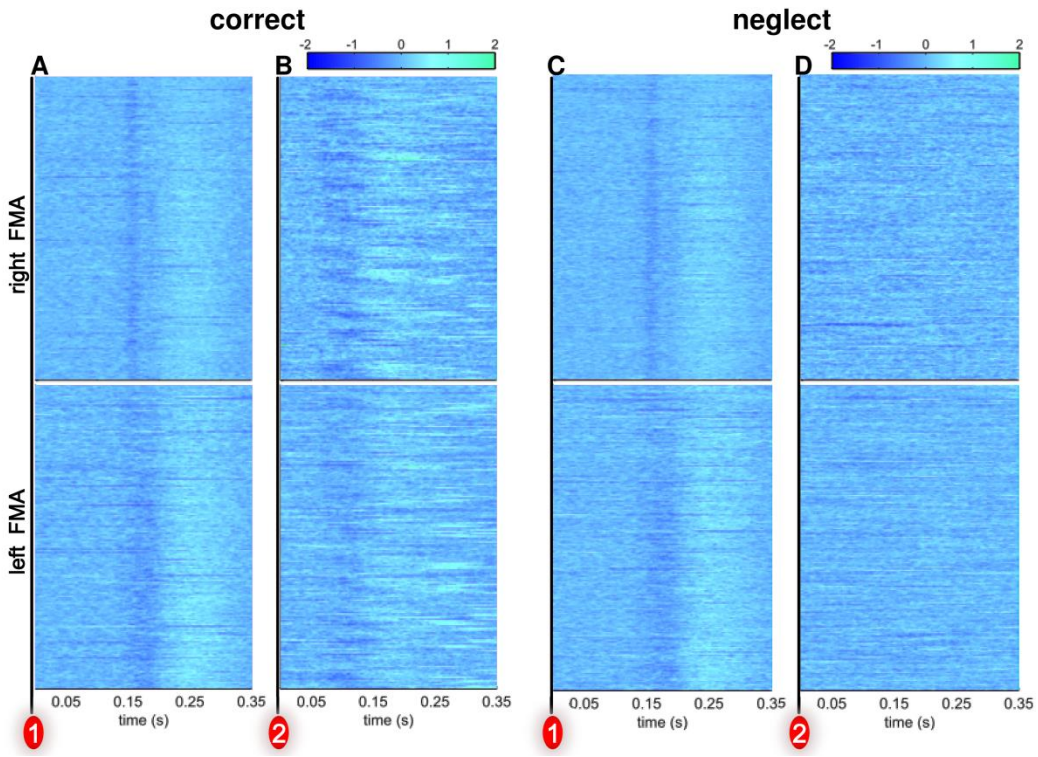

Figure 3.14 Rasterized post-lesional LFP results from cat L2. Shown is the post-lesion period 3. **(A, C)** LFP changes in response to the fixation LED. The 1st LED evoked a distinct negative peak at circa 175 ms followed by a positive peak at ~ 200 ms after LED onset. **(B)** When the target stimulus was attended to, the typical response pattern was evoked. **(D)** No changes in LFP amplitude were observed for neglected targets. correct trials n = 173; neglected trials n = 205.

3.4.1.2 *Spectral analysis of neuronal activity during neglect*

A spectral analysis of ipsilesionally recorded signals in response to stimuli that were presented in the contralesional hemifield was performed. For this stimulus condition, two behavioral outcomes were possible: (1) The cat neglected the target LED or (2) the cat correctly attended to the target stimulus. The neglect behavioral condition was more likely to occur in the first days after the pMS lesion. In order to rule out possible training-induced effects on neuronal activity, only target locations for which the cat exhibited a pre-lesion performance level above 75 % were considered. Therefore, the correct responses only included recovered targets. Additionally, the spectral profiles of 'catch' trials, in which the target stimulus was absent, were also presented. Here, only 'catch' trials of post-lesion periods were selected in which the overall performance level did not exceeded the pre-lesion performance level. The spectrograms show an average over all electrodes from the ipsilesional FMA and over all post-lesion periods. The normalization was done by subtraction of 'catch' trials (trials without the second LED stimulus). For each condition the evoked as well as the induced activity was calculated.

Cat R1

Figure 3.15 shows cat R1 time-frequency (TF) plots of the three behavioral conditions (neglect, correct, and catch). The time axis ranges from 200 ms prior to stimulus presentation up to 250 ms post 2nd LED onset. In cat R1 the spectral analysis of neglected targets revealed moderate alterations in low frequency signal power (Figure 3.15 A). Neglect resulted in a slight power increase for frequencies below 10 Hz that started circa 100 ms after stimulus onset. For comparison, when the target LED was attended to correctly, a gradual increase in power in the frequency range of 0 -18 Hz, started approximately 20 ms after the target LED onset. The 'catch' condition did not show any changes in signal power over the time course. The time- frequency calculations containing induced activity are shown in the lower plot row (Fig. 3.15 B). In general, the induced activity displayed a high amount of power in the frequency range up to 45 Hz. When the cat correctly attended to the target LED, an increase in low frequency power (< 18 Hz), linked to stimulus onset, could be observed. Trials in which the stimulus was neglected resulted in an enhancement of low frequency oscillations in the range of up to 8 Hz.

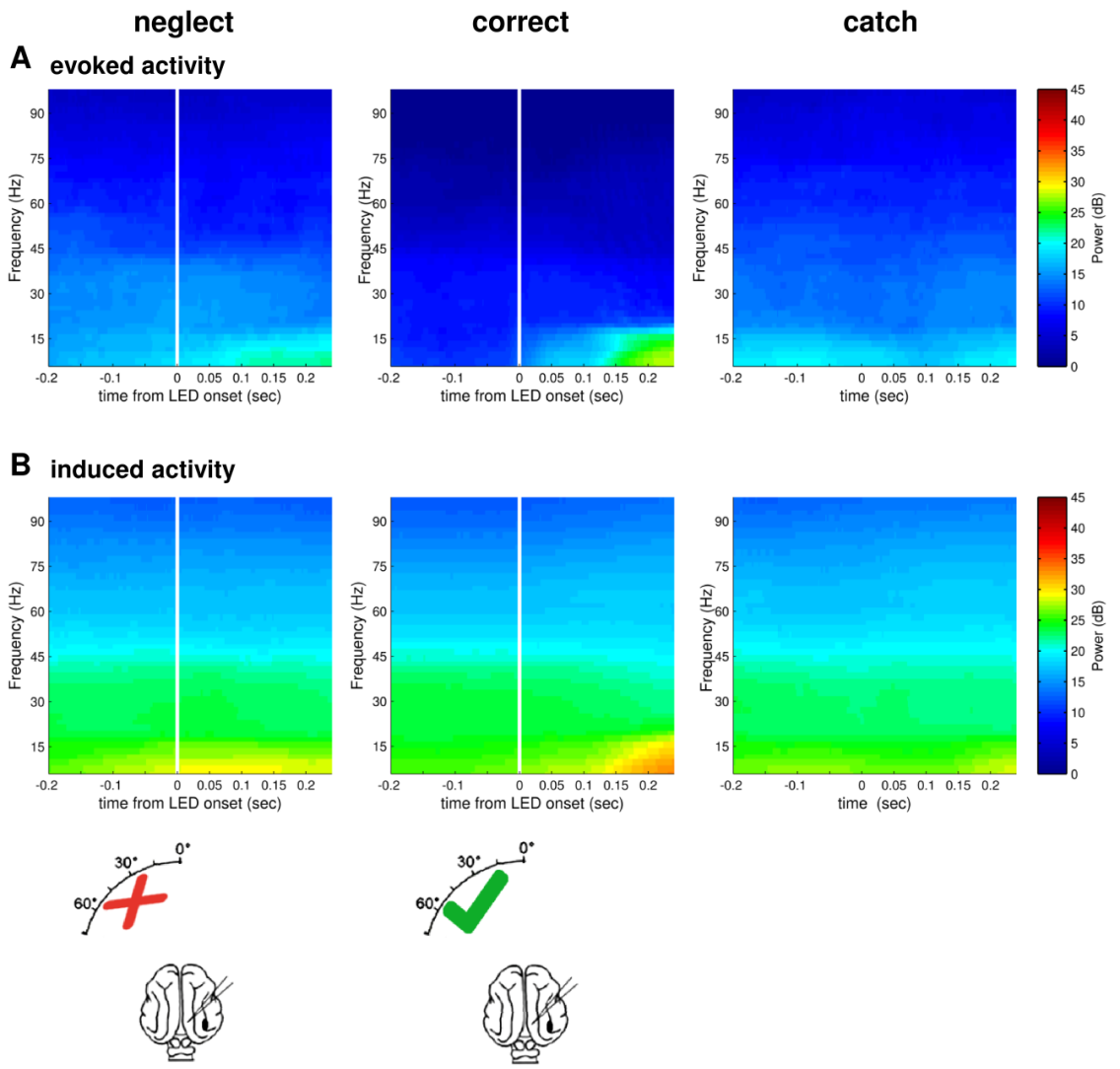

Figure 3.15 Spectral analysis of the LFP recorded from ipsilesional area 18. The cat R1 either neglected (left column) or correctly attended to (middle column) stimuli that were presented in the contralesional hemifield (see pictogram). The right column shows the spectral decomposition for 'catch' trials, where the target LED was absent. Spectrograms color-code for the relative signal power in decibel. The lesion was located in the right pMS cortex (depicted in black in the cat brain icons below). The vertical white line indicates the onset of the target LED. **(A)** Evoked activity for neglected stimuli (left spectrogram) compared to correctly detected and localized stimuli (middle spectrogram) and 'catch' trials. For the correct trials, a response signature in the form of a gradual increase in low frequency power (< 18 Hz), which started 40 ms after stimulus onset, was observed. Neglected stimuli did evoke at 100 ms after LED onset a weak enhancement in the frequency range up to 10 Hz. 'Catch' trials indicated no alterations in frequency power. **(B)** Analysis of induced activity revealed generally stronger signal power than evoked activity. Only if R1 correctly attended to the target LED, a response signature in the low frequency range (< 18 Hz) that was time-locked to the LED onset was evoked. Trials, in which the stimulus was neglected, resulted in an enhancement of low frequency oscillations in the range of up to 8 Hz. Neglect trials n = 93; correct trials n = 604; catch trials n = 97.

An analysis of the normalized evoked activity revealed substantial differences in the time-frequency distribution when comparing the two conditions (Figure 3.16 A). A correct performance exhibited around 40 ms after target LED onset a gradual increase in signal power in the frequency range up to 18 Hz. When the target LED was neglected, an abrupt increase of oscillatory activity below 15 Hz could be observed. Additionally,

the ‘neglect’ condition indicated at approximately 100 ms prior to stimulus presentation a weak enhancement in the frequency range between 18 – 40 Hz, which continued until 100 ms after stimulus onset.

When compared to evoked activity, the spectral composition of normalized induced activity revealed a weaker gradual increase of low-frequency oscillations when the cat had seen the target LED (Figure 3.16 B, right column). A neglected target resulted in an enhancement of low-frequency power, starting 50 ms prior to stimulus presentation and lasting until 175 ms after LED onset.

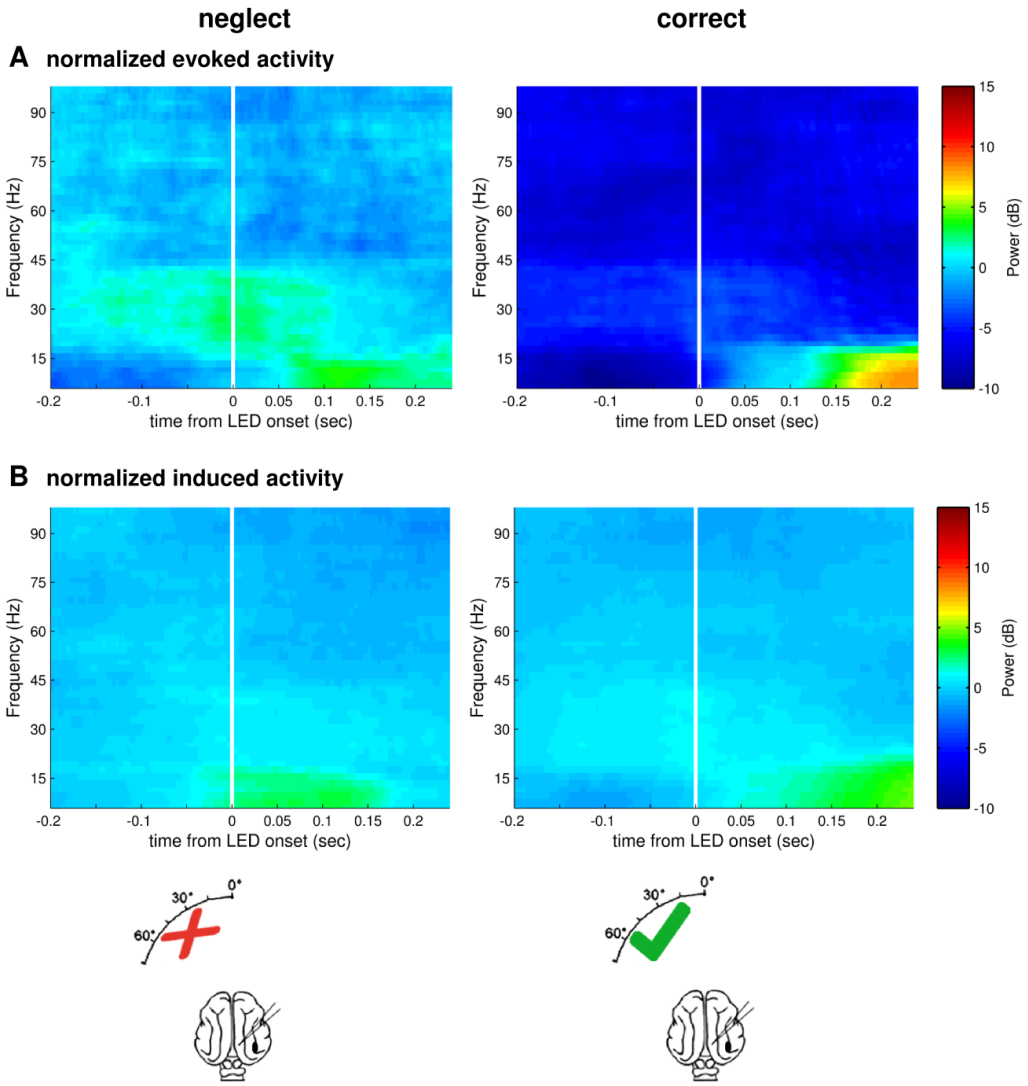

Figure 3.16 Ipsilesional recorded normalized spectrograms of neglected (left column) and correctly attended to (right column) trials from cat R1. For normalization, the ‘catch’ trials were subtracted from the respective condition. **(A)** The upper row shows the normalized evoked activity of neglected stimuli compared to correct responses. Neglected targets resulted in an abrupt increase of low-frequency oscillations at circa 50 ms after LED onset followed by a delayed attenuation of frequencies in the middle range (18-40 Hz) at ~100 ms. Correct responses evoked a gradual increase in low-frequency power (3-18 Hz) at approximately 30 ms after LED onset. **(B)** When compared to evoked activity, the spectral composition of normalized induced activity revealed a weaker gradual increase of low-frequency power if the cat had seen the target LED (right plot). TF-analysis of the neglect situation indicated an enhancement of low-frequency oscillations ~50 ms prior to stimulus presentation, which was attenuated at ~175 ms after LED onset. Neglect trials n = 93; correct trials n = 604.

Cat L1

Time-frequency analysis of the neglect condition in cat L1 indicated a slight and nonspecific increase in evoked low-frequency power that was not time-locked to the LED onset (Figure 3.17 A, left panel). The induced activity did not reveal any alterations in spectral power (Figure 3.17 B, left panel). Evoked and induced activity in the 'correct' condition showed a gradually increasing response signature in the low-frequency range up to 18 Hz (Figure 3.17, middle column). In evoked activity, the latency of the stimulus signature was around 100 ms post LED onset. An assessment of induced activity revealed a response signature latency of ~ 50 ms after stimulus onset. At this time point, together with the gradual increase (broadening) in the frequency range, a power increase could also be observed. In the 'catch' condition the evoked activity displayed a strong level of low-frequency oscillations below 10 Hz which then broadened to include 18 Hz (Figure 3.17 A, right panel). Additionally, a moderate increase in power occurred ~30 ms after the stimulus would have been illuminated. A similar spectral pattern was observed for induced activity (Figure 3.17 B, right panel). In this case, the increase in spectral power occurred simultaneous with the time at which the stimulus would have been presented to the cat.

The assessment of normalized evoked activity revealed no alterations in spectral power over the time course for either of the two analyzed conditions (Figure 3.18 A). This was presumably due to the high amount of low-frequency power in the 'catch' condition, since the normalization was done by a subtraction of the non-stimulus condition. The normalized induced activity in the neglect behavioral condition showed a moderate enhancement of low-frequency oscillations (< 18 Hz) starting ~100 ms prior to stimulus presentation and lasting until ~150 ms after stimulus onset (Figure 3.18 B, left panel). Consequently, the power change was not stimulus-locked. The spectral composition of normalized induced activity when the cat had seen the target LED did not display any changes in oscillatory power (Figure 3.18 B, right panel).

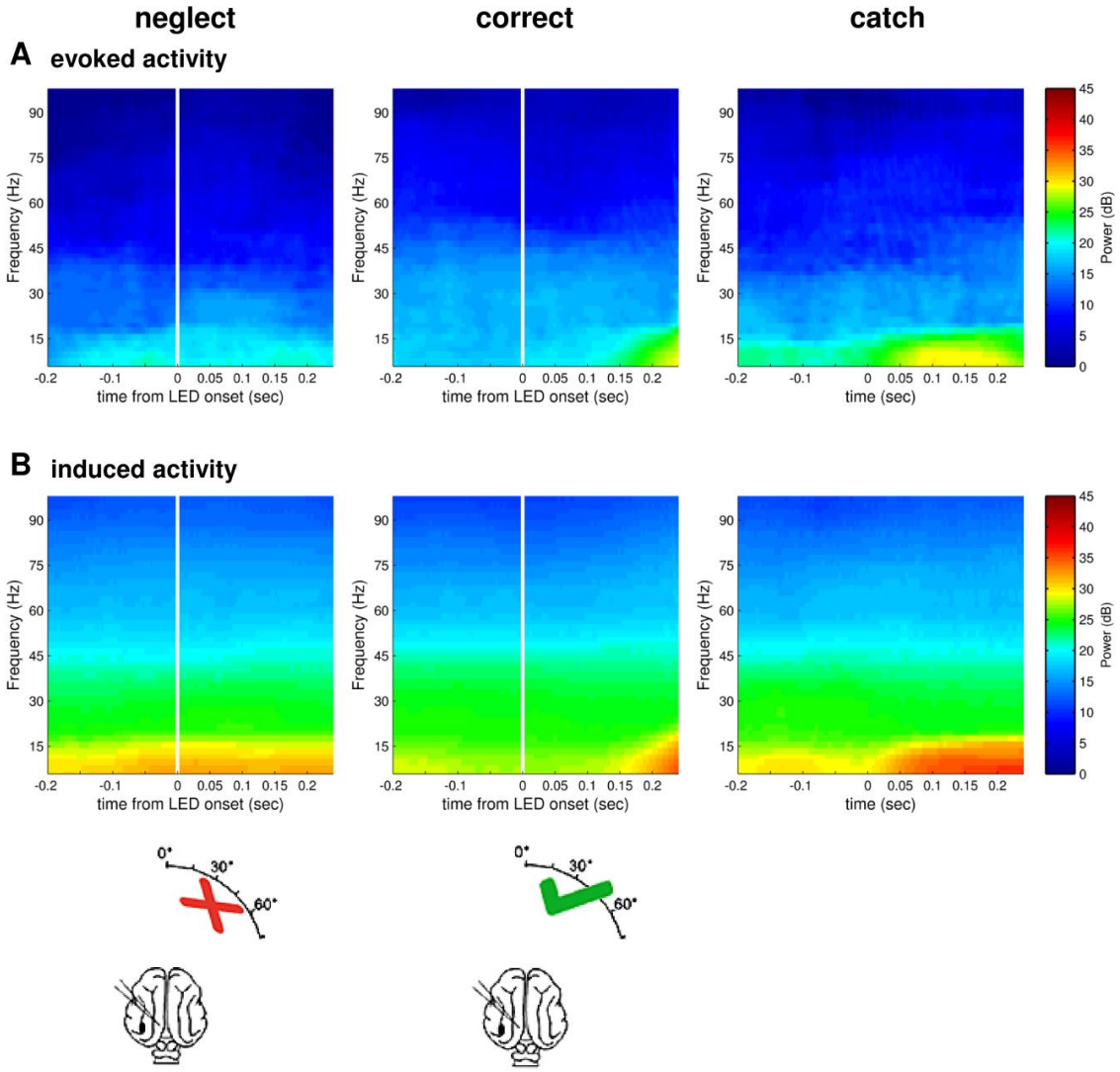

Figure 3.17 Spectral analysis of the LFP recorded from ipsilesional area 18. The cat L1 either neglected (left column) or correctly attended to (middle column) stimuli that were presented in the contralesional hemifield (see pictogram). The right column shows the spectral decomposition for 'catch' trials, where the target LED was absent. The lesion was located in the left pMS cortex (depicted in black in the cat brain icons below). Other conventions as in Figure 3.15. **(A)** TF-plots illustrating evoked LFP activity. The 'neglect' condition is shown in the left spectrogram, the 'correct' condition in the middle spectrogram and the 'catch' condition on the right. For the correct trials, a response signature in the form of a gradual increase in low frequency power (< 18 Hz), with a latency of ~100 ms after stimulus onset, was observed. Neglected stimuli did not evoke any alterations in signal power that were related to the LED onset. 'Catch' trials indicated a moderate increase of low-frequency oscillations after the stimulus would have been presented to L1. **(B)** Analysis of induced activity revealed generally stronger signal power than evoked activity. Only if L1 correctly attended to the target LED, a response signature in the low frequency range (< 18 Hz) that was time-locked to the LED onset was evoked. Trials, in which the stimulus was neglected, did not elicit any alterations in signal power. The 'catch' condition resulted in an increase of low-frequency oscillations. Neglect trials n = 64; correct trials n = 81; catch trials n = 31.

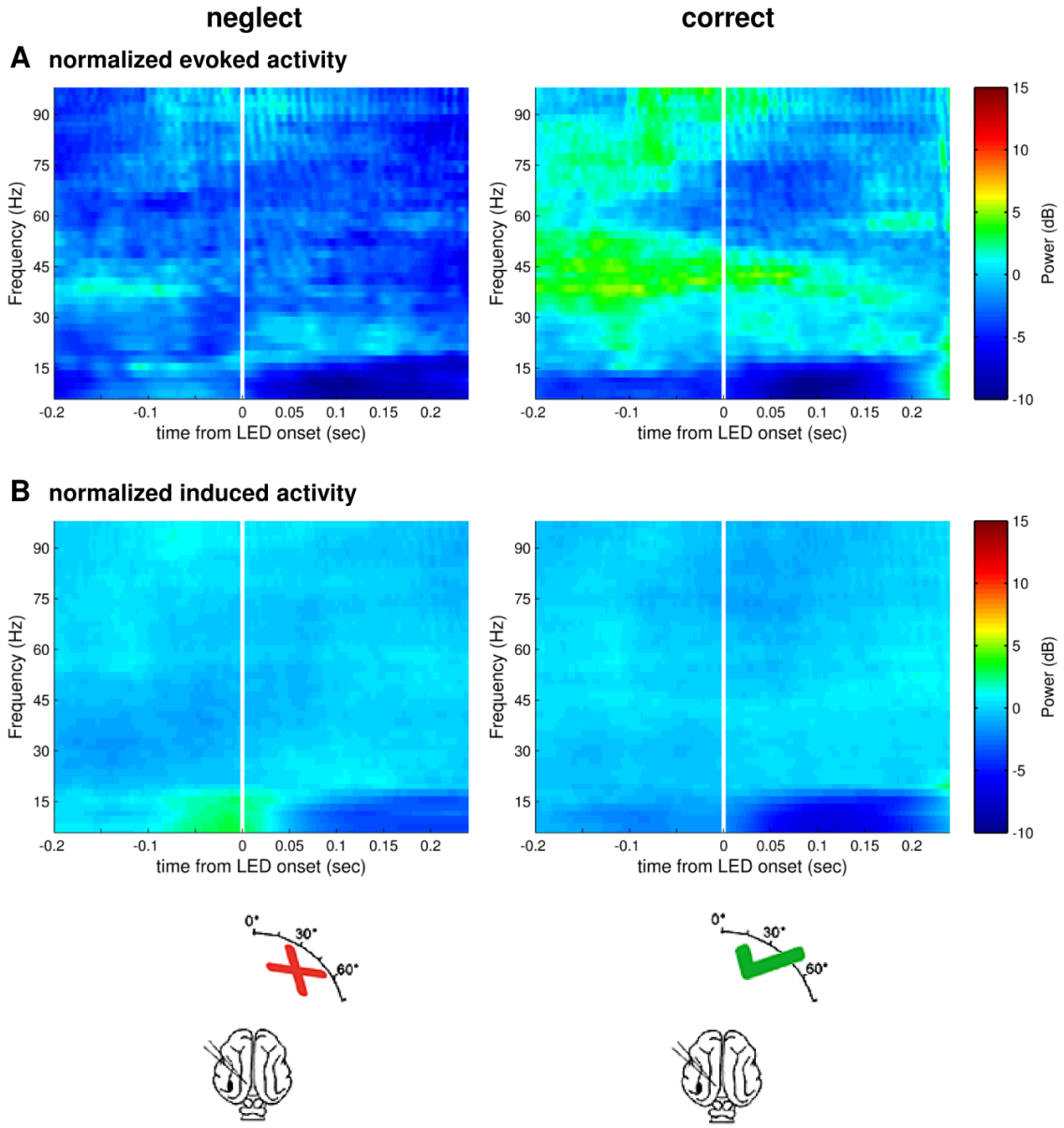

Figure 3.18 Ipsilesional recorded normalized spectrograms of neglected (left column) and correctly attended to (right column) trials from cat L1. For normalization, the 'catch' trials were subtracted from the respective condition. **(A)** The upper row shows the normalized evoked activity of neglected stimuli compared to correct responses. In none of the two conditions, a change in oscillatory power was observed. **(B)** The same outcome was also observed for the spectral composition of normalized induced activity when the cat had seen the target LED (right plot). TF-analysis of the neglect situation indicated an enhancement of low-frequency oscillations ~100 ms prior to stimulus presentation, which was attenuated at ~50 ms after LED onset. Neglect trials n = 64; correct trials n = 81.

Cat L2

Since the cat L2 exhibited no functional recovery for stimuli located in the contralesional hemifield, only a comparison between the 'neglect' and the 'catch' condition was possible. In the neglect situation the evoked activity showed a slight increase in low-frequency power (<15 Hz) from ~30 ms until ~200 ms post LED onset (Figure 3.19 A, left panel). The time-frequency distribution in the 'catch' condition indicated a general enhancement of oscillations in the low-frequency range (<18 Hz) with the highest power in the range below 10 Hz (Figure 3.19 A, right panel). Spectral analysis of induced activity displayed throughout the entire time course an increased level of signal power in the frequency range up to ~55 Hz with the highest power within low-frequency oscillations up to 15 Hz (Figure 3.19 B). Remarkably, the spectral profile of the neglect situation demonstrated very close resemblance to that of the 'catch' condition.

The normalized spectrograms of the neglect condition did not show any oscillatory changes. This held true for both the normalized evoked as well as the induced activity (Figure 3.20).

Summary of results from all three cats

A common characteristic of the spectral analysis was the fact that almost all changes in oscillatory power occurred in the low-frequency range up to 18 Hz. This observation applied to evoked as well as to induced activity.

The neglect condition elicited only weak changes in evoked signal power that were not time-locked to the stimulus onset and, in general, showed a high individual variability in time and magnitude.

Correctly detected and localized targets resulted in a gradual gain of evoked and induced oscillatory power in the low-frequency range (<18 Hz). The latency of this increase was ~50 ms or ~100 ms after stimulus onset in cat R1 and cat L1, respectively.

The 'catch' condition did not elicit any oscillatory power changes in either of the cats R1 and L2. However, cat L1 showed a precisely timed enhancement of evoked as well as induced low-frequency power (<18 Hz). This gain could be an error signal that is the neuronal correlate of unmet cognitive predictions.

The normalized spectra displaying the neglect condition revealed no oscillatory power changes over the entire time course in cats L1 and L2. Only cat R1 exhibited a moderate power increase in the low-frequency range, which however, differed considerably from the spectral profile evoked by correctly detected targets.

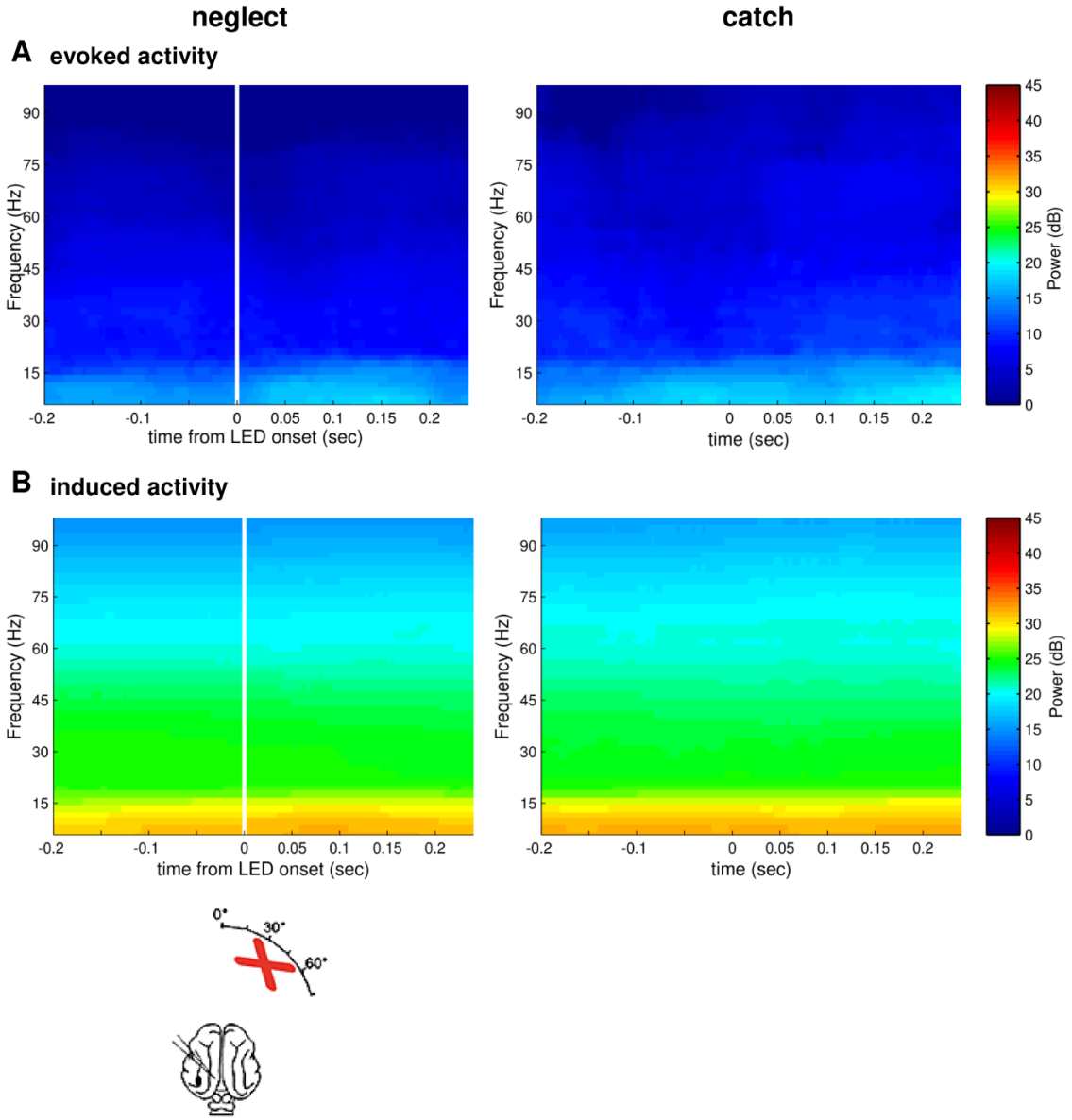

Figure 3.19 Spectral analysis of the LFP recorded from ipsilesional area 18 in cat L2. The left column illustrates changes in spectral power if the cat L2 had neglected targets that were presented in the contralesional hemifield (see pictogram). The right column shows the spectral decomposition for 'catch' trials, where the target LED was absent. Other conventions as in Figure 3.15. **(A)** Evoked activity for neglected stimuli (left spectrogram) compared to 'catch' trials (right spectrogram). Neglected stimuli did evoke at 30 ms until 200 ms after LED onset a weak enhancement in the frequency range up to 10 Hz. 'Catch' trials indicated no alterations in frequency power. **(B)** Analysis of induced activity revealed generally stronger signal power than evoked activity. The 'neglect' condition looked very similar to the 'catch' condition, in which a stimulus was absent. In both conditions, no changes in frequency power over the entire time course were observed. Neglect trials n = 538; catch trials n = 131.

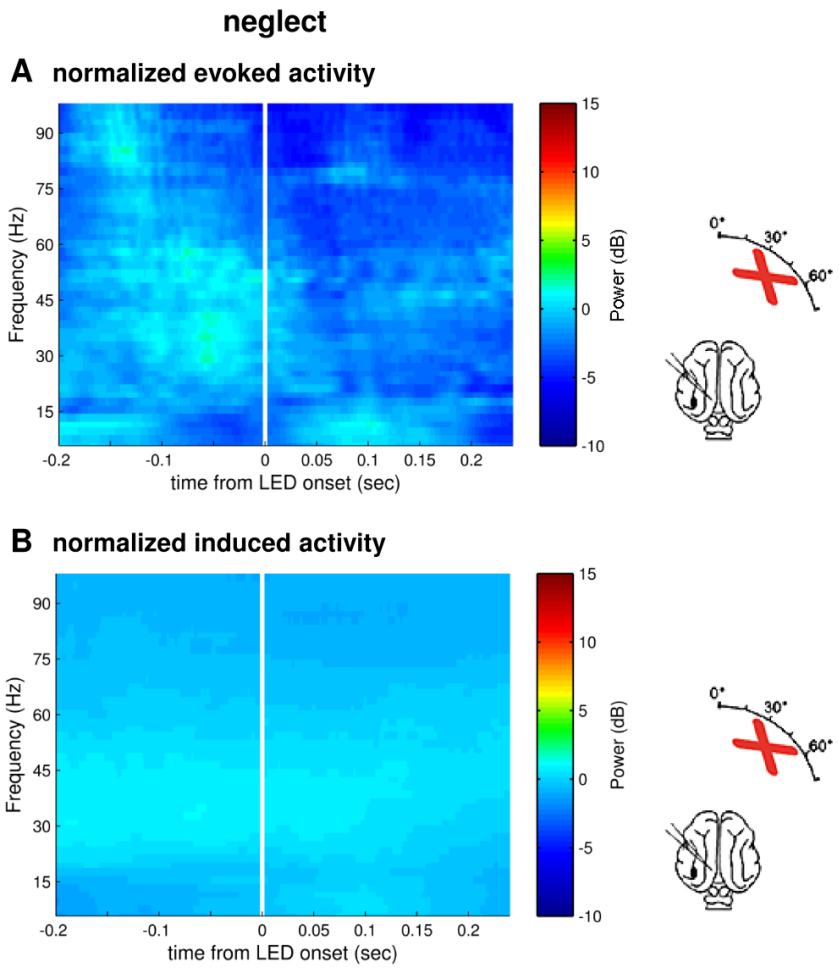

Figure 3.20 Ipsilesionally recorded normalized spectrograms of neglected trials from cat L2. For normalization, the 'catch' trials were subtracted from the 'neglect' condition. **(A)** The upper row shows the normalized evoked activity of neglected stimuli. Neglected targets resulted in no alterations of oscillatory power. **(B)** The same result was true for normalized induced activity during the neglect situation. Neglect trials n = 538.

3.4.1.3 *Frequency band analysis of neuronal activity during neglect*

In order to compare the spectral changes caused by the target stimulus during the 'neglect' and 'correct' condition, the change in power for each frequency band was calculated by normalization to the pre-stimulus (pre 1st LED) spontaneous activity. Thus, the following results illustrate the changes in power relative to the power in each frequency band during the pre-stimulus analysis window (AW1). Again, only trials were considered for which the cat showed a pre-lesion performance level above 75%. The relative power changes are expressed as percent change.

Cat R1

The neglect situation resulted in a decrease of power in almost all frequency bands except for the ipsilesional recorded theta and gamma2 band (Figure 3.21 A). In these two bands a slight power increase occurred (ipsilesional: theta: +11.4%; gamma2: +3.8%). The contralesionally recorded theta and gamma1 band, as well as the bilateral alpha band activity had a mild power decrease as compared to pre-stimulus activity (contralesional: theta: -5.1%; alpha: -6.5%; gamma1: -14.4%; ipsilesional: alpha: -16.6%). Statistically significant power reductions were observed for the beta band (contralesional: beta: -20.4% $p<.01$; ipsilesional: beta: -21.9% $p<.001$, U) and for the ipsilesionally recorded gamma1 band activity (ipsilesional: gamma1: -16.7% $p<.05$, U). Power in the contralesionally recorded gamma2 band activity remained unchanged (contralesional: gamma2 :+0.1%).

A correct response to contralesional targets produced a clear increase in the theta and alpha band and in the ipsilesional recorded gamma2 band activity (ipsilesional: theta: +65.5% $p<.0001$; alpha: +69.2% $p<.0001$; gamma2: +10.7% $p<.0001$; contralesional: theta: +28.2% $p<.0001$; alpha: +58.7% $p<.0001$, U; Figure 3.21 B). Activity in all other frequency bands was decreased (ipsilesional: beta: -19.3% $p<.0001$; gamma1: -19.5% $p<.0001$; contralesional: beta: -13.2% $p<.001$; gamma1: -16.7% $p<.0001$; gamma2: -4.8%, U).

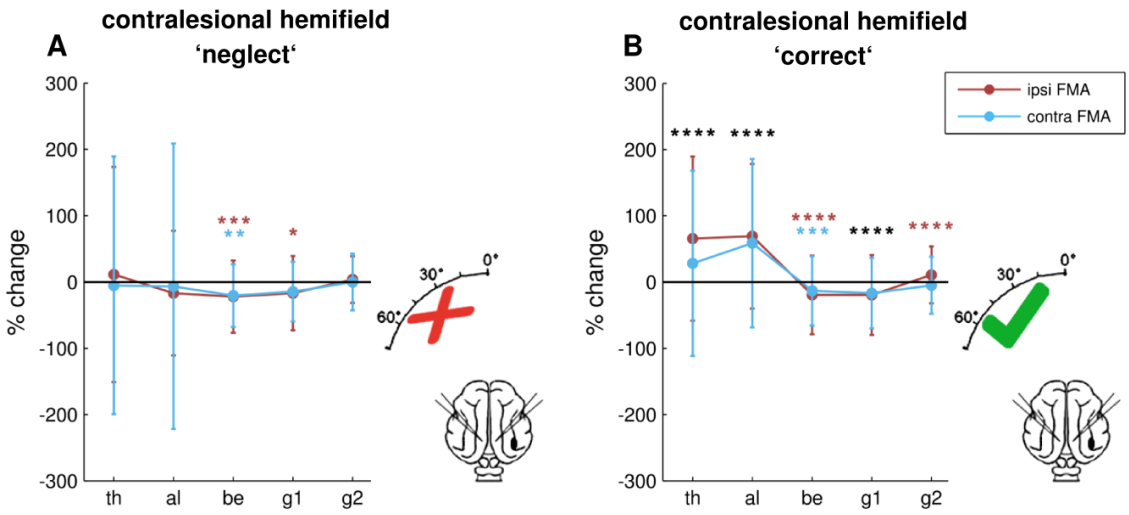

Figure 3.21 Comparison of frequency band power during the 'neglect' or 'correct' condition in cat R1. Icons next to the plots indicate the lesion site, the recording sites and the behavioral outcome (either 'neglect' or 'correct'). The y-axis shows the power change of the post-stimulus condition (AW4) in percent relative to the pre-stimulus condition (AW 1), the x-axis displays the frequency bands: th = theta, al = alpha, be = beta; g1 = gamma1, g2 = gamma2. Ipsi FMA denotes the averaged signal recorded from the ipsilesional primary visual cortex, contra FMA denotes the averaged signal recorded from the contralesional V1. The asterisks represent significant power differences in either one of the two possible conditions relative to pre-stimulus power. Black asterisks indicate bilateral significance. Significant values were obtained by performing a Mann-Whitney U-test (U). * = significant at p<.05; ** = significant at p<.01; *** = significant at p<.001; **** = significant at p<.0001. **(A)** The neglect situation evoked in almost all frequency bands a minor power decrease, which was most pronounced in the beta and gamma1 band. **(B)** If R1 had correctly responded to contralesional targets, a strong increase of theta and alpha band power was observed for both hemispheres. Both, the beta and gamma1 band exhibited a moderate power decrease that was comparable to the response profile in the neglect situation. 'neglect' trials n = 93; 'correct' trials n = 604; (error bars: SD).

Cat L1

When the cat L1 neglected the target LED, a general enhancement of oscillatory power was observed in both hemispheres (Figure 3.22 A). The contralesional primary visual cortex displayed for all frequency bands, with the exception of the gamma2 band, a stronger power increase than the ipsilesionally recorded V1 (contralesional: theta: +59.4% p<.05; alpha: +66.6% p<.05; beta: +35.2%; gamma1: +16.6%; gamma2: +10.6%; ipsilesional: theta: +33.6% p<.01; alpha: +38.9% p<.05; beta: +10.2%; gamma1: +11.9%; gamma2: +13.1%, U).

When cat L1 correctly attended to stimuli in the contralesional hemifield, the lower frequency bands theta and alpha as well as the high gamma band, gamma2, also showed an increase in power, whereas the beta and ipsilesional gamma1 bands displayed a moderate decrease relative to the pre-stimulus analysis window (Figure 3.22 B).

No substantial power differences between the ipsi- and contralesionally recorded primary visual cortex were observed (contralesional: theta: +78.3% p<.001; alpha: +39.2% p<.05; beta: -5.6%; gamma1: +8.0%; gamma2: +23.1% p<.01; ipsilesional: theta: +72.0% p<.01; alpha: +36.8% p<.05; beta: -13.2%; gamma1: -3.3%; gamma2: +27.3% p<.001, U).

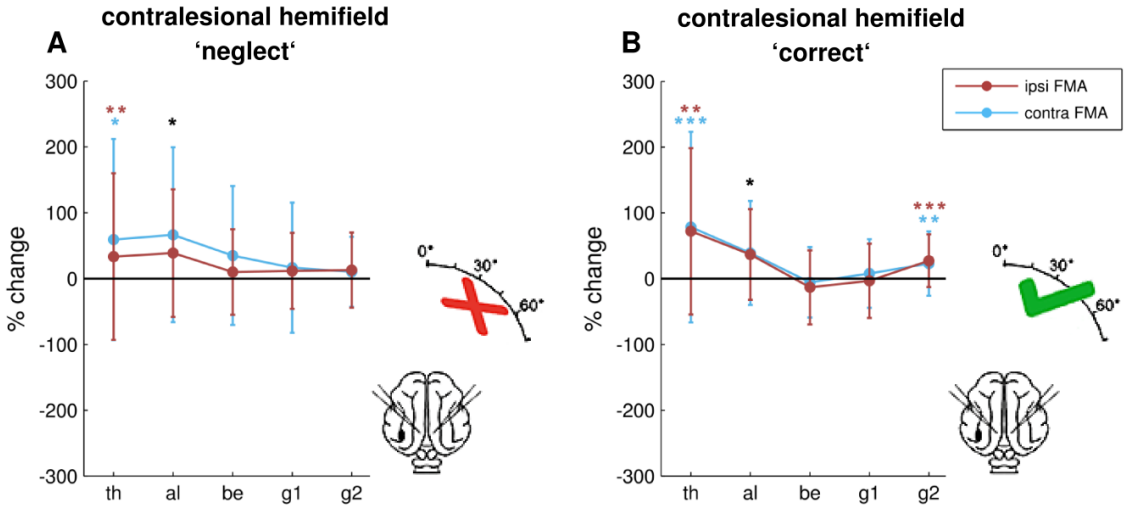

Figure 3.22 Comparison of frequency band power during the 'neglect' or 'correct' condition in cat L1. Same conventions and abbreviations as in Figure 3.21 **(A)** Neglected targets elicited an increase in oscillatory power in all frequency bands that was most evident in the contralesional recorded theta, alpha and beta band. **(B)** Perceived target stimuli resulted in a bilateral power enhancement in the theta, alpha and gamma2 range. The beta and gamma1 band showed relative to pre-stimulus power, a slight reduction. 'neglect' trials n = 64; 'correct' trials n = 81; (error bars: SD).

Cat L2

In cat L2 there was no recovery from neglect. Thus, only 'neglect' trials could be analyzed. The neglect situation produced a significant increase in theta and alpha band power on both hemispheres as compared to the pre-stimulus condition (Figure 3.23 A). This effect was slightly more pronounced in the ipsilesionally recorded primary visual cortex (contralesional: theta: +83.8% p<.0001; alpha: +44.8% p<.0001; ipsilesional: theta: +111.2% p<.0001; alpha: +69.7% p<.0001, U). Furthermore, the gamma2 band showed a moderate enhancement of oscillatory power with a magnitude of +19.4% on the ipsilesional and +5.7% on the contralesional recording site. The remaining frequency bands, beta and gamma1, bilaterally exhibited a decrease in power relative to pre-stimulus activity (contralesional: beta: -11.8% p<.001; gamma1: -13.7% p<.001; ipsilesional: beta: -7.2% p<.01; gamma1: -7.2% p<.05, U).

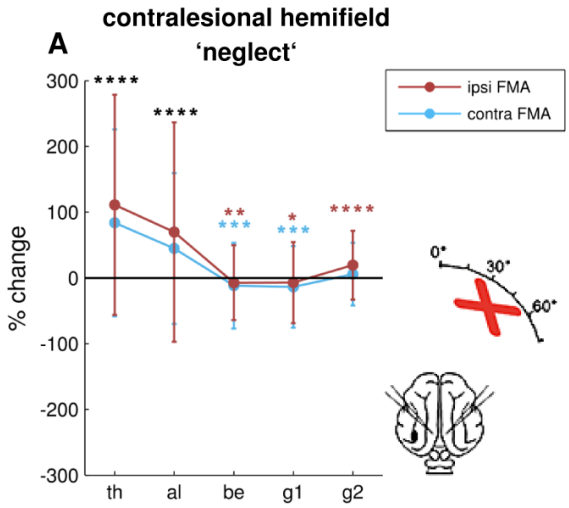

Figure 3.23 Oscillatory power in the different frequency bands during the 'neglect' condition in cat L2. Same conventions and abbreviations as in Figure 3.21 **(A)** In cat L2, the neglect situation resulted in an enhancement of theta, alpha and gamma2 band power. 'neglect' trials n = 538; (error bars: SD)

Summary

The most prominent change in frequency band power relative to the pre-stimulus condition was a large increase in low-frequency power, namely the theta and alpha band, on both recorded hemispheres. This increase was reflected in all three cats throughout all conditions examined. Only the neglect profile of cat R1 was an exception to this. In addition, the analysis revealed, with the exception of the 'correct' condition in cat R1,a bilateral modest increase in high gamma power in all tested conditions. In general, oscillatory power in the medium-frequency range, comprising the beta and gamma1 band, was slightly decreased. The only exception here was the neglect profile of cat L1.

Although the spectral profiles of the 'correct' condition in cats R1 and L1 displayed some similarities, the effects described above did not seem to be linked to the behavioral outcome. The finding that the neglect profile of cat L2 resembled the spectral profiles of cat R1 and L1 when both attended to the target stimuli, supports this evaluation. An additional comparison between the ipsi- and contralesional recording sites regarding the magnitude of power increase or decrease, respectively, did not yield effects that were specific to one hemisphere.

3.4.2 LESION-INDUCED CHANGES OF STIMULUS PROCESSING IN THE NON-NEGLECTED VISUAL HEMIFIELD

To determine whether the lesion has additional effects on the processing of stimuli that appear in the intact (non-neglected) hemifield, bilateral recordings while the cat attended to ipsilesional targets were examined.

3.4.2.1 *Analysis of event related potentials*

The ERPs from each post-lesion period were calculated in the same manner as described in section 3.1.2 and the peak latencies for the three components N1, P1 and P2 were extracted. To assess lesion-induced changes in stimulus processing, the peak latency values were normalized by subtracting the corresponding peak latencies of the pre-lesion period. Resulting negative values corresponded to an earlier occurrence of a component, positive values corresponded to a later occurrence of a component with respect to the pre-lesion period. As before, the results of cat R1 were selected as a representative example. In order to maintain a better overview, the individual post-lesion periods were grouped into three blocks. The classification was made according to the behavioral results (see section 3.2).

The analysis of ERP peak latency changes revealed for all target locations that the late P2 component occurred considerably earlier relative to the pre-lesion condition (Figure 3.24 E, F). These peak latency differences were largest for the target locations 30° and 45° and smallest for the most peripheral target location 75°. In addition, with the exception of the stimulus location at 75°, the peak latency differences were larger in the late post-lesion periods 6-18 than in the early post-lesion periods (post-lesion 1-5).

Decreased peak latencies relative to the pre-lesion period were also evident for the N1 component although to a lesser extent than for the P2 component (Figure 3.24 A, B). This component showed some differences between the recorded hemispheres, especially for the fixation cue, the center and 15° location. For the fixation cue and the 0° location the ipsilaterally recorded hemisphere exhibited a clearly earlier occurrence of the N1 component with respect to the pre-lesion period whereas the contralateral hemisphere showed a earlier occurrence of the N1 component at the 15° target location.

In contrast to the decreased peak latencies of the components N1 and P2, the P1 component indicated a distinct tendency to occur later with respect to the pre-lesion period (Figure 3.24 C, D).

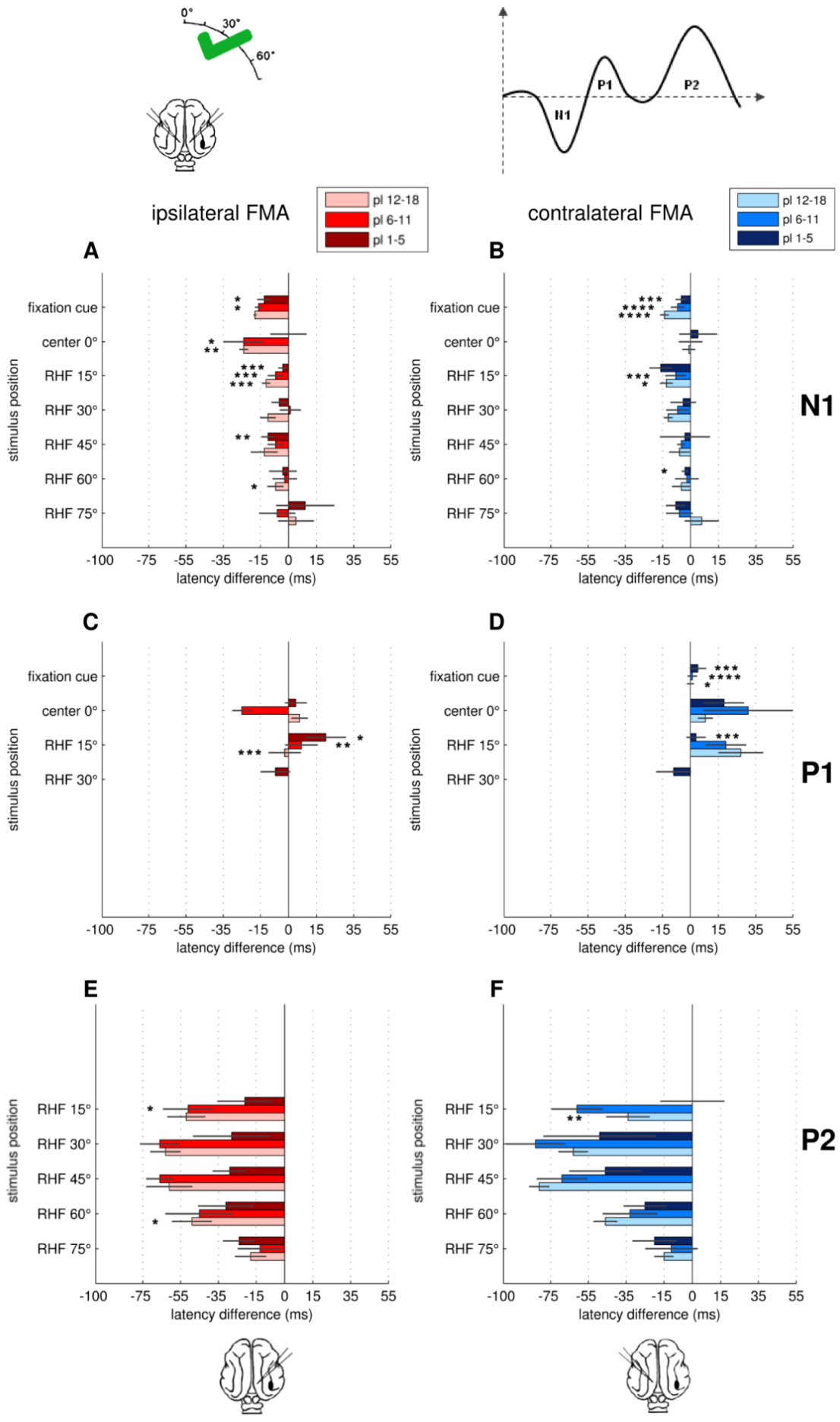
0°
30°
60°
P1
N1
P2
ipsilateral FMA
pl 12-18
pl 6-11
pl 1-5
contralateral FMA
pl 12-18
pl 6-11
pl 1-5
A
B
C
D
E
F
fixation cue
center 0°
RHF 15°
RHF 30°
RHF 45°
RHF 60°
RHF 75°
stimulus position
-100 -75 -55 -35 -15 0 15 35 55
latency difference (ms)
N1
P1
P2

Figure 3.24 ERP peak latency differences between the pre-lesion period and all post-lesion periods of correctly detected targets in the ipsilesional hemifield of cat R1. The cat brain icon above the plot illustrates the lesion site, the recording sites and the behavioral condition that was used in the analysis. Next to the icon, a schematic diagram of an ERP with all three components is shown. As indicated by the icons below the plots, the left plot column **(A, C, E)** shows the ipsilesionally recorded hemisphere and the right plot column **(B, D, F)** shows the results from the contralesionally located FMA. In each plot, the stimulus position is indicated on the y-axis and peak latency differences relative to the pre-lesion period in milliseconds are shown on the x-axis. Negative values mean an earlier occurrence of the respective component; positive values correspond to a later occurrence. The asterisks represent significant peak latency differences for each component with respect to the related component in the pre-lesion period. Significant values were obtained by performing a Wilcoxon signed rank test (WSR). * = significant at p< .05; ** = significant at p< .01; *** = significant at p< .001; **** = significant at p< .0001; **(A, B)** Bilateral peak latency differences of N1. When compared to the pre-lesion period the N1 peak displayed a generally earlier occurrence for almost every target location. **(C, D)** Bilateral peak latency differences of P1. The P1 peak showed, in the contralesional V1 more clearly than in the ipsilesional V1, a tendency to occur later with respect to the pre-lesion period. **(E, F)** Bilateral peak latency differences of P2. The P2 component displayed a clearly earlier occurrence relative to the pre-lesion period, which was further accelerated the later in the post-lesional time course the analysis was performed.
fixation cue: pl 1-5 n = 252; pl 6-11 n = 441; pl 12-18 n = 899; center 0°: pl 1-5 n = 28; pl 6-11 n = 45; pl 12-18 n = 79; RHF 15°: pl 1-5 n = 30; pl 6-11 n = 43; pl 12-18 n = 73; RHF 30°: pl 1-5 n = 21; pl 6-11 n = 43; pl 12-18 n = 87; RHF 45°: pl 1-5 n = 22; pl 6-11 n = 43; pl 12-18 n = 51; RHF 60°: pl 1-5 n = 25; pl 6-11 n = 40; pl 12-18 n = 74; RHF 75°: pl 1-5 n = 12; pl 6-11 n = 32; pl 12-18 n = 71; Abbreviations: pl: post-lesion; RHF: right hemifield; (error bars: SEM)

Summary

Although stimuli were presented in the non-neglected hemifield, the processing was altered in both primary visual cortices, as revealed by this analysis. The decreased peak latencies of N1 and P2, but not P1, indicated a faster stimulus processing at certain stages of sensory signal processing. The further acceleration of the P2 peak latencies, which was observed over the post-lesional time course, might be related to training-induced effects on neuronal activity.

3.4.2.2 *Frequency band analysis of ipsilesionally attended targets*

I. Comparison of oscillatory power between ipsilesionally attended and recovered, contralesionally attended targets

The normalized frequency band power changes, which resulted from correctly detected targets in the intact (ipsilesional) visual hemifield, were compared to normalized power changes of correct responses to contralesionally presented targets. The latter condition comprised the post-lesional recovered responses. Similar to the previous analysis, the power in each frequency band was normalized to the frequency band power in the pre-stimulus analysis window (AW1) and expressed in percent change. Again, only target locations for which the cat exhibited a pre-lesional performance level above 75% correct were considered.

A correct response to targets in the ipsilesional as well as contralesional visual hemifield evoked a similar general pattern of frequency band changes with a strong increase of activity in the theta and alpha band and a moderate increase in the high-gamma band (Figure 3.25, upper row). The beta and gamma1 band displayed a mild decrease when compared to the pre-stimulus analysis window. However, in both recorded hemispheres the increase in the theta and alpha band in response to ipsilesional targets was more than twice as high as in response to contralesionally located targets (Table 3.3).

Generally, the increase in the high-gamma band was more pronounced in cat L1 than in cat R1 (Figure 3.25, lower row). In addition, Cat L1 displayed a stronger enhancement of low frequency band power on the intact (contralesional) hemisphere than on the ipsilesional hemisphere when the attended target was located ipsilesionally (Table 3.4).

Summary

In both cats, correctly detected targets produced a similar response signature, with a bilateral, significant increase of theta and alpha band power. The comparison between the response profiles of ipsi- and contralesional targets revealed an excessively strong representation of ipsilesionally attended stimuli.

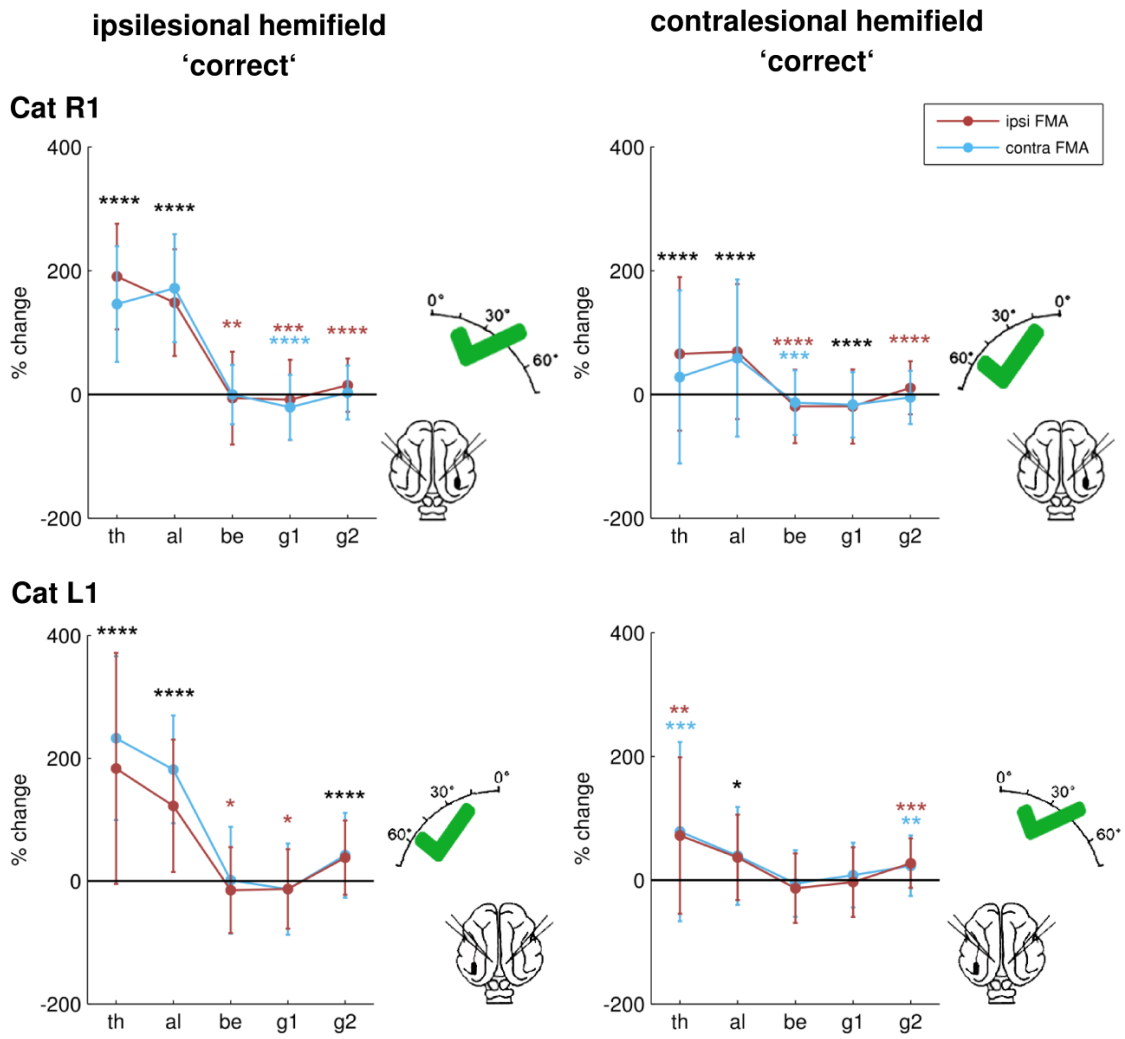

Figure 3.25 Comparison of frequency band power changes of correctly detected targets in the ipsi- and contralesional visual hemifield. The upper plot row shows the results from cat R1, the lower plot row has the results from cat L1. The y-axis indicates the power change in percent relative to the pre-stimulus condition (AW1). Other conventions and abbreviations as in Figure 3.21. The increase in the theta and alpha band in response to ipsilesionally presented targets was at least twice the increase as in response to contralesional targets.
Cat R1: ipsilesional hemifield n = 671; contralesional hemifield n = 604;
Cat L1: ipsilesional hemifield n = 122; contralesional hemifield n = 84; (error bars: SD)

Table 3.3 Percent change of frequency band power relative to AW1 for correctly attended targets. Results obtained from cat R1.

	Ipsilesional hemifield; correct				
Recorded FMA	**Theta**	**Alpha**	**Beta**	**Gamma 1**	**Gamma 2**
Ipsilesional FMA	+190.6****	+148.5****	-5.8**	-8.7****	+14.9****
Contralesional FMA	+146.2****	+171.9****	-0.3†	-20.8****	+3.0†
	Contralesional hemifield; correct				
Ipsilesional FMA	+65.5****	+69.2****	-19.3****	-19.5****	+10.8****
Contralesional FMA	+28.2****	+58.8****	-13.3***	-16.7****	-4.8†

* = significant at p< .05; ** = significant at p< .01; *** = significant at p< .001; **** = significant at p< .0001;
†= nonsignificant
Significant values were obtained by performing a Mann-Whitney U-test (U).

Table 3.4 Percent change of frequency band power relative to AW1 for correctly attended targets. Results obtained from cat L1.

	Ipsilesional hemifield; correct				
Recorded FMA	**Theta**	**Alpha**	**Beta**	**Gamma 1**	**Gamma 2**
Ipsilesional FMA	+183.4****	+122.4****	-14.9*	-13.0****	+37.9****
Contralesional FMA	+232.6****	+181.7****	+1.2†	-13.2†	+41.9****
	Contralesional hemifield; correct				
Ipsilesional FMA	+72.0**	+39.2*	-13.2†	-3.3†	+27.3***
Contralesional FMA	+78.3***	+36.8*	-5.6†	+8.0†	+23.1**

* = significant at p< .05; ** = significant at p< .01; *** = significant at p< .001; **** = significant at p< .0001;
†= nonsignificant
Significant values were obtained by performing a Mann-Whitney U-test (U).

II. Comparative analysis of pre- and post-lesional stimulus processing in the non-neglected hemifield

To further investigate how the lesion generally affects the processing of stimuli in the non-neglected hemifield a comparison between the pre- and post-lesion periods was performed.

As a first step, the frequency band power in the pre-lesion period for correctly detected targets in the corresponding hemifield[1] was computed for each cat. This was done to evaluate possible differences between the cats and between the hemispheres within each cat. The frequency bands were normalized relative to all frequencies.

None of the cats revealed a substantial interhemispheric difference. Furthermore, all three cats exhibited a similar response profile to stimuli in the relevant visual hemifield (Figure 3.26).

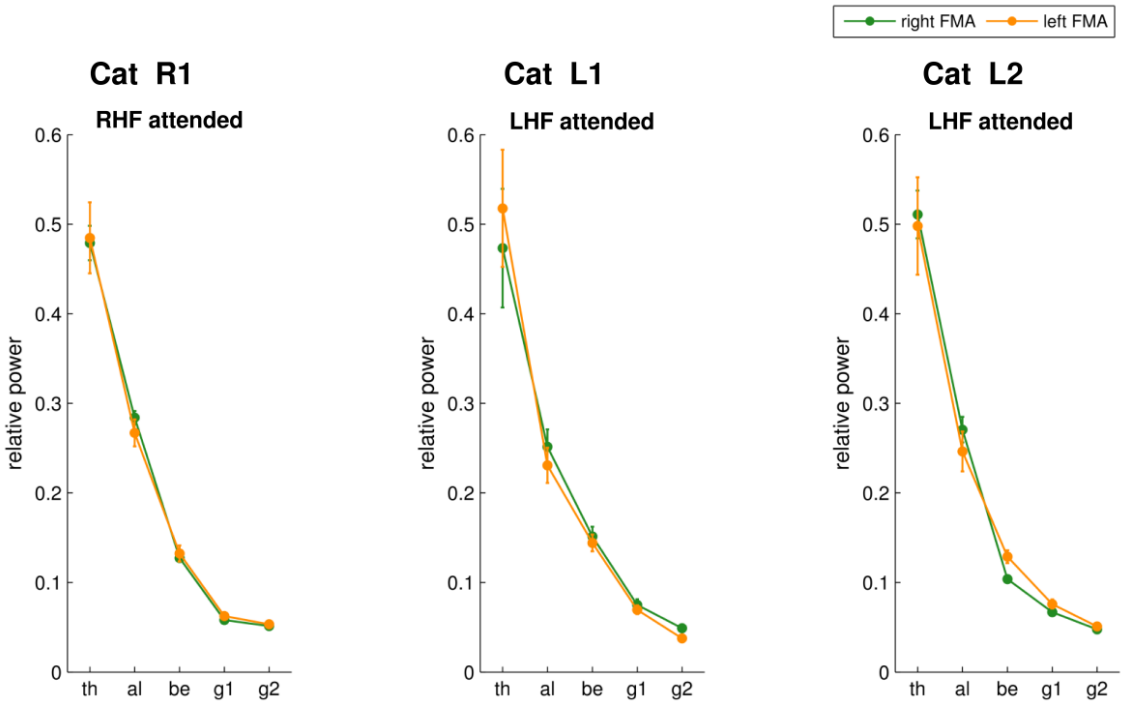

Figure 3.26 Frequency band power in the pre-lesion period for attended targets in the relevant visual hemifield. The power relative to all frequencies is shown on the y-axis, the frequency bands are specified on the x-axis: Neither between the hemispheres within each cat, nor between the three cats, were considerable differences in power observed.
Cat R1 n = 50; cat L1 n = 50; cat L2 n = 22; Abbreviations: RHF: right hemifield; LHF: left hemifield; FMA: floating micro-electrode array; (error bars: SD)

[1] The hemifield that was located ipsilateral to the subsequent lesion site

As a second step, the lesion-induced alterations in stimulus processing were assessed by computing the power changes in the entire post-lesion period with respect to the pre-lesion period in percent (Figure 3.27). The behavioral condition was 'ipsilesionally attended'.Tto minimize spurious effects (e.g. training effects) target locations for which the cat showed a pre-lesion performance of less than 75% correct, were excluded from the analysis.

The comparison revealed stronger disparities not only between the cats but also between the individual hemispheres.

Cat R1

Relative to the pre-lesion period, cat R1 exhibited a global increase in oscillatory power (Figure 3.27 A). The most prominent gain in power was observed for contralesionally recorded theta oscillations (+232.1%, $p<.0001$, WSR) but also the ipsilesionally recorded V1 showed a significant increase in theta power (+69.2%, $p<.01$, WSR). In addition to the theta band, only the alpha band showed a larger increase in oscillatory power in the intact (contralesional) than in the impaired (ipsilesional) hemisphere (contralesional: alpha: +105.2%, $p<.001$; ipsilesional: alpha: +28.9%, WSR). The remaining frequency bands; beta, gamma1 and gamma2, displayed in the ipsi- as well as contralesionally recorded V1 a significant increase in power relative to the pre-lesion period, with the largest gain of ipsilesional power in the gamma1 band (contralesional: beta: +28.0%, $p<.01$; gamma1: +49.0%, $p<.0001$; gamma2: +55.2%, $p<.0001$; ipsilesional: beta: +83.6%, $p<.0001$; gamma1: +156.7%, $p<.0001$; gamma2: +102.8%, $p<.0001$, WSR).

Cat L1

The results from cat L1 showed a large deviation from the results obtained from the two other cats (Figure 3.27 B). This was mainly because ipsilesionally attended targets produced a significant reduction of oscillatory power in all frequency bands in the contralesional hemisphere (contralesional: theta: -34.3, $p<.0001$; alpha: -37.8%, $p<.0001$; beta: -44.4%, $p<.0001$; gamma1: -40.0%, $p<.0001$; gamma2: -26.9%, $p<.0001$, WSR). Ipsilesionally recorded V1 exhibited a power decrease in the low-frequency range (theta and alpha) and an increase of oscillatory power in the beta and gamma range when compared to the pre-lesion period (ipsilesional: theta: -21.1%, $p<.0001$; alpha: -0.2%, $p<.001$; beta: +17.2%; gamma1: +19.5%; gamma2: +34.2%, $p<.05$, WSR).

Cat L2

Correct detection of ipsilesionally presented targets evoked a bilateral enhancement of oscillatory power in the entire frequency range as compared to the pre-lesion period (Figure 3.27 C). A comparison between the hemispheres revealed, with the exception of theta band power, for the intact (contralesional) hemisphere a generally stronger power increase as in the impaired (ipsilesional) hemisphere. The contralesional V1 indicated the largest changes with respect to the pre-lesion period in the theta and high-gamma range and the smallest change in the gamma1 band (contralesional: theta: +97.3%, $p<.001$; alpha: +75.3%, $p<.01$; beta: +61.3%, p<,001; gamma1: +51.8%, $p<.01$; gamma2: +100.6%, $p<.0001$, WSR). The ipsilesional hemisphere displayed nearly the same pattern of power gain, but with the smallest power increase relative to pre-lesion in the beta band (ipsilesional: theta: +97.3%, $p<.001$; alpha: +66.5%; beta: 13.5%; gamma1: +31.8%; gamma2: +76.8%, $p<.0001$, WSR).

Summary

The lesion induced in cats R1 and L2 a general increase in oscillatory power across the entire frequency range as compared to the pre-lesion period. This enhancement was most pronounced and highly significant in both cats. One possible reason for this finding might be a stronger, lesion-induced representation of ipsilesionally located targets. In addition, both cats exhibited, with respect to the pre-lesion period, a bilateral significant power increase in the theta and high-gamma band. This finding further supports this hypothesis, because an increase in these two bands is part of the general response profile for the target LED. However, the results from cat L1 displayed an entirely different picture. Only a significant power gain in the ipsilesionally recorded high-gamma band was similar in all three cats. The pronounced reduction of contralesionally recorded power in cat L1 might be related to the large expansion of the lesion in this cat since all three cats exhibited a comparable pre-lesional response profile of oscillatory power.

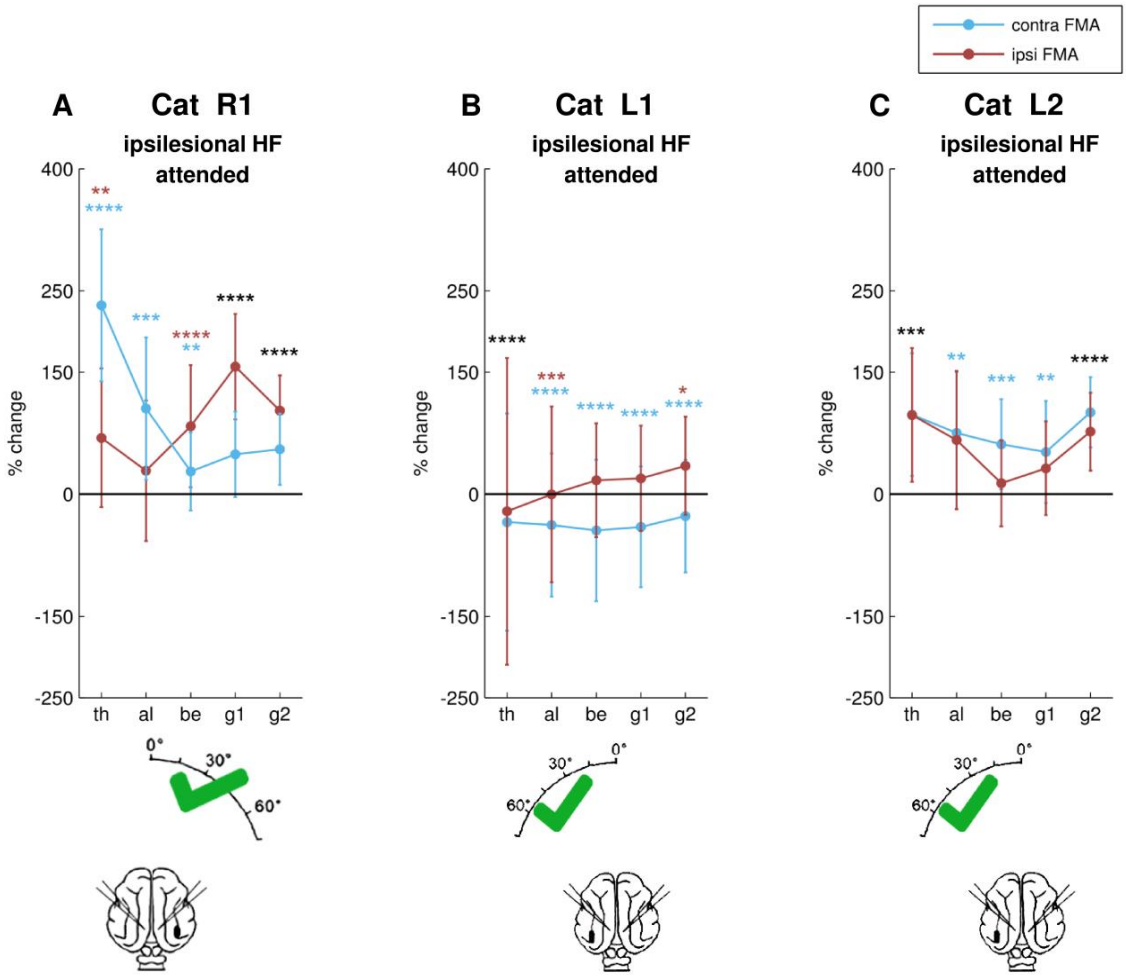

Figure 3.27 Normalized frequency band power changes for ipsilesionally attended targets in the entire post-lesion period. Shown is the percent change in power relative to the pre-lesion period. The cat brain icons below the plots illustrate the lesion site, the recording sites and the respective ipsilesional visual hemifield. The y-axis indicates the power change in percent relative to the pre-lesion period. The asterisks represent significant power differences in the 'ipsilesionally attended' condition relative to pre-lesional power. **(A)** Cat R1 showed a general power increase with a strong gain in the contralesional theta and alpha band and ipsilesional gamma 1 band. **(B)** Cat L1 displayed a highly significant reduction of contralesionally recorded oscillatory power. **(C)** In cat L2, the lesion produced also a bilateral enhancement of oscillatory power, which was strongest in the theta and high gamma bands. Cat R1: n = 671; Cat L1: n = 122; Cat L2: n = 613; (error bars: SD). Significant values were obtained by performing a Wilcoxon signed rank test (WSR). Other conventions and abbreviations as in Figure 3.21.

3.4.3 LESION-INDUCED CHANGES OF ONGOING ACTIVITY

In order to study endogenous (stimulus-independent) changes of oscillatory activity that were caused by the lesion and to reveal possible long-term mechanisms, which are related to a restoration of function, an analysis window ($AW_{baseline}$) between the fixation cue and the target LED was chosen. The $AW_{baseline}$ was part of the expectation phase and offered, due to the fixation performed by the cat, constant and therefore comparable conditions over the entire recording period. The main questions to be answered with this analysis were: (i) Does the neglect-syndrome manifest itself through an alternated neuronal baseline activity already at the early processing level of the primary visual cortex? (ii) Are changes that were caused by the loss of feedback-signals observable across the entire frequency spectrum or in a particular frequency range? (iii) Is a recovery of function on the behavioral level accompanied by a restoration of neuronal activity to pre-lesion levels? To answer these questions, the power of the averaged signal was calculated as above and the lesion-induced effects were quantified by computing a modulation index (MI) for each frequency band. The MI describes the ratio between the power in the single post-lesion periods and the power in the pre-lesion period in every frequency band. A MI less than zero corresponds to a decrease, a MI greater than zero means an increase in power relative to pre-lesional baseline power.

Cat L1 indicated a permanent, substantial reduction of contralesionally recorded baseline power across all frequency bands and it was highly questionable whether this finding was related to the neglect syndrome or rather generated by a different cause. Therefore, the results from cat L1 were excluded from this analysis.

3.4.3.1 *Comparative analysis of single frequency bands*

Cat R1

Immediately after the lesion, an increase in power across all frequency bands was observed in the impaired hemisphere (Figure 3.28 - Figure 3.30 cat R1, pl1). In the further experimental course, the ipsilesionally recorded delta power displayed a moderate fluctuation around the zero line (Figure 3.28 upper panel). For the last post-lesional period, a slight delta decrease in relation to the pre-lesion period was observed. However, this difference was not significant. The intact hemisphere showed a permanent decrease of delta band power throughout the entire experimental duration as compared to pre-lesion power levels.

The strongest changes in ipsilesionally recorded theta power were observed in the 1st and 9th post-lesional period (Figure 3.28, lower panel). Both periods indicated a pronounced increase in power relative to the pre-lesion period. The contralesionally recorded theta power was reduced in almost all post-lesional periods. Exceptions were the 9th, 10th and 12th post-lesion periods, which displayed an enhancement in theta oscillations.

The relative power in the alpha range indicated a substantial increase in the entire post-lesional period in both hemispheres (Figure 3.29, upper panel), that was strongest on the ipsilesional hemisphere during the acute phase of neglect (pl1). Together with the 2nd post-lesion period, these were the only two periods where the relative power increase on the ipsilesional recording site was larger than in the contralesional V1.

In the high-frequency range (beta, gamma1 and gamma2) the lesion led to a pronounced bilateral increase of oscillatory power (Figure 3.29, lower panel and Figure 3.30). For all three frequency-bands, the power enhancement was stronger on the impaired hemisphere than on the intact hemisphere.

Cat L2

Generally, cat L2 showed only moderate lesion-induced changes of oscillatory power in the low-frequency range (delta, theta and alpha band) with fluctuations around the zero line. However, directly after the pMS-lesion, the intact hemisphere indicated an enhancement whereas the impaired hemisphere displayed a decrease of oscillatory low-frequency power when compared to pre-lesional power levels (Figure 3.28 - Figure 3.30 cat L2, pl1). In the subsequent post-lesion periods 2 and 3, all three frequency bands indicated a bilateral power increase. With the exception of the contralesionally recorded alpha power, oscillations in the post-lesion periods were reduced bilaterally with respect to pre-lesional power.

The high-frequency range (beta, gamma1 and gamma2) displayed a bilateral power enhancement throughout all post-lesional periods (Figure 3.29, lower panel and Figure 3.30). Moreover, this increase was more distinct in the gamma range than in the beta band. A comparison between the two recording sites revealed in the intact hemisphere a substantially larger increase of power in the first post-lesion period.

Summary

Immediately after the lesion, both cats indicated an opposing pattern of low-frequency power alterations. In cat R1, an increase of power was observed on the impaired hemisphere whereas in cat L2 the intact hemisphere displayed an enhancement of oscillatory power.

A somewhat different picture emerged in the high-frequency range. Here, both cats showed a persistent bilateral increase of oscillatory power relative to pre-lesion power levels.

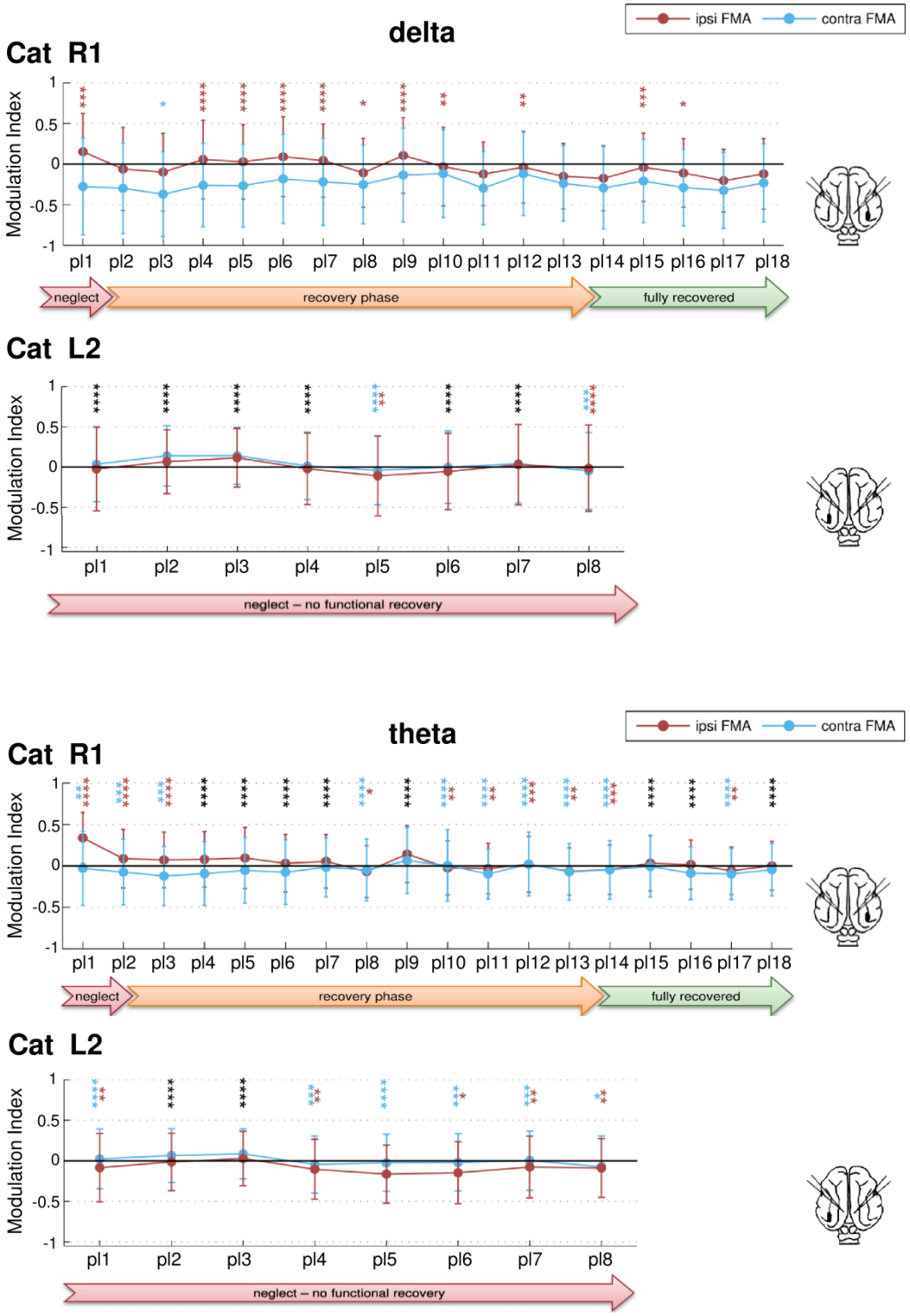

Figure 3.28 Lesion-induced changes in delta and theta band power of all post-lesional recording periods of cats R1 and L2. The lesion sites are depicted in the cat brain icons. The power changes are illustrated in relation to the pre-lesion period and expressed on the y-axis as modulation index (MI). The x-axis of each subplot holds the single post-lesional recording periods. Significant values were obtained by performing a Wilcoxon signed rank-test (WSR).Other conventions as in Figure 3.21 The timeline below the plots show the behavioral time course of the experiment. **(Cat R1)** The lesion resulted on the contralesional hemisphere in a lasting decrease of delta band power. In addition, ipsilesionally recorded delta and theta band was significantly increased in the acute phase of neglect. **(Cat L2)** Immediately after the lesion (pl1), the contralesional hemisphere indicated an increase, whereas the ipsilesional hemisphere showed a decrease of low-frequency power. number of trials are given in Figure 3.29.

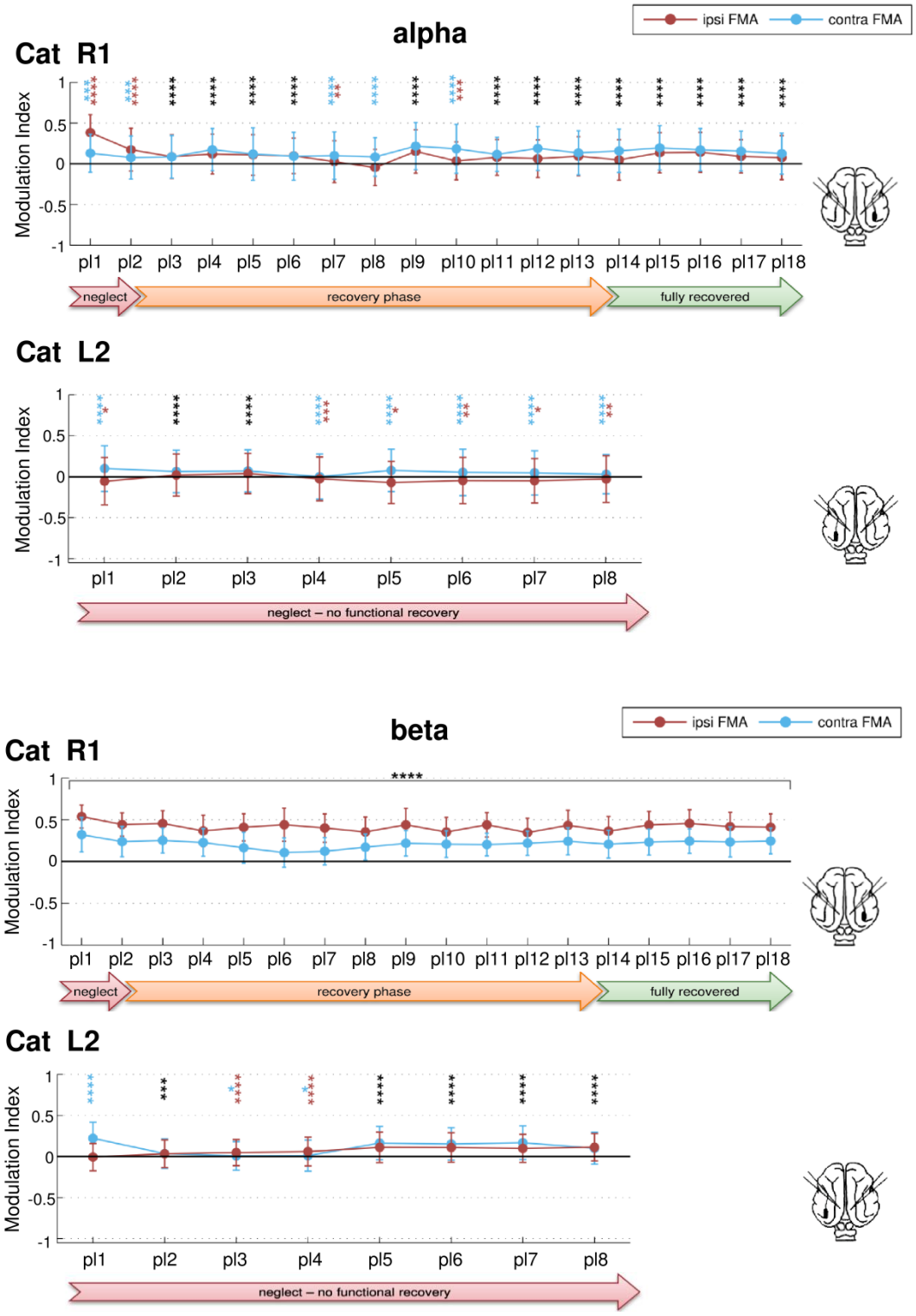

Figure 3.29 Lesion-induced changes in alpha and beta band power of all post-lesional recording periods of cats R1 and L2. (Cat R1) With the exception of post-lesion period 8, alpha band power was permanently bilaterally increased with a strong increase on the ipsilesional hemisphere in the acute neglect phase. In the beta band the lesion caused a persistent bilateral increase of oscillatory power that was stronger on the impaired hemisphere relative to the intact hemisphere. **(Cat L2)** The lesion caused a reduction of ipsilesionally recorded alpha band power whereas a bilateral enhancement of power was observed in the beta range. Other conventions as in Figure 3.28.
number of trials: R1:pl1:n = 22; pl2:n = 57; pl3:n = 68; pl4:n = 112; pl5:n = 86; pl6:n = 106; pl7:n = 90; pl8: n = 97; pl9:n = 124; pl10:n = 117; pl11:n = 72; pl12:n = 89; pl13:n = 215; pl14:n = 235; pl15:n = 121; pl16: n = 177; pl17:n = 128; pl18:n = 114; L2; pl1:n = 366; pl2:n = 472; pl3:n = 466; pl4:n = 459; pl5:n = 283; pl6: n = 207; pl7:n = 128; pl8:n = 117; (error bars: SD)

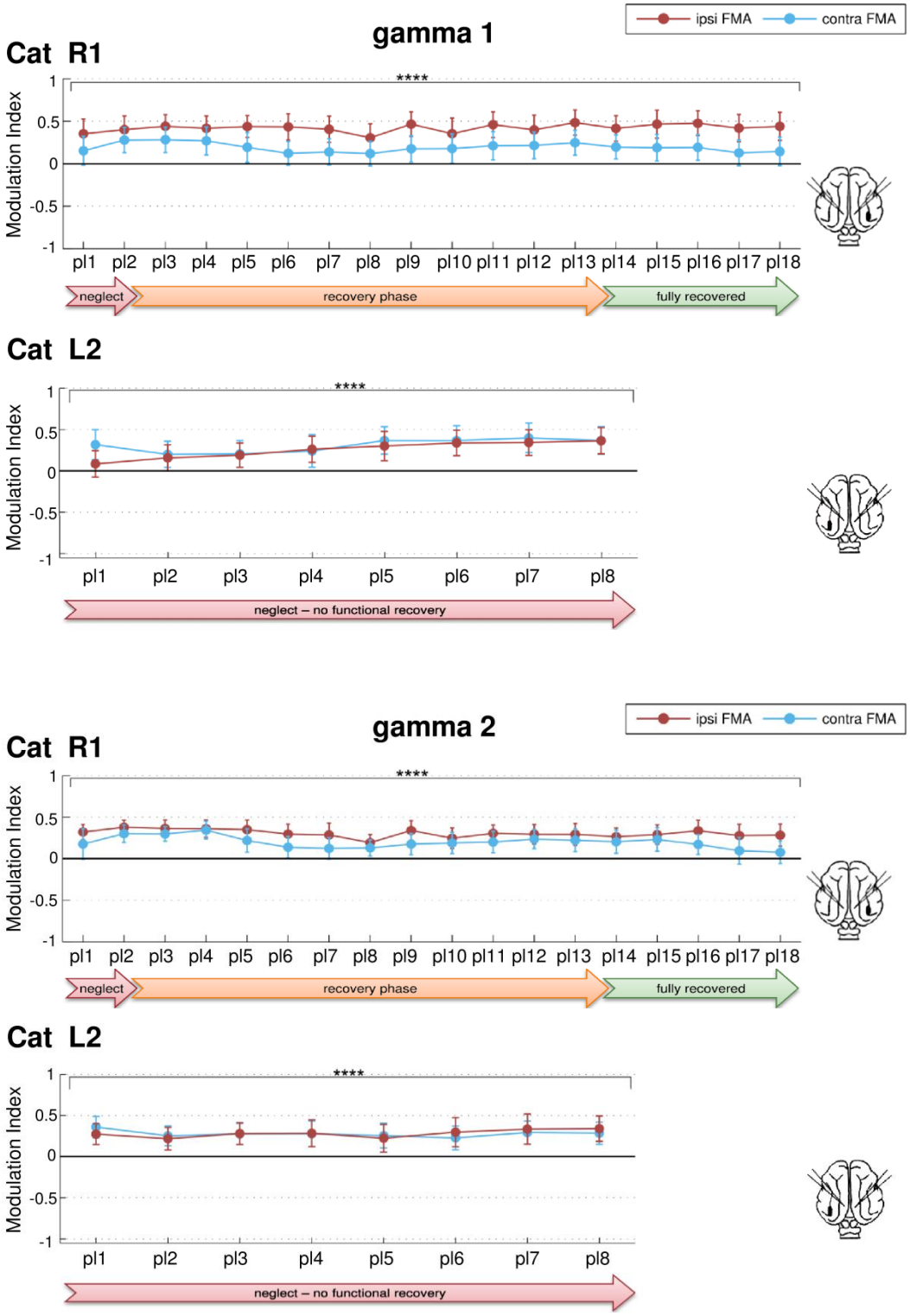

Figure 3.30 Lesion-induced changes in gamma band power of all post-lesional recording periods of cats R1 and L2. (Cat R1) In the gamma range the lesion caused a persistent bilateral increase of oscillatory power that was stronger on the impaired hemisphere than on the intact side. **(Cat L2)** With the exception of post-lesion period 1 the lesion resulted in a comparable power increase on both recording sites. Other conventions as in Figure 3.28.

3.4.4 LESION-INDUCED CHANGES OF INTERHEMISPHERIC COHERENCE

In order to investigate how the lesion affects interhemispheric interactions at the level of the primary visual cortices, the coherence between the two hemispheres was computed. The neuronal coherence is an estimator of synchrony between spatially distributed oscillatory signals. After calculating the coherence in a certain frequency range for every possible electrode pair, the obtained values were averaged. The changes in coherence for each post-lesion period were assessed relative to the pre-lesion period and expressed as percent change.

In this evaluation, the results of cat L2 were of particular interest, since this cat showed a lasting impairment in the detection and localization of contralesional static stimuli. Therefore, only the results of cat L2 are shown in Figure 3.31.

3.4.4.1 *Cat L2*

The most striking result was a sustained increase of interhemispheric coherence in the low frequency range that was strongest in the first four post-lesion periods (Figure 3.31). By contrast, the coherence in all other frequency ranges was permanently decreased relative to the pre-lesional interhemispheric coherence. The persistent increase of coherence in the low-frequency range was observed exclusively in cat L2. Moreover, the other two cats, R1 and L1, showed an increased coherence in this range only during the neglect phase. Therefore, this finding might provide an indication for neglect-associated changes of ongoing activity even in the early visual cortex.

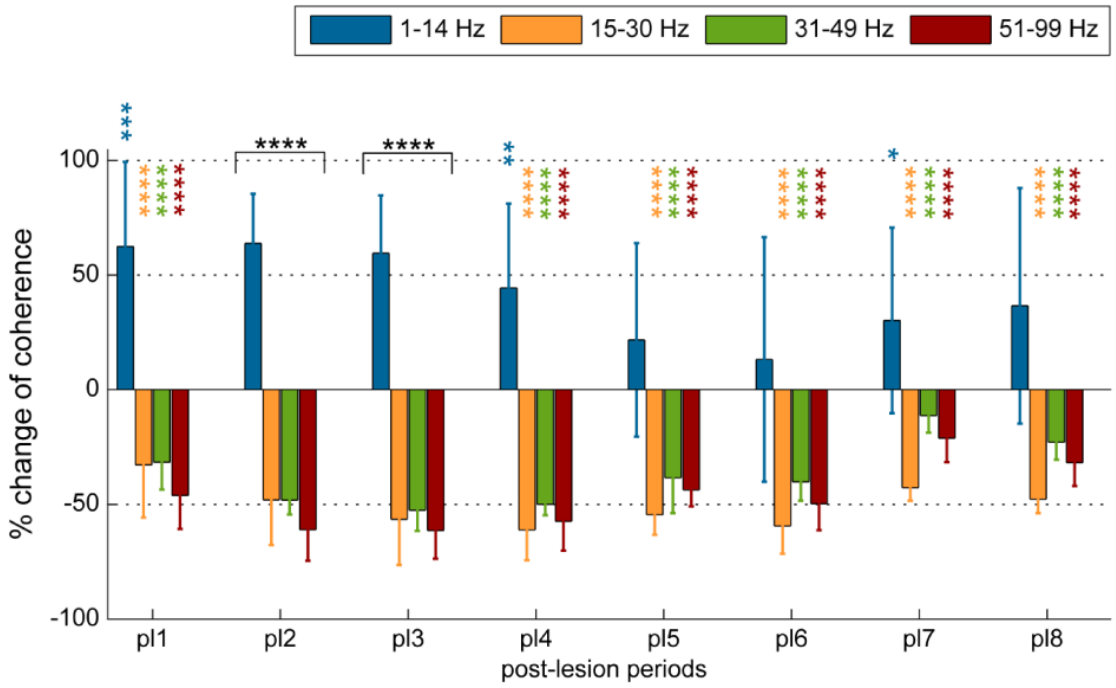

Figure 3.31 Changes of interhemispheric coherence in the primary visual cortex of cat L2. This cat exhibited over the entire experimental period no functional recovery. The figure shows changes of coherence in all post-lesion periods relative to the pre-lesion period in percent. The legend illustrates four different frequency ranges. The asterisks represent significant differences in coherence between the relevant post-lesion period and the pre-lesion period in the respective frequency range. Significant values were obtained by performing a Wilcoxon signed rank test (WSR). Same conventions as in Figure 3.27. Note the persistently increased coherence in the low-frequency range (blue bars).
number of trials: pl1: n = 366; pl2: n = 472; pl3: n = 466; pl4: n = 459; pl5: n = 283; pl6: n = 207; pl7: n = 128; pl8: n = 117; (error bars: SD)

4 DISCUSSION

4.1 METHODOLOGICAL CONSIDERATIONS

The investigation of neural network interactions in behaviorally relevant disorders, such as the neglect syndrome, requires electrophysiological recording in awake behaving animals. These experimental approaches, however, are often accompanied by a set of challenges, which complicate experimental control, and interpretation of results. In the present study, FMAs were used to record from behaving cats over a period of several months. These electrode arrays, specifically designed for long-term chronic applications, provided high quality and stable recordings of LFP-signals over the entire experimental time course. Moreover, post mortem histology showed minimal damage in the tissue surrounding the electrodes (3.3.3). However, a drawback of chronic recordings is the ongoing gliosis around the electrode tip. This glial scarring is known to decrease the signal-to-noise ratio over time (Suner *et al.*, 2005; Griffith & Humphrey, 2006). An additional drawback of the chronic electrodes is the predefined position of electrodes within an array, which does not allow for targeted recording from specific single units.

Another major issue related to the experimental design is the considerably high degree of variability in the results due to inherent individual and inter-individual differences in performance and motivation levels. This had a direct effect on the number of trials for each experimental condition. Consequently, to avoid a bias in favor of one of the cats, rather than grouping the data, a comparative analysis was chosen to evaluate the dataset.

4.1.1 EFFECTS OF LESION SIZE AND DIMENSION ON FUNCTIONAL QUALITIES

In vision research, lesion studies in animals have provided important insights in the functional interactions between network components and the neural processes that guide behavior. Despite the numerous advantages of using ibotenic acid lesions to selectively deactivate a network structure, there are certain limitations to this technique. One difficulty lies in the control of the spread of ibotenic acid. The histological results of cat L1 revealed a large encroachment of the neurotoxin into several regions distant from the injection site, which presumably affected the results of the frequency analysis. Cat L1 indicated a general power decrease within all frequency ranges on the contralesional hemisphere. Importantly, no power differences between the two hemispheres or between the three cats were obvious prior to the lesion (3.4.2.2 Fig. 3.26). This finding implies that the ibotenic acid might have affected cortical circuits that have an impact on interhemispheric interactions.

Besides the undesired diffusion of ibotenic acid, the precise targeting of ibotenic acid injections based on stereotactic coordinates could also pose a problem due to a pronounced variance in the macroscopic as well as in the functional structure of the suprasylvian region (Otsuka & Hassler, 1962; Hubel & Wiesel, 1969b; Sherk, 2010). It is therefore likely that in cat L2 the ibotenic acid led to a lesion not only in the pMS region but also in portions of the anterior middle suprasylvian (aMS) cortex. As already mentioned in the introduction, it has been demonstrated that an additional lesion in the aMS regions produces a profound and long-lasting deficit in visual orienting behavior (Lomber *et al.*, 2006).

4.2 INTERPRETATION OF THE STIMULUS-RELATED RESPONSE SIGNATURE IN THE LFP

Based on the results obtained in this study, three major implications regarding top-down processes and their affects on hemineglect can be made:

I. The response signature elicited by the stimulus constitutes a recurrent feedback signal

Several lines of evidence support this hypothesis. First, in all three cats the receptive fields (RF) of the recorded neural populations are mainly located around the 30° eccentricity in the lower visual hemifield (3.1.3). Thus, one would expect strong feedforward activity to be almost exclusively elicited by stimuli appearing at the 30° position, in particular, in the RFs of the recorded neuronal population. The response signature, however, is visible in the channel averaged LFP whenever the cat attended to either the fixation cue or to the target LED, independent of its position (3.1.1). Therefore, it is unlikely that the response signature is a net stimulus-induced feedforward signal. Presumably, the feedforward activation evoked by the static LED is too weak to be detected and averaged out in the further course of the analysis. Compared to a moving stimulus or a stimulus covering a larger part of the visual field, the static LED has a low inherent physical salience and activates a smaller neuronal population.

The idea that the response signature constitutes a recurrent feedback signal is further supported by the late onset of peak latencies found in the ERP (3.1.2). Studies examining the response latencies at different stages along the visual pathway in the cat found in area 18 a mean firing onset of 40 ms following stimulus presentation (Dinse & Krüger, 1994). In addition, the onset latency of the stimulus-locked visual evoked potential (VEP) in area 18 was found to be around 40 ms (Salazar *et al.*, 2004). By comparison, in the present study, the first visible ERP component occurred at the earliest 90 ms after LED onset.

A third observation was the temporal variability in response to the 1st and 2nd LED. The peak onset of the first component (N1) in response to the target LED was always earlier than in response to the fixation cue, even when both were presented at the same location in the visual hemifield. Furthermore, the N1 peak latency was positively correlated to the target LED distance from the central position (Figure 4.1.). Both findings imply that the onset latency of the response signature is partly determined by internal aspects, such as relevance criteria and partly by external features like the stimulus position within the visual field. The earlier onset of N1 in response to the target LED

likely reflects a higher significance of the target LED relative to the fixation cue, since only correct responses to the 2nd LED were rewarded with a high incentive food reward. Support for this hypothesis comes from studies on top-down attention showing that enhanced top-down signaling leads to improved task performance and shorter reaction times (Carrasco, 2011). Importantly, the effects of spatial attention can vary for the center and the periphery; it has been proposed that the orienting of attention describes a bell-shaped distribution along the horizontal axis (Karnath *et al.*, 1996; Karnath, 1997).

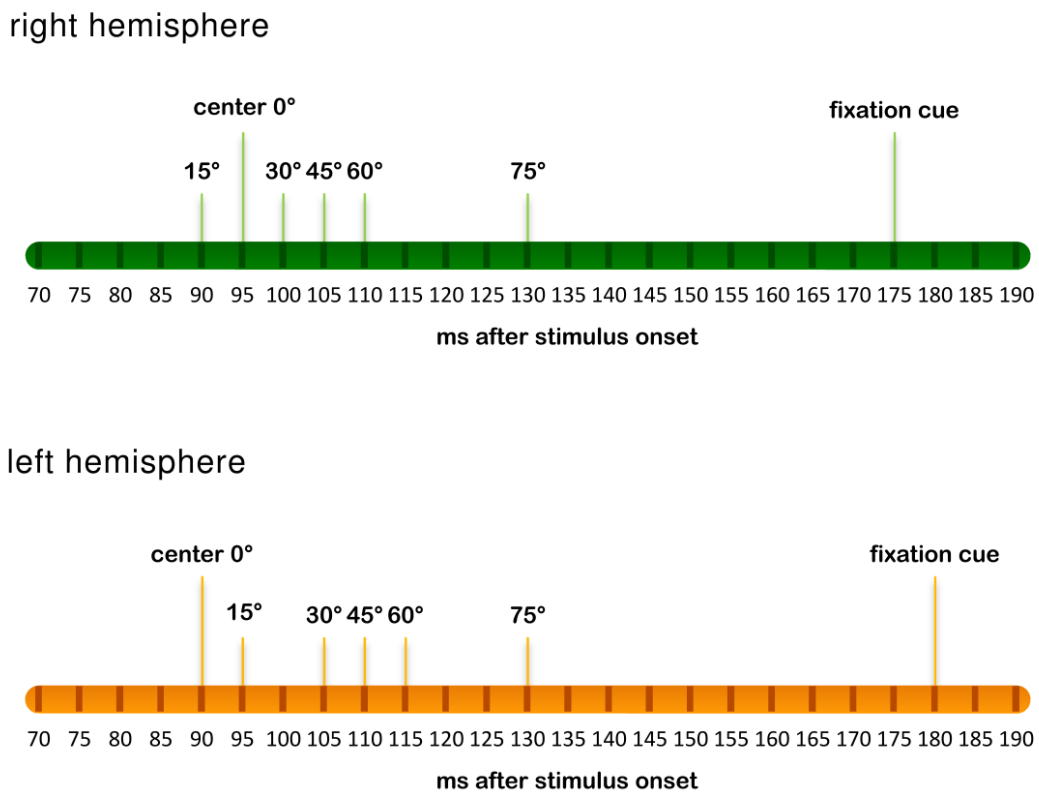

Figure 4.1 Timeline of ERP N1 peak latencies in response to the fixation cue and to different locations of the target LED The upper row shows the N1 peak latencies recorded in the right hemisphere, the lower row the respective results obtained from the left hemisphere. The N1 component in response to the fixation cue occurred always later than in response to any target LED. A comparison of N1 peak latencies in response to different target LED locations revealed a later N1 occurrence the more peripheral a stimulus was located.

II. The response signature is characterized by activation in distinct frequency ranges – functional implications

Spectral analysis of the response signature revealed a significant increase of oscillatory theta and alpha power together with a minor increase of power in the high gamma range (3.4.1).

Synchronous oscillatory activity has long been known to play a crucial role in the integration of sensory signals across multiple cortical scales (Singer & Gray, 1995). Moreover, it has been proposed that different frequency bands reflect different features of the integrated signal. Specifically, feedforward and feedback components are believed to oscillate in distinct frequency ranges and therefore could be used to measure the direction of information transmission (van Kerkoerle *et al.*, 2014; Bastos *et al.*, 2015).

It has been suggested that low-frequency oscillations, particularly in the theta and alpha range, predominantly reflect top-down processes whereas gamma oscillations primarily but not exclusively have been related to bottom-up processing (von Stein & Sarnthein, 2000; Engel *et al.*, 2001; Bressler & Richter, 2014; van Kerkoerle *et al.*, 2014). Besides its general role in long-range communication, theta oscillations have also been found to play a critical role in working memory, episodic-memory encoding and spatial navigation (Kahana *et al.*, 2001; Jensen & Tesche, 2002; Rizzuto *et al.*, 2003). In this context, the existence of theta- synchronized recurrent loops of neural activity between the cortex and the hippocampus has been proposed by several authors (Miller, 1991; Young, 2011; Lega *et al.*, 2012).

It is also possible, however, that low- and high-frequency ranges simultaneously cooperate to integrate neural activity across different spatial and temporal scales (Canolty & Knight, 2010). Theta-gamma and alpha-gamma cross-frequency interactions have been claimed to play an important role in learning, memory and attention (Bruns & Eckhorn, 2004; Canolty *et al.*, 2006; Osipova *et al.*, 2008; Sauseng *et al.*, 2008; Holz *et al.*, 2010).

To summarize, these findings provide further support to the idea that the response signatures as observed in the current paradigm in area 18, are dominated by recurrent feedback activity. However, it is important to note that due to the integrative character of sensory processing, a complete dissociation of feedforward and feedback signals is almost impossible.

III. In the neglect condition, the response signature is absent

When a target was behaviorally neglected, the corresponding response signature was absent as revealed by the results from the raster LFP (3.4.1.1) and time-frequency analysis (3.4.1.2). Likewise, in the neglect situation an ERP was not elicited.

One possible explanation for this observation could be that the respective LED stimulus may not reach the cortical processing level due to neglect-induced disturbances already on the subcortical level or within the thalamocortical network. It has been demonstrated that a lesion in the parietal cortex results in an activity decrease in the ipsilesional SC accompanied by a simultaneous increase of activity in the contralesional SC (Hardy & Stein, 1988; Hilgetag *et al.*, 1999). In this regard, the pattern of anatomical connectivity, as described in the introduction (1.4.3.3), suggests that damage to the parietal region also might have substantial impact on the LGN and the LP pulvinar complex. Consequently, disturbances in sensory processing at the level of the LGN, the main cortical input source of visual signals, raises the possibility that a visual stimulus is not transmitted to the cortex for further processing. However, two important experimental findings from earlier studies tend to work against this hypothesis. First, Marshall and Halligan (1988) demonstrated in a case study that neglected stimuli are processed at some level, although not consciously. In their study, a patient was presented with two drawings of a house, in one of which the neglected side was on fire. As expected, the patient reported that the two houses were identical. However, when asked in which house she would prefer to live in, she reliably chose the non-burning house at a level well above chance. Second, EEG studies that compared the transient visual-evoked potentials (VEPs) to neglected and non-neglected stimuli showed that bottom-up processing up to 130 ms is not impaired in neglect patients and that neglect specific deficits, in the form of VEP amplitude and latency changes, occur at the level of feedback reactivation of the primary visual cortex (Di Russo *et al.*, 2008).

Under the assumption that in visual neglect the primary visual cortex is indeed activated by stimuli, even though they escape awareness, another interpretation of the current findings could be that the lesion produces a deficit in attentive vision. Lamme and Roelfsema (2000) proposed a dichotomy between attentive and pre-attentive visual processing and identified the former with recurrent (feedback) activation and the latter with feedforward activation. The authors further suggested that low-level areas such as V1 are involved in pre-attentive vision whereas higher-order areas in the parietal region are involved in attentive vision. Thus, when a stimulus is presented, the initial (< 80 ms) stimulus-locked response, mediated by feedforward signals is followed by recurrent

feedback signals at longer latencies. These recurrent feedback signals are thought to mainly reflect cognitive or behavioral aspects of sensory processing.

Interestingly, an electrophysiological study assessing V1 activity changes in a 'stimulus detected' versus 'stimulus not detected' paradigm carried out in the monkey, demonstrated that a late component (> 100 ms), representing contextual modulation, was selectively suppressed when the stimulus was not perceived (Supèr *et al.*, 2001). Importantly, the preceding neuronal activity pattern did not differ in the 'seen' condition from that in the 'not seen' condition indicating that the stimulus reached the primary visual cortex in both cases. Based on these findings, the authors suggested a specific role for recurrent feedback processing when a stimulus reaches a perceptual level of processing.

In this context, the recurrent feedback signals from the pMS region to the primary visual cortex and the SC may be essential to attentively perceive the stimulus and to trigger attentional orienting behavior. Consequently, damage to the pMS cortex results in a lateralized disruption of attentive vision.

4.3 Neglect in the context of the interhemispheric imbalance model: Evidence for strong interactions between the two hemispheres

According to the hypothesis of Payne and Rushmore (2004,) in the cat the orienting deficit in hemineglect is the consequence of an interhemispheric imbalance of activity levels. Unilateral damage to the parietal regions results in a disinhibition and subsequent hyperexcitability of the intact hemisphere and increased (pathological) inhibition of the impaired hemisphere.

The results obtained in the present study indeed suggest a hyperactivation of the intact hemisphere. This was shown by an enhancement of oscillatory power in the response signature to ipsilesionally presented stimuli (3.4.2.2) and a substantial decrease of ERP peak latencies relative to the pre-lesion period (3.4.2.1). Interestingly, this stronger activation in response to ipsilesional targets occurred in *both* hemispheres. To summarize, these findings support the idea that the orienting deficit in neglect is partly based on a hyperexcitability of the intact hemisphere. However, ipsilesionally presented stimuli elicited an exceedingly strong response signature in both primary visual cortices, leading to a more complex picture of interhemispheric interactions presumably mediated through the corpus callosum.

4.3.1 UNDERLYING CIRCUITS OF INTERHEMISPHERIC COMMUNICATION

Visual cortical areas of the two hemispheres are interconnected by fibers belonging to the corpus callosum. In the primary visual cortex, the callosal connections originate in the area 17/18 transition zone, corresponding to the representation of the vertical meridian (Hubel & Wiesel, 1967; Houzel *et al.*, 1994). Anatomical studies have demonstrated that these reciprocal callosal connections terminate in regions of contralateral areas 17, 18, 19 and the pMS sulcus, representing the vertical midline (Sanides, 1978; Segraves & Rosenquist, 1982) (Figure 4.2, top). By contrast, it has been found that the callosal connections between the two pMS sulci were not restricted to the narrow midline representation of the visual field and can reach 50° or more into the ipsilateral hemifield (Antonini *et al.*, 1983) (Figure 4.2, bottom). Besides these projections that connect the two pMS sulci, it is also known that area 18 receives direct input from the contralateral MS region (Payne & Lomber, 2003).

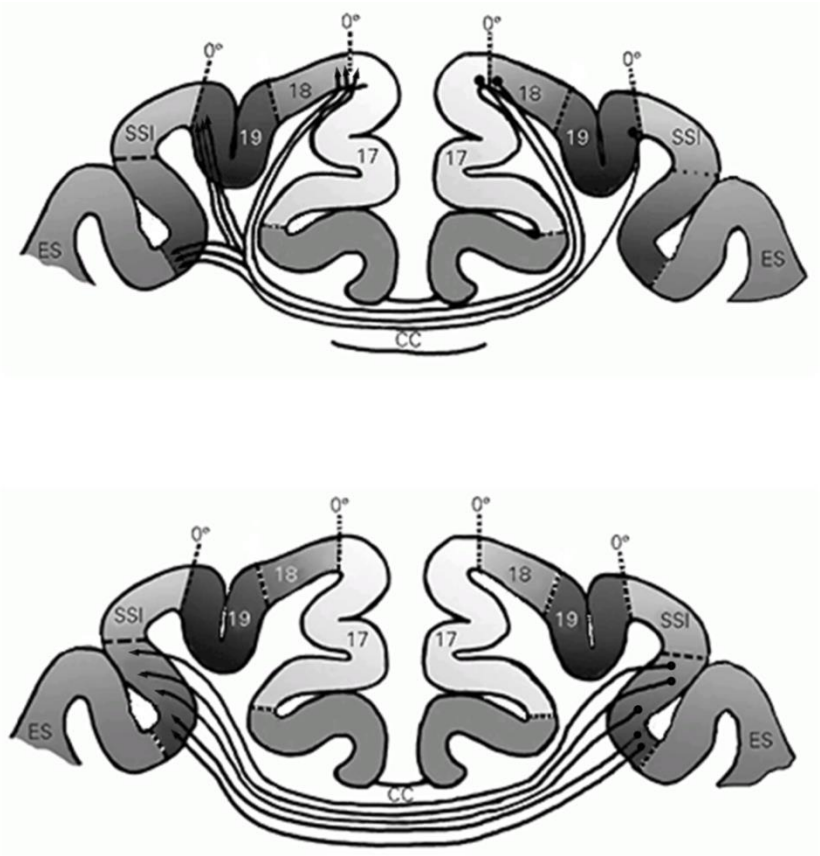

Figure 4.2 The distribution of callosal fibers in the primary visual cortex and the MS region of the cat. Upper diagram: Fibers originating in the area 17/18 transition zone project to several areas representing visually equivalent points along the vertical midline (0°). Lower diagram: Fibers connecting the two pMS sulci are not restricted to the narrow representation of the vertical meridian. Abbreviations: CC, corpus callosum; ES, ectosylvian cortex; SSI, suprasylvian cortex. Adapted from Aboitiz and Montiel (2003).

On the functional side, it has been shown that the callosal input can both facilitate and attenuate interhemispheric interactions in a stimulus-dependent manner, although most of the callosal fibers are excitatory (Innocenti, 1986, 2009; Makarov *et al.*, 2008). It has been proposed that a key function of the corpus callosum is the establishment of interhemispheric neuronal assemblies by synchronizing the activity of neurons in the two hemispheres, which is a prerequisite for the integration of lateralized input signals for further higher-order processing and unified motor responses (Engel *et al.*, 1991; Stephan *et al.*, 2003; Pietrasanta *et al.*, 2012).). In this context, it is conceivable that the strong responses on the impaired side evoked by ipsilesionally presented stimuli are mediated by excitatory feedback signals originating in the contralateral pMS region (Fig. 4.3). Without the feedback signals from the lesioned pMS the contralateral VP cortex becomes now the dominant source for synchronizing feedback input to both primary visual cortices. This idea is further supported by the finding that the activation pattern of both hemispheres in response to ipsilesional stimuli has a similar shape (3.4.2.2), thus suggesting a common input to both hemispheres. Moreover, the lesion-induced loss of contralateral feedback signals from the impaired pMS to area 18 in the intact hemisphere could provide a possible explanation for the stronger activation in response to ipsilesional vs. contralesional stimuli.

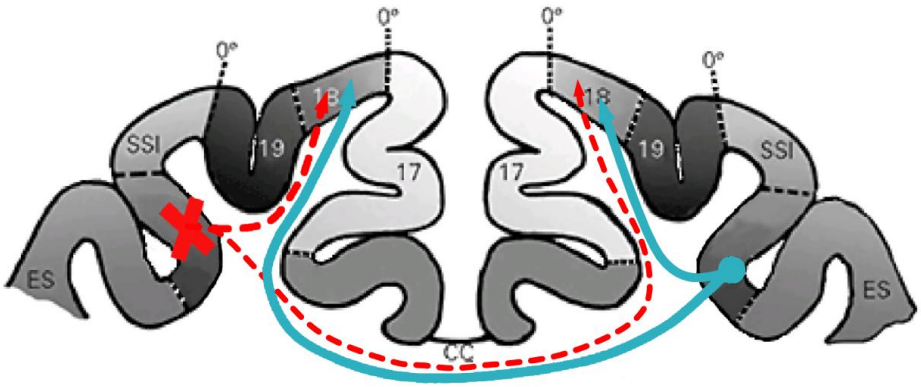

Figure 4.3 Altered feedback input to area 18 after a unilateral lesion of the pMS cortex. Without the feedback signals from the lesioned pMS (depicted in red dashed lines) the contralateral VP cortex becomes now the dominant source for feedback input to both primary visual cortices (depicted in blue lines). Abbreviations as in figure 4.2. Modified from Aboitiz and Montiel (2003).

However, the corpus callosum is not the only pathway connecting the two hemispheres. For example, the two superior colliculi communicate via the intercollicular commissure. Importantly, collicular interactions have been shown to be predominantly inhibitory and unilateral damage to the SC results in a robust inhibition by the contralateral SC and induces a profound neglect (Waleszczyk *et al.*, 1993; Hilgetag *et al.*, 1999; Payne & Rushmore, 2004).

4.3.2 POSSIBLE MECHANISMS UNDERLYING NEGLECT

In line with the predictions made in the interhemispheric imbalance model, the results clearly indicate a lesion-induced hyperexcitability of the intact hemisphere in response to ipsilesionally presented stimuli. Intriguingly, however, no indications for inhibitory mechanisms affecting the compromised hemisphere have been found in the present study. By contrast, ipsilesionally presented stimuli evoked stronger and faster responses on both sides (3.4.2.; Figure 3.24 and 3.25). Taken together, these findings argue against the existence of a functional mutual inhibition between the two hemispheres on the cortical level. Additional support for this view comes from studies in humans and primates, where it has been shown that sectioning the corpus callosum increases and not, as predicted by the inhibition model, reduces the severity of hemineglect (Watson *et al.*, 1984; Heilman & Adams, 2003).

Another conclusion, which can be drawn from the analysis of the ongoing activity (3.4.3), is that hemineglect does not introduce a hemispheric imbalance, in the form of a push-pull pattern, of activity levels *per se*. These results differ from the observations made by Corbetta et al. (2005) in an fMRI study with neglect patients. By using the Blood Oxygenation Level Dependent (BOLD) signal the authors found a relative imbalance of activity in the visual cortex with a hyperactivation of the intact hemisphere and a relative hypoactivation of the impaired side. Although their findings support the interhemispheric imbalance hypothesis, it is highly questionable whether the observed fMRI BOLD push-pull pattern between the hemispheres reflect functional changes that are specific to the neglect syndrome. In fact, there is growing evidence that stroke has a systematic effect on the BOLD signal in perilesional areas, as shown by de Haan and colleagues (2013). They observed an abnormal interhemispheric imbalance of the BOLD signal, similar to that reported by Corbetta et al. (2005) , in right hemisphere damaged patients without neglect performing a non-spatial attention task. To conclude, the interhemispheric imbalance observed in the fMRI BOLD signal may not necessarily underlie the subjects' spatial hemineglect. Rather a loss of balance in the integration of endogenous and exogenous components seems to be a key mechanism underlying visual hemineglect. This idea is largely consistent with the attentional priority account of neglect, already mentioned in the introduction (1.2.4). In this theoretical framework, the parietal region integrates bottom-up and top-down signals to compute a spatial representation of attentional priority (priority map) (Serences & Yantis, 2006). Accordingly, unilateral damage to this region should cause disturbances in the spatial distribution of attention (Ptak & Fellrath, 2013).

Based on studies with monkeys and human neglect patients, it has been proposed that a parietal lesion results in an ipsilesional bias of attentional orienting, i.e. a shift of the bell-shaped distribution of attention toward the ipsilesional side (Figure 4.4) (Karnath, 1997; Karnath *et al.*, 1998; Pouget & Driver, 2000; Ptak *et al.*, 2009).

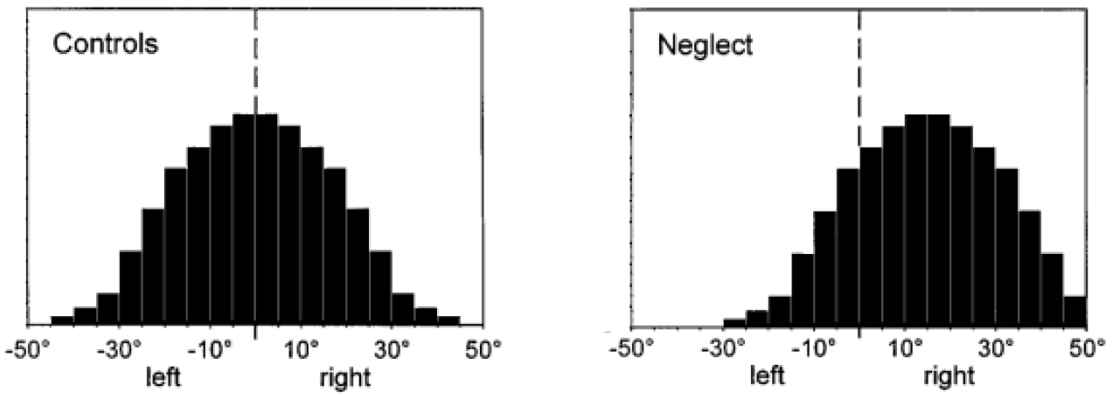

Figure 4.4 Theoretical distributions of attention along the horizontal axis in healthy participants (left panel) and in neglect patients (right panel). Neglect patients show a pathological bias of attentional orienting toward the ipsilesional visual hemifield. Adapted from Karnath (1997).

Importantly, the ipsilesional shift of the attentional focus stands in contrast to the interhemispheric imbalance model that predicts a laterally increasing gradient of attentional orienting with its maximum at the most peripheral margin of the non-neglected hemifield (Kinsbourne, 1970b; Payne & Rushmore, 2004; Corbetta & Shulman, 2011). Consequently, the performance level for peripheral targets in the ipsilesional visual hemifield should be markedly improved during the acute neglect phase. However, in contrast to this prediction the analysis of the behavioral performance of all three cats did not show an increase in performance levels for peripheral targets in the ipsilesional hemifield (Figure 4.5). Moreover, the observed pattern in the neglect condition largely resembled the predicted ipsilesional bias, with an increase in performance only observable for center near stimulus locations.

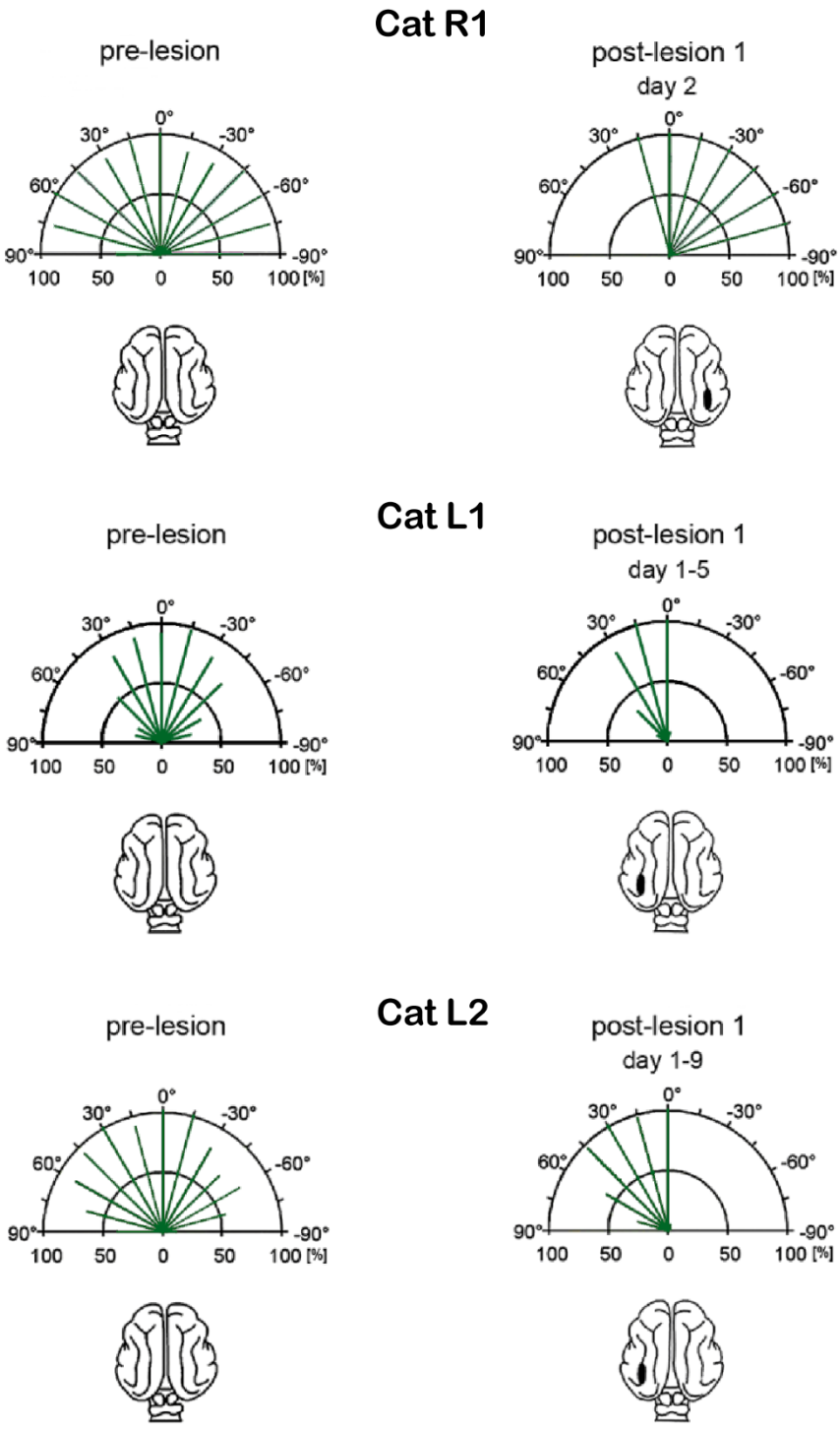

Figure 4.5 Distributions of attentional orienting before and after a lesion in the pMS cortex of the three cats used in the current study. During the acute neglect phase (right column) performance level toward the ipsilesional visual hemifield largely resembled the individual pre-lesion performance. An increased performance was only observable for center near stimulus locations. See figs. 3.6, 3.7, and 3,8 for conventions and number of trials.

The attentional priority hypothesis could also provide a possible explanation for the large bilateral activation in response to ipsilateral targets (3.4.2). According to this concept, damage to the parietal region results in increased priority (in the form of stronger activation) of ipsi- relative to contralesional representations. The outcome would be, that ipsilesional stimuli have competitive advantages and are, therefore, selected by a "winner-takes all" - mechanism of attentional selection (Ptak & Fellrath, 2013). Subsequently, this strong priority signal that is given to stimuli in the ipsilesional visual hemifield is then transmitted via the altered feedback pathways (Figure 4.3) to both primary cortices. In this view, the bilaterally enhanced response signature would be the partial reflection of an attentional priority signal.

The strong interhemispheric coherence in the theta (and alpha) range during the expectation phase (3.4.4) gives rise to an alternative hypothesis about the underlying mechanisms of neglect that is closely related to the concept of an attentional priority map. Theta oscillations play a key role in coordinating interactions between the hippocampus, a structure crucial for learning and memory processes, and the neocortex (Jones & Wilson, 2005; Siapas *et al.*, 2005; Sirota *et al.*, 2008; Battaglia *et al.*, 2011). Interestingly, oscillatory theta coherence has been found to occur between the hippocampus and prefrontal cortical regions and between the hippocampus and the parietal cortex during task conditions that required spatial working memory (Jones & Wilson, 2005; Sirota *et al.*, 2008). In light of this, Whitlock and colleagues (2008) hypothesized that the parietal cortex transforms coordinate information from spatial maps formed by grid cells in the entorhinal cortex and place cells in the hippocampus into a body-centered spatial representation necessary for goal-directed motor actions. Damage to the parietal cortex would lead to a failure to construct one half of the spatiotopic mental map and, subsequently, to an incomplete representation of the environment. The high theta coherence between the two hemispheres may be an indicator for such a deficient coordinate system that is dominated by the spatial representation of only one side.

4.4 Neglect and Recovery

At the behavioral level, analysis of the course of recovery revealed a characteristic spatial pattern (3.2.1 and 3.2.2). In both cats R1 and L1, recovery started with the central stimulus locations and continued to more peripheral target locations, thus, suggesting a gradual reduction of the previously discussed pathological spatial bias. By contrast, cat L2 displayed a lasting impairment in the detection and localization of contralesional stimuli. However, this lasting deficit was only restricted to static but not moving stimuli. The capacity to respond to a moving target, as tested with a laser pointer, recovered within a week. Such a stimulus domain dependent recovery has been previously described in cats by Rushmore et al. (2010). The authors suggested a redundancy of function for the detection of moving but not static stimuli and identified the ipsilesional SC as the most likely structure that mediates this function. In fact, the network character of the visual system with its multiple and parallel feedforward and feedback pathways strongly argues, at least to some degree, for redundancy of function (cf. Figure 0.1). Another important aspect that could account for this behavioral difference in response to static versus moving stimuli might be the perceptual salience of these two types. While the onset of the static LED, due to its small size, only activates a few neurons in a small portion of the visual field, the moving stimulus activates a large neuronal population as it moves across a larger area of the hemifield. In this context, and under the assumption that neglect reflects a unilateral failure to integrate saliency information with top-down signals (Ptak & Fellrath, 2013) one could make the following two predictions for the course of a functional recovery from neglect. First, a gradual amelioration of the pathological spatial bias, similar to the findings of the present study, should be observable and second, stimuli that are more salient should have a higher probability to be attentively perceived than less salient stimuli. Possibly, this is reflected in the results of cat L2.

At the neuronal level, a comparison of frequency-band power changes between ipsilesionally attended and recovered stimulus locations revealed substantial differences in the strength of the concomitant response signature (3.4.2.2 I.). Notably, the general shape of the response signature with the characteristic increase in the theta, alpha and high gamma range was preserved but the magnitude of power increase was approximately twice as large in response to ipsilesional targets as in response to recovered stimuli. These differences in activation strength for ipsi- and contralesional stimuli possibly indicate generally stronger representations of ipsilesionally appearing stimuli and might also underlie the emergence of visual spatial extinction, a deficit that frequently occurs in humans (Driver & Mattingley, 1998; Mesulam, 1999; Driver & Vuilleumier, 2001)

and in cats (Payne & Rushmore, 2004) during the course of recovery from neglect. In visual extinction individual stimuli in both visual hemifields are perceived correctly, but when contralesional stimuli are presented simultaneously with an ipsilesional stimulus, the contralesional stimulus is neglected. This deficiency may indicate a lasting deficit of the impaired hemisphere that is most prominent in competitive situations.

5 CONCLUDING REMARKS AND FUTURE RESEARCH

The research reported in this thesis has investigated the impact of pMS-lesions and the consequent loss of feedback signals on neuronal dynamics in primary visual cortex and has monitored activity changes related to a behavioral restitution. The findings have demonstrated that even in this early visual processing stage, neuronal activity patterns are highly modulated by internally generated goal-related signals. Furthermore it has been shown that a lesion-induced deficit in orienting behavior is accompanied by a selective and full suppression of the late feedback component of sensory processing signals thereby adding support to our understanding of neglect as a post-sensory phenomenon that is directed to an internal representation (Mesulam, 1999). Future studies using a more salient stimulus (e.g. moving targets) that evokes stronger feedforward activation should be performed. In combination with the present findings this could provide a more differentiated picture of feedforward and feedback activity changes in neglect and the subsequent processes of behavioral restitution.

Another major finding was a pronounced hyperactivation in response to stimuli in the non-neglected visual hemifield that appeared in both hemispheres. This result has led to the suggestion that, at least at the cortical level, the neurophysiological basis of neglect is more complex than a mere push-pull pattern of activity levels, as proposed by Payne and Rushmore (2004) in the interhemispheric imbalance model of neglect. However, it is important to note that the focus of this study has been on a single component of a highly complex network. To further elucidate the role of feedback signals to the primary visual cortex and to develop a full picture of the mechanisms underlying neglect, further studies are needed that also include electrophysiological recordings from the contralesional pMS cortex. Possibly, these simultaneous recordings from area 18 and pMS cortex could be compared to recordings from the ipsilesional aMS cortex in order to examine its role in the recovery of function in neglect more closely.

6 BIBLIOGRAPHY

Aboitiz, F. & Montiel, J. (2003) One hundred million years of interhemispheric communication: the history of the corpus callosum. *Braz. J. Med. Biol. Res.*, **36**, 409–420.

Abramson, B.P. & Chalupa, L.M. (1985) The laminar distribution of cortical connections with the tecto- and cortico-recipient zones in the cat's lateral posterior nucleus. *Neuroscience*, **15**, 81–95.

Abramson, B.P. & Chalupa, L.M. (1988) Multiple pathways from the superior colliculus to the extrageniculate visual thalamus of the cat. *J. Comp. Neurol.*, **271**, 397–418.

Albus, K. (1979) 14C-deoxyglucose mapping of orientation subunits in the cats visual cortical areas. *Exp. brain Res.*, **37**, 609–613.

Albus, K. & Beckmann, R. (1980) Second and third visual areas of the cat: interindividual variability in retinotopic arrangement and cortical location. *J. Physiol.*, **299**, 247–276.

Antonini, A., Berlucchi, G., & Lepore, F. (1983) Physiological organization of callosal connections of a visual lateral suprasylvian cortical area in the cat. *J. Neurophysiol.* , **49** , 902–921.

Arend, I., Machado, L., Ward, R., McGrath, M., Ro, T., & Rafal, R.D. (2008) The role of the human pulvinar in visual attention and action: evidence from temporal-order judgment, saccade decision, and antisaccade tasks. *Prog. Brain Res.*, **171**, 475–483.

Awh, E., Belopolsky, A.V., & Theeuwes, J. (2012) Top-down versus bottom-up attentional control: a failed theoretical dichotomy. *Trends Cogn. Sci.*, **16**, 437–443.

Baluch, F. & Itti, L. (2011) Mechanisms of top-down attention. *Trends Neurosci.*, **34**, 210–224.

Bartolomeo, P. (2007) Visual neglect. *Curr. Opin. Neurol.*, **20**, 381–386.

Bartolomeo, P. & Chokron, S. (2002) Orienting of attention in left unilateral neglect. *Neurosci. Biobehav. Rev.*, **26**, 217–234.

Bastos, A.M., Vezoli, J., Bosman, C.A., Schoffelen, J.-M., Oostenveld, R., Dowdall, J.R., De Weerd, P., Kennedy, H., & Fries, P. (2015) Visual areas exert feedforward and feedback influences through distinct frequency channels. *Neuron*, **85**, 390–401.

Battaglia, F.P., Benchenane, K., Sirota, A., Pennartz, C.M.A., & Wiener, S.I. (2011) The hippocampus: Hub of brain network communication for memory. *Trends Cogn. Sci.*, **15**, 310–318.

Bishop, P.O., Kozak, W., & Vakkur, G.J. (1962) Some quantitative aspects of the cat's eye: axis and plane of reference, visual field co-ordinates and optics. *J. Physiol.*, **163**, 466–502.2.

Bisiach, E. & Luzzatti, C. (1978) Unilateral neglect of representational space. *Cortex.*, **14**, 129–133.

Bisley, J.W. (2011) The neural basis of visual attention. *J. Physiol.*, **589**, 49–57.

Bisley, J.W. & Goldberg, M.E. (2010) Attention, intention, and priority in the parietal lobe. *Annu. Rev. Neurosci.*, **33**, 1–21.

Bokil, H., Andrews, P., Kulkarni, J.E., Mehta, S., & Mitra, P.P. (2010) Chronux: A platform for analyzing neural signals. *J. Neurosci. Methods*, **192**, 146–151.

Bosman, C.A., Schoffelen, J.-M., Brunet, N., Oostenveld, R., Bastos, A.M., Womelsdorf, T., Rubehn, B., Stieglitz, T., De Weerd, P., & Fries, P. (2012) Attentional stimulus selection through selective synchronization between monkey visual areas. *Neuron*, **75**, 875–888.

Bowling, D. & Michael, C. (1984) Terminal patterns of single, physiologically characterized optic tract fibers in the cat's lateral geniculate nucleus. *J. Neurosci.*, **4**, 198–216.

Braitenberg, V. & Braitenberg, C. (1979) Geometry of orientation columns in the visual cortex. *Biol. Cybern.*, **33**, 179–186.

Bressler, S.L. & Richter, C.G. (2014) Interareal oscillatory synchronization in top-down neocortical processing. *Curr. Opin. Neurobiol.*, **31C**, 62–66.

Bruns, A. & Eckhorn, R. (2004) Task-related coupling from high- to low-frequency signals among visual cortical areas in human subdural recordings. *Int. J. Psychophysiol.*, **51**, 97–116.

Bullier, J., Hupe, J.M., James, A.C., & Girard, P. (2001) The role of feedback connections in shaping the responses of visual cortical neurons. *Prog Brain Res*, **134**, 193–204.

Buschman, T.J. & Miller, E.K. (2007) Top-down versus bottom-up control of attention in the prefrontal and posterior parietal cortices. *Science*, **315**, 1860–1862.

Canolty, R. & Knight, R. (2010) The functional role of cross-frequency coupling. *Trends Cogn. Sci.*, **14**, 506–515.

Canolty, R.T., Edwards, E., Dalal, S.S., Soltani, M., Nagarajan, S.S., Kirsch, H.E., Berger, M.S., Barbaro, N.M., & Knight, R.T. (2006) High gamma power is phase-locked to theta oscillations in human neocortex. *Science*, **313**, 1626–1628.

Carrasco, M. (2011) Visual attention: The past 25 years. *Vision Res.*, **51**, 1484–1525.

Carrera, E. & Tononi, G. (2014) Diaschisis: past, present, future. *Brain*, **137**, 2408–

2422.

Chelazzi, L., Miller, E.K., Duncan, J., & Desimone, R. (1993) A neural basis for visual search in inferior temporal cortex. *Nature*, **363**, 345–347.

Cleland, B.G., Dubin, M.W., & Levick, W.R. (1971a) Sustained and transient neurones in the cat's retina and lateral geniculate nucleus. *J. Physiol.*, **217**, 473–496.

Cleland, B.G., Dubin, M.W., & Levick, W.R. (1971b) Sustained and transient neurones in the cat's retina and lateral geniculate nucleus. *J. Physiol.*, **217**, 473–496.

Cohen, M.R. & Maunsell, J.H.R. (2009) Attention improves performance primarily by reducing interneuronal correlations. *Nat. Neurosci.*, **12**, 1594–1600.

Connor, C.E., Preddie, D.C., Gallant, J.L., & Van Essen, D.C. (1997) Spatial attention effects in macaque area V4. *J. Neurosci.*, **17**, 3201–3214.

Corbetta, M., Kincade, M.J., Lewis, C., Snyder, A.Z., & Sapir, A. (2005) Neural basis and recovery of spatial attention deficits in spatial neglect. *Nat. Neurosci.*, **8**, 1603–1610.

Corbetta, M. & Shulman, G.L. (2011) *Spatial Neglect and Attention Networks.*, Annual review of neuroscience.

Cutrell, E. & Marrocco, R. (2002) Electrical microstimulation of primate posterior parietal cortex initiates orienting and alerting components of covert attention. *Exp. Brain Res.*, **144**, 103–113.

de Haan, B., Rorden, C., & Karnath, H.-O. (2013) Abnormal perilesional BOLD signal is not correlated with stroke patients' behavior. *Front. Hum. Neurosci.*, **7**, 669.

Desimone, R. & Duncan, J. (1995) Neural mechanisms of selective visual attention. *Annu. Rev. Neurosci.*, **18**, 193–222.

Di Russo, F., Aprile, T., Spitoni, G., & Spinelli, D. (2008) Impaired visual processing of contralesional stimuli in neglect patients: A visual-evoked potential study. *Brain*, **131**, 842–854.

Dinse, H.R. & Krüger, K. (1994) The timing of processing along the visual pathway in the cat. *Neuroreport*, **5**, 893–897.

Donner, T.H. & Siegel, M. (2011) A framework for local cortical oscillation patterns. *Trends Cogn. Sci.*, **15**, 191–199.

Dreher, B., Leventhal, a G., & Hale, P.T. (1980) Geniculate input to cat visual cortex: a comparison of area 19 with areas 17 and 18. *J. Neurophysiol.*, **44**, 804–826.

Dreher, B., Wang, C., & Burke, W. (1996) Limits of parallel processing: Excitatory convergence of different information channels on single neurons in striate and extrastriate visual cortices. *Clin. Exp. Pharmacol. Physiol.*, **23**, 913–925.

Dreher, B., Wang, C., Turlejski, K.J., Djavadian, R.L., & Burke, W. (1996) Areas PMLS and 21a of cat visual cortex: two functionally distinct areas. *Cereb. Cortex*, **6**, 585–599.

Driver, J. & Mattingley, J.B. (1998) Parietal neglect and visual awareness. *Nat. Neurosci.*, **1**, 17–22.

Driver, J. & Vuilleumier, P. (2001) Perceptual awareness and its loss in unilateral neglect and extinction. *Cognition*, **79**, 39–88.

Dumbrava, D., Faubert, J., & Casanova, C. (2001) Global motion integration in the cat's lateral posterior-pulvinar complex. *Eur. J. …*, **13**, 2218–2226.

Duncan, J. (1984) Selective attention and the organization of visual information. *J. Exp. Psychol. Gen.*, **113**, 501–517.

Engel, a K., Fries, P., & Singer, W. (2001) Dynamic predictions: oscillations and synchrony in top-down processing. *Nat. Rev. Neurosci.*, **2**, 704–716.

Engel, a K. & Singer, W. (2001) Temporal binding and the neural correlates of sensory awareness. *Trends Cogn. Sci.*, **5**, 16–25.

Engel, A.K., Kreiter, A.K., König, P., & Singer, W. (1991) Synchronization of oscillatory neuronal responses between striate and extrastriate visual cortical areas of the cat. *Proc. Natl. Acad. Sci. U. S. A.*, **88**, 6048–6052.

Eysel, U.T. & Schweigart, G. (1999) Increased receptive field size in the surround of chronic lesions in the adult cat visual cortex. *Cereb. Cortex*, **9**, 101–109.

Felleman, D.J. & Van Essen, D.C. (1991) Distributed Hierarchical Processing in the Primate Cerebral Cortex. *Cereb. Cortex*, **1**, 1–47.

Fries, P., Womelsdorf, T., Oostenveld, R., & Desimone, R. (2008) The effects of visual stimulation and selective visual attention on rhythmic neuronal synchronization in macaque area V4. *J. Neurosci.*, **28**, 4823–4835.

Fukada, Y. & Saito, H. (1971) The relationship between response characteristics to flicker stimulation and receptive field organization in the cat's optic nerve fibers. *Vision Res.*, **11**, 227–240.

Galuske, R. a W., Schmidt, K.E., Goebel, R., Lomber, S.G., & Payne, B.R. (2002) The role of feedback in shaping neural representations in cat visual cortex. *Proc. Natl. Acad. Sci. U. S. A.*, **99**, 17083–17088.

Gilbert, C.D. & Li, W. (2013) Top-down influences on visual processing. *Nat. Rev. Neurosci.*, **14**, 350–363.

Gilbert, C.D. & Sigman, M. (2007) Brain states: top-down influences in sensory processing. *Neuron*, **54**, 677–696.

Grant, S. & Shipp, S. (1991) Visuotopic organization of the lateral suprasylvian area and of an adjacent area of the ectosylvian gyrus of cat cortex: a physiological and connectional study. *Vis. Neurosci.*, **6**, 315–338.

Graybiel, A.M. & Berson, D.M. (1980) Histochemical identification and afferent connections of subdivisions in the lateralis posterior-pulvinar complex and related thalamic nuclei in the cat. *Neuroscience*, **5**, 1175–1238.

Grieve, K., Rivadulla, C., & Cudeiro, J. (2009) Visual Role of the Pulvinar. In Binder, M., Hirokawa, N., & Windhorst, U. (eds), *Encyclopedia of Neuroscience SE - 6370*. Springer Berlin Heidelberg, pp. 4333–4336.

Griffith, R.W. & Humphrey, D.R. (2006) Long-term gliosis around chronically implanted platinum electrodes in the Rhesus macaque motor cortex. *Neurosci. Lett.*, **406**, 81–86.

Guldin, W.O. & Markowitsch, H.J. (1982) Epidural kainate, but not ibotenate, produces lesions in local and distant regions of the brain. A comparison of the intracerebral actions of kainic acid and ibotenic acid. *J. Neurosci. Methods*, **5**, 83–93.

Hardy, S.C. & Stein, B.E. (1988) Small lateral suprasylvian cortex lesions produce visual neglect and decreased visual activity in the superior colliculus. *J. Comp. Neurol.*, **273**, 527–542.

Heilman, K.M. & Adams, D.J. (2003) Callosal neglect. *Arch. Neurol.*, **60**, 276–279.

Hier, D.B., Mondlock, J., & Caplan, L.R. (1983) Recovery of behavioral abnormalities after right hemisphere stroke. *Neurology*, **33**, 345–350.

Hilgetag, C.C., Kötter, R., & Young, M.P. (1999) Inter-hemispheric competition of sub-cortical structures is a crucial mechanism in paradoxical lesion effects and spatial neglect. *Prog. Brain Res.*,.

Holz, E.M., Glennon, M., Prendergast, K., & Sauseng, P. (2010) Theta-gamma phase synchronization during memory matching in visual working memory. *Neuroimage*, **52**, 326–335.

Hoshino, K., Horie, M., Nagy, A., Berényi, A., Benedek, G., & Norita, M. (2010) Direct synaptic connections between superior colliculus afferents and thalamo-insular projection neurons in the feline suprageniculate nucleus: A double-labeling study with WGA-HRP and kainic acid. *Neurosci. Res.*, **66**, 7–13.

Houzel, J.C., Milleret, C., & Innocenti, G. (1994) Morphology of callosal axons interconnecting areas 17 and 18 of the cat. *Eur. J. Neurosci.*, **6**, 898–917.

Hubel, D. & Wiesel, T. (1962) Receptive fields, binocular interaction and functional architecture in the cat's visual cortex. *J. Physiol.*, **26**, 285–292.

Hubel, D. & Wiesel, T. (1965) Receptive fields and functional architecture in two nonstriate visual areas (18 and 19) of the cat. *J. Neurophysiol.*, 229–289.

Hubel, D. & Wiesel, T. (1969a) Visual area of the lateral suprasylvian gyrus (Clare—Bishop area) of the cat. *J. Physiol.*,.

Hubel, D. & Wiesel, T. (1969b) Visual area of the lateral suprasylvian gyrus (Clare—Bishop area) of the cat. *J. Physiol.*, 251–260.

Hubel, D.H. & Wiesel, T.N. (1967) Cortical and callosal connections concerned with the vertical meridian of visual fields in the cat. *J. Neurophysiol.*, **30**, 1561–1573.

Hupé, J.M., James, A.C., Payne, B.R., Lomber, S.G., Girard, P., & Bullier, J. (1998) Cortical feedback improves discrimination between figure and background by V1, V2 and V3 neurons. *Nature*, **394**, 784–787.

Ibos, G., Duhamel, J.-R., & Ben Hamed, S. (2013) A functional hierarchy within the parietofrontal network in stimulus selection and attention control. *J. Neurosci.*, **33**, 8359–8369.

Ignashchenkova, A., Dicke, P.W., Haarmeier, T., & Thier, P. (2004) Neuron-specific contribution of the superior colliculus to overt and covert shifts of attention. *Nat. Neurosci.*, **7**, 56–64.

Illing, R.B. & Wässle, H. (1981) The retinal projection to the thalamus in the cat: a quantitative investigation and a comparison with the retinotectal pathway. *J. Comp. Neurol.*, **202**, 265–285.

Innocenti, G. (1986) General organization of callosal connections in the cerebral cortex. In *Sensory-Motor Areas and Aspects of Cortical Connectivity*.

Innocenti, G.M. (2009) Dynamic interactions between the cerebral hemispheres. *Exp. brain Res.*, **192**, 417–423.

Jensen, O. & Tesche, C.D. (2002) Frontal theta activity in humans increases with memory load in a working memory task. *Neuroscience*, **15**, 1395–1399.

Jones, M.W. & Wilson, M.A. (2005) Theta rhythms coordinate hippocampal-prefrontal interactions in a spatial memory task. *PLoS Biol.*, **3**, 1–13.

Kahana, M.J., Seelig, D., & Madsen, J.R. (2001) Theta returns. *Curr. Opin. Neurobiol.*, **11**, 739–744.

Karnath, H.O. (1997) Spatial orientation and the representation of space with parietal lobe lesions. *Philos.Trans.R.Soc.Lond.B.Biol.Sci.*, **352**, 1411–1419.

Karnath, H.O., Fetter, M., & Dichgans, J. (1996) Ocular exploration of space as a function of neck proprioceptive and vestibular input--observations in normal subjects and patients with spatial neglect after parietal lesions. *Exp. Brain Res.*, **109**, 333–342.

Karnath, H.O., Niemeier, M., & Dichgans, J. (1998) Space exploration in neglect. *Brain*, **121 (Pt 1**, 2357–2367.

Kastner, S. & Ungerleider, L.G. (2000) Mechanisms of visual attention in the human cortex. *Annu. Rev. Neurosci.*, **23**, 315–341.

Kerkhoff, G. & Schenk, T. (2012) Rehabilitation of neglect: an update. *Neuropsychologia*, **50**, 1072–1079.

Kinsbourne, M. (1970a) A model for the mechanism of unilateral neglect of space. *Trans. Am. Neurol. Assoc.*, **95**, 143–146.

Kinsbourne, M. (1970b) A model for the mechanism of unilateral neglect of space. *Trans. Am. Neurol. Assoc.*, **95**, 143–146.

Kleim, J. a (2011) Neural plasticity and neurorehabilitation: teaching the new brain old tricks. *J. Commun. Disord.*, **44**, 521–528.

Kopell, N., Ermentrout, G.B., Whittington, M. a, & Traub, R.D. (2000) Gamma rhythms and beta rhythms have different synchronization properties. *Proc. Natl. Acad. Sci. U. S. A.*, **97**, 1867–1872.

Krauzlis, R.J., Lovejoy, L.P., & Zénon, A. (2013) Superior colliculus and visual spatial attention. *Annu. Rev. Neurosci.*, **36**, 165–182.

Krout, K.E., Loewy, A.D., Westby, G.W., & Redgrave, P. (2001) Superior colliculus projections to midline and intralaminar thalamic nuclei of the rat. *J. Comp. Neurol.*, **431**, 198–216.

Làdavas, E., Petronio, A., & Umiltà, C. (1990) The deployment of visual attention in the intact field of hemineglect patients. *Cortex.*, **26**, 307–317.

Lakatos, P., Karmos, G., Mehta, A.D., Ulbert, I., & Schroeder, C.E. (2008) Entrainment of neuronal oscillations as a mechanism of attentional selection. *Science*, **320**, 110–113.

Lamme, V. a & Roelfsema, P.R. (2000) The distinct modes of vision offered by feedforward and recurrent processing. *Trends Neurosci.*, **23**, 571–579.

Lega, B.C., Jacobs, J., & Kahana, M. (2012) Human hippocampal theta oscillations and the formation of episodic memories. *Hippocampus*, **22**, 748–761.

Livingstone, M. & Hubel, D. (1988) Segregation of Form, Color, Movement, and Depth: Anatomy, Physiology, and Perception. *Science (80-.).*, **240**, 740–749.

Lomber, S.G. & Payne, B.R. (1996) Removal of two halves restores the whole: reversal of visual hemineglect during bilateral cortical or collicular inactivation in the cat. *Vis. Neurosci.*, **13**, 1143–1156.

Lomber, S.G. & Payne, B.R. (2004) Cerebral areas mediating visual redirection of gaze: cooling deactivation of 15 loci in the cat. *J. Comp. Neurol.*, **474**, 190–208.

Lomber, S.G., Payne, B.R., Cornwell, P., & Long, K.D. (1996) Perceptual and cognitive visual functions of parietal and temporal cortices in the cat. *Cereb. Cortex*, **6**, 673–695.

Lomber, S.G., Yi, S.K., & Woller, E.M. (2006) Relocation of specific visual functions following damage of mature posterior parietal cortex. *Prog. Brain Res.*, **157**, 157–172.

Makarov, V.A., Schmidt, K.E., Castellanos, N.P., Lopez-Aguado, L., & Innocenti, G.M. (2008) Stimulus-dependent interaction between the visual areas 17 and 18 of the 2 hemispheres of the ferret (Mustela putorius). *Cereb. Cortex*, **18**, 1951–1960.

Marshall, J.C. & Halligan, P.W. (1988) Blindsight and insight in visuo-spatial neglect. *Nature*, **336**, 766–767.

Marshall, J.C. & Halligan, P.W. (1989) When right goes left: an investigation of line bisection in a case of visual neglect. *Cortex.*, **25**, 503–515.

Mather, G. (2006) Visual physiology. In *Foundations of Perception*, *Psychology/Neuroscience*. Taylor & Francis, pp. 192–193.

Mazzoni, A., Logothetis, N., & Panzeri, S. (2012) The information content of Local Field Potentials: experiments and models. *arXiv Prepr. arXiv1206.0560*, 1–32.

McAdams, C.J. & Maunsell, J.H. (1999) Effects of attention on the reliability of individual neurons in monkey visual cortex. *Neuron*, **23**, 765–773.

McAlonan, K., Cavanaugh, J., & Wurtz, R.H. (2008a) Guarding the gateway to cortex with attention in visual thalamus. *Nature*, **456**, 391–394.

McAlonan, K., Cavanaugh, J., & Wurtz, R.H. (2008b) Guarding the gateway to cortex with attention in visual thalamus. *Nature*, **456**, 391–394.

McHaffie, J.G., Stanford, T.R., Stein, B.E., Coizet, V., & Redgrave, P. (2005) Subcortical loops through the basal ganglia. *Trends Neurosci.*, **28**, 401–407.

McMains, S. & Kastner, S. (2011) Interactions of top-down and bottom-up mechanisms in human visual cortex. *J Neurosci*, **31**, 587–597.

Meredith, M.A. & Stein, B.E. (1986) Spatial factors determine the activity of multisensory neurons in cat superior colliculus. *Brain Res.*, **365**, 350–354.

Mesulam, M.M. (1981) A cortical network for directed attention and unilateral neglect. *Ann. Neurol.*, **10**, 309–325.

Mesulam, M.M. (1999) Spatial attention and neglect: parietal, frontal and cingulate contributions to the mental representation and attentional targeting of salient extrapersonal events. *Philos. Trans. R. Soc. Lond. B. Biol. Sci.*, **354**, 1325–1346.

Mignard, M. & Malpeli, J.G. (1991) Paths of information flow through visual cortex. *Science*, **251**, 1249–1251.

Miller, R. (1991) *Cortico-Hippocampal Interplay and the Representation of Contexts in the Brain*, Studies of Brain Function, Studies of Brain Function. Springer Berlin Heidelberg, Berlin, Heidelberg.

Mitchell, J., Sundberg, K., & Reynolds, J. (2007) Differential attention-dependent response modulation across cell classes in macaque visual area V4 - Supplemental Data. *Neuron*, **55**, 1–14.

Moore, T. & Armstrong, K.M. (2003) Selective gating of visual signals by microstimulation of frontal cortex. *Nature*, **421**, 370–373.

Moore, T. & Fallah, M. (2004) Microstimulation of the frontal eye field and its effects on covert spatial attention. *J. Neurophysiol.*, **91**, 152–162.

Moran, J. & Desimone, R. (1985) Selective attention gates visual processing in the extrastriate cortex. *Science*, **229**, 782–784.

Mort, D.J., Malhotra, P., Mannan, S.K., Rorden, C., Pambakian, A., Kennard, C., & Husain, M. (2003) The anatomy of visual neglect. *Brain*, **126**, 1986–1997.

Mozer, M.C., Halligan, P.W., & Marshall, J.C. (1997) The end of the line for a brain-damaged model of unilateral neglect. *J. Cogn. Neurosci.*, **9**, 171–190.

Müller, J.R., Philiastides, M.G., & Newsome, W.T. (2005) Microstimulation of the superior colliculus focuses attention without moving the eyes. *Proc. Natl. Acad. Sci. U. S. A.*, **102**, 524–529.

Noudoost, B., Chang, M.H., Steinmetz, N. a, & Moore, T. (2010) Top-down control of visual attention. *Curr. Opin. Neurobiol.*, **20**, 183–190.

Nudo, R.J. (2011) Neural bases of recovery after brain injury. *J. Commun. Disord.*, **44**, 515–520.

Osipova, D., Hermes, D., & Jensen, O. (2008) Gamma power is phase-locked to posterior alpha activity. *PLoS One*, **3**, e3990.

Otsuka, R. & Hassler, R. (1962) Über Aufbau und Gliederung der corticalen Sehsphäre bei der Katze. *Arch. Psychiatr. Nervenkr.*, **234**, 212–234.

Palmer, L. a, Rosenquist, a C., & Tusa, R.J. (1978) The retinotopic organization of lateral suprasylvian visual areas in the cat. *J. Comp. Neurol.*, **177**, 237–256.

Payne, B. & Lomber, S. (2003) Quantitative analyses of principal and secondary compound parieto-occipital feedback pathways in cat. *Exp. brain Res.*, **152**, 420–433.

Payne, B. & Peters, A. (2001) The Concept of Cat Primary Visual Cortex. In Payne, B.R. & Peters, A. (eds), *The Cat Primary Visual Cortex*. Academic Press, pp. 1–129.

Payne, B.R. (1993) Evidence for visual cortical area homologs in cat and macaque monkey. *Cereb. Cortex*, **3**, 1–25.

Payne, B.R., Lomber, S.G., Geeraerts, S., van der Gucht, E., & Vandenbussche, E. (1996) Reversible visual hemineglect. *Proc. Natl. Acad. Sci.*, **93**, 290–294.

Payne, B.R. & Rushmore, R.J. (2003) Animal models of cerebral neglect and its cancellation. *Neuroscientist*, **9**, 446–454.

Payne, B.R. & Rushmore, R.J. (2004) Functional circuitry underlying natural and interventional cancellation of visual neglect. *Exp. brain Res.*, **154**, 127–153.

Percival, D.B. & Walden, A.T. (1993) *Spectral Analysis for Physical Applications*, Cambridge Univ. Press, New York. Cambridge University Press, Cambridge.

Petersen, S.E., Robinson, D.L., & Morris, J.D. (1987) Contributions of the pulvinar to visual spatial attention. *Neuropsychologia*, **25**, 97–105.

Pietrasanta, M., Restani, L., & Caleo, M. (2012) The corpus callosum and the visual cortex: plasticity is a game for two. *Neural Plast.*, **2012**, 1–10.

Posner, M.I. (1980) Orienting of attention. *Q. J. Exp. Psychol.*, **32**, 3–25.

Pouget, A. & Driver, J. (2000) Relating unilateral neglect to the neural coding of space. *Curr. Opin. Neurobiol.*, **10**, 242–249.

Ptak, R. & Fellrath, J. (2013) Spatial neglect and the neural coding of attentional priority. *Neurosci. Biobehav. Rev.*, **37**, 705–722.

Ptak, R., Golay, L., Müri, R.M., & Schnider, A. (2009) Looking left with left neglect: The role of spatial attention when active vision selects local image features for fixation. *Cortex*, **45**, 1156–1166.

Quiroga, R.Q., Nadasdy, Z., & Ben-Shaul, Y. (2004) Unsupervised spike detection and sorting with wavelets and superparamagnetic clustering. *Neural Comput.*, **16**, 1661–1687.

Raczkowski, D. & Rosenquist, A. (1983) Connections of the multiple visual cortical areas with the lateral posterior-pulvinar complex and adjacent thalamic nuclei in the cat. *J. Neurosci.*, **3**, 1912–1942.

Raczkowski, D. & Rosenquist, A.C. (1981) Retinotopic organization in the cat lateral posterior-pulvinar complex. *Brain Res.*, **221**, 185–191.

Rafal, R.D. (1994) Neglect. *Curr. Opin. Neurobiol.*, **4**, 231–236.

Rastelli, F., Funes, M.-J., Lupiáñez, J., Duret, C., & Bartolomeo, P. (2008) Left visual neglect: is the disengage deficit space- or object-based? *Exp. brain Res.*, **187**, 439–446.

Reinoso-Suárez, F. (1961) *Topographischer Hirnatlas Der Katze Für Experimental-Physiologische Untersuchungen*. Merck.

Reynolds, J.H., Chelazzi, L., & Desimone, R. (1999) Competitive mechanisms subserve attention in macaque areas V2 and V4. *J. Neurosci.*, **19**, 1736–1753.

Rizzuto, D.S., Madsen, J.R., Bromfield, E.B., Schulze-Bonhage, a, Seelig, D., Aschenbrenner-Scheibe, R., & Kahana, M.J. (2003) Reset of human neocortical oscillations during a working memory task. *Proc. Natl. Acad. Sci. U. S. A.*, **100**, 7931–7936.

Romo, P.A., Wang, C., Zeater, N., Solomon, S.G., & Dreher, B. (2011) Phase sensitivities, excitatory summation fields, and silent suppressive receptive fields of single neurons in the parastriate cortex of the cat. *J. Neurophysiol.*, **106**, 1688–1712.

Rosenquist, A. (1985) Connections of visual cortical areas in the cat. In Jones, E.G. & Peters, A.A. (eds), *Cerebral Cortex Vol. 3 : Visual Cortex*, 1st edn. Plenum Publishing Corporation, New York and London, pp. 81–117.

Rushmore, R.J., Payne, B., & Valero-Cabre, A. (2010) Recovery of function following unilateral damage to visuoparietal cortex. *Exp. brain Res.*, **203**, 693–700.

Salazar, R.F., König, P., & Kayser, C. (2004) Directed interactions between visual areas and their role in processing image structure and expectancy. *Eur. J. Neurosci.*, **20**, 1391–1401.

Salin, P.A. & Bullier, J. (1995) Corticocortical connections in the visual system: structure and function. *Physiol. Rev.*, **75**, 107–154.

Salinas, E. & Sejnowski, T.J. (2001) Correlated neuronal activity and the flow of neural information. *Nat. Rev. Neurosci.*, **2**, 539–550.

Sandell, J.H. & Schiller, P.H. (1982) Effect of cooling area 18 on striate cortex cells in the squirrel monkey. *J. Neurophysiol.*, **48**, 38–48.

Sanderson, K.J. (1971) The projection of the visual field to the lateral geniculate and medial interlaminar nuclei in the cat. *J. Comp. Neurol.*, **143**, 101–108.

Sanides, D. (1978) The retinotopic distribution of visual callosal projections in the suprasylvian visual areas compared to the classical visual areas (17, 18, 19) in the cat. *Exp. Brain Res.*, **33**, 435–443.

Sauseng, P., Klimesch, W., Gruber, W.R., & Birbaumer, N. (2008) Cross-frequency phase synchronization: a brain mechanism of memory matching and attention. *Neuroimage*, **40**, 308–317.

Scannell, J.W., Blakemore, C., & Young, M.P. (1995) Analysis of connectivity in the cat cerebral cortex. *J. Neurosci.*, **15**, 1463–1483.

Schwarcz, R., Hökfelt, T., Fuxe, K., Jonsson, G., Goldstein, M., & Terenius, L. (1979) Ibotenic acid-induced neuronal degeneration: A morphological and neurochemical study. *Exp. Brain Res.*, **37**, 199–216.

Segal, R.L. & Beckstead, R.M. (1984) The lateral suprasylvian corticotectal projection in cats. *J. Comp. Neurol.*, **225**, 259–275.

Segraves, M. a & Rosenquist, a C. (1982) The afferent and efferent callosal connections of retinotopically defined areas in cat cortex. *J. Neurosci.*, **2**, 1090–1107.

Serences, J.T. & Yantis, S. (2006) Selective visual attention and perceptual coherence. *Trends Cogn. Sci.*, **10**, 38–45.

Sherk, H. (1986) Location and connections of visual cortical areas in the cat's suprasylvian sulcus. *J. Comp. Neurol.*, **247**, 1–31.

Sherk, H. (2010) Evidence regarding the integrity of the posterior medial lateral suprasylvian visual area in the cat. *J. Comp. Neurol.*, **518**, 3343–3358.

Sherman, S.M. & Spear, P.D. (1982a) Organization of visual pathways in normal and visually deprived cats. *Physiol. Rev.*, **62**, 738–855.

Sherman, S.M. & Spear, P.D. (1982b) Organization of visual pathways in normal and visually deprived cats. *Physiol. Rev.*, **62**, 738–855.

Siapas, A.G., Lubenov, E. V, & Wilson, M. a (2005) Prefrontal phase locking to hippocampal theta oscillations. *Neuron*, **46**, 141–151.

Singer, W. (1999) Neuronal Synchrony : A Versatile Code for the Definition of Relations ? Most of our knowledge about the functional organization **24**, 49–65.

Singer, W. & Gray, C.M. (1995) Visual feature integration and the temporal correlation hypothesis. *Annu. Rev. Neurosci.*, **18**, 555–586.

Sirota, A., Montgomery, S., Fujisawa, S., Isomura, Y., Zugaro, M., & Buzs??ki, G. (2008) Entrainment of Neocortical Neurons and Gamma Oscillations by the Hippocampal Theta Rhythm. *Neuron*, **60**, 683–697.

Sprague, J.M. (1966) Interaction of cortex and superior colliculus in mediation of visually guided behavior in the cat. *Science*, **153**, 1544–1547.

Stein, B., Stanford, T., Godwin, D., & McHaffie, J. (2013) The Superior Colliculus and Visual Thalamus. *Neurosci. 21st Century*, 1591–1620.

Stephan, K.E., Marshall, J.C., Friston, K.J., Rowe, J.B., Ritzl, A., Zilles, K., & Fink, G.R. (2003) Lateralized cognitive processes and lateralized task control in the human brain. *Science*, **301**, 384–386.

Stone, J. & Hoffmann, K.P. (1972a) Very slow-conducting ganglion cells in the cat's retina: a major, new functional type? *Brain Res.*, **43**, 610–616.

Stone, J. & Hoffmann, K.P. (1972b) Very slow-conducting ganglion cells in the cat's retina: a major, new functional type? *Brain Res.*, **43**, 610–616.

Suner, S., Fellows, M.R., Vargas-Irwin, C., Nakata, K., & Donoghue, J.P. (2005) Reliability of signals from a chronically implanted, silicon-gased electrode array in non-human primate primary motor cortex. *IEEE Trans Neural Syst Rehabil Eng*, **13**, 524–541.

Supèr, H., Spekreijse, H., & Lamme, V. a (2001) Two distinct modes of sensory processing observed in monkey primary visual cortex (V1). *Nat. Neurosci.*, **4**, 304–310.

Symonds, L.L. & Rosenquist, a C. (1984a) Laminar origins of visual corticocortical connections in the cat. *J. Comp. Neurol.*, **229**, 39–47.

Symonds, L.L. & Rosenquist, a C. (1984b) Corticocortical connections among visual areas in the cat. *J. Comp. Neurol.*, **229**, 1–38.

Symonds, L.L., Rosenquist, A.C., Edwards, S.B., & Palmer, L.A. (1981) Projections of the pulvinar-lateral posterior complex to visual cortical areas in the cat. *Neuroscience*, **6**, 1995–2020.

Tallon-Baudry, C. & Bertrand, O. (1999a) Oscillatory gamma activity in humans and its role in object representation. *Trends Cogn. Sci.*, **3**, 151–162.

Tallon-Baudry, C. & Bertrand, O. (1999b) Oscillatory gamma activity in humans and its role in object representation. *Trends Cogn. Sci.*, **3**, 151–162.

Thompson, K.G. & Bichot, N.P. (2005) *Development, Dynamics and Pathiology of Neuronal Networks: From Molecules to Functional Circuits*, Progress in brain research, Progress in Brain Research. Elsevier.

Tiesinga, P.H.E., Fellous, J.-M., Salinas, E., José, J. V, & Sejnowski, T.J. (2004) Synchronization as a mechanism for attentional gain modulation. *Neurocomputing*, **58-60**, 641–646.

Tong, L., Kalil, R.E., & Spear, P.D. (1982) Thalamic projections to visual areas of the middle suprasylvian sulcus in the cat. *J. Comp. Neurol.*, **212**, 103–117.

Tusa, R.J., Palmer, L. a, & Rosenquist, a C. (1978) The retinotopic organization of area 17 (striate cortex) in the cat. *J. Comp. Neurol.*, **177**, 213–235.

Tusa, R.J., Palmer, L.A., & Rosenquist, A.C. (1981a) Multiple Cortical Visual Areas. In *Multiple Visual Areas SE - 1*, *Cortical Sensory Organization*. Humana Press, pp. 1–31.

Tusa, R.J., Palmer, L.A., & Rosenquist, A.C. (1981b) Multiple Cortical Visual Areas. In *Multiple Visual Areas SE - 1*, *Cortical Sensory Organization*. Humana Press, pp. 1–31.

Tusa, R.J., Rosenquist, A.C., & Palmer, L.A. (1979) Retinotopic organization of areas 18 and 19 in the cat. *J. Comp. Neurol.*, **185**, 657–678.

Updyke, B. V (1981) Projections from visual areas of the middle suprasylvian sulcus onto the lateral posterior complex and adjacent thalamic nuclei in cat. *J. Comp. Neurol.*, **201**, 477–506.

Updyke, B. V (1983) A reevaluation of the functional organization and cytoarchitecture of the feline lateral posterior complex, with observations on adjoining cell groups. *J. Comp. Neurol.*, **219**, 143–181.

van Kerkoerle, T., Self, M.W., Dagnino, B., Gariel-Mathis, M. -a., Poort, J., van der Togt, C., & Roelfsema, P.R. (2014) Alpha and gamma oscillations characterize feedback and feedforward processing in monkey visual cortex. *Proc. Natl. Acad. Sci.*, **111**, 14332–14341.

Vanduffel, W., Payne, B.R., Lomber, S.G., & Orban, G. a (1997) Functional impact of cerebral connections. *Proc. Natl. Acad. Sci. U. S. A.*, **94**, 7617–7620.

von Stein, a, Chiang, C., & König, P. (2000) Top-down processing mediated by interareal synchronization. *Proc. Natl. Acad. Sci. U. S. A.*, **97**, 14748–14753.

von Stein, a & Sarnthein, J. (2000) Different frequencies for different scales of cortical integration: from local gamma to long range alpha/theta synchronization. *Int. J. Psychophysiol.*, **38**, 301–313.

Waleszczyk, W.J., Dec, K., & Hekimian, A.A. (1993) Influence of the intertectal connection upon visual responses in the cat's superior colliculus. *Acta Neurobiol. Exp. (Wars).*, **53**, 409–414.

Wardak, C., Olivier, E., & Duhamel, J.-R. (2004) A deficit in covert attention after parietal cortex inactivation in the monkey. *Neuron*, **42**, 501–508.

Wässle, H. & Illing, R.B. (1980) The retinal projection to the superior colliculus in the cat: a quantitative study with HRP. *J. Comp. Neurol.*, **190**, 333–356.

Watson, R.T., Valenstein, E., Day, A.L., & Heilman, K.M. (1984) The effect of corpus callosum lesions on unilateral neglect in monkeys. *Neurology*, **34**, 812–815.

Whitlock, J.R., Sutherland, R.J., Witter, M.P., Moser, M.-B., & Moser, E.I. (2008) Navigating from hippocampus to parietal cortex. *Proc. Natl. Acad. Sci. U. S. A.*, **105**, 14755–14762.

Womelsdorf, T., Anton-Erxleben, K., Pieper, F., & Treue, S. (2006) Dynamic shifts of visual receptive fields in cortical area MT by spatial attention. *Nat. Neurosci.*, **9**, 1156–1160.

Young, C.K. (2011) Behavioral significance of hippocampal θ oscillations: looking elsewhere to find the right answers. *J. Neurophysiol.*, **106**, 497–499.

Zelinsky, G.J. & Bisley, J.W. (2015) The what, where, and why of priority maps and their interactions with visual working memory. *Ann. N. Y. Acad. Sci.*, **1339**, 154–164.

Zénon, A., Ben Hamed, S., Duhamel, J.-R., & Olivier, E. (2009) Attentional guidance relies on a winner-take-all mechanism. *Vision Res.*, **49**, 1522–1531.

Zumbroich, T.J., von Grünau, M., Poulin, C., & Blakemore, C. (1986) Differences of visual field representation in the medial and lateral banks of the suprasylvian cortex (PMLS/PLLS) of the cat. *Exp. brain Res.*, **64**, 77–93.

ACKNOWLEDGEMENTS

I would like to express my gratitude to Prof. Dr. Ralf A. W. Galuske my research supervisor, for his patient guidance, enthusiastic encouragement and useful critiques of this research work.

My sincere thanks also goes to Prof. Dr. Dr. h. c. mult. Wolf Singer who provided me an opportunity to join his group and who gave access to the laboratory, research facilities and an office. Without his precious support, it would not have been possible to conduct this research.

I am particularly grateful for the active assistance and expertise given by Prof Dr. Richard Jarrett Rushmore III in conducting the lesion experiments.

I would like to offer my special thanks to my colleagues from the Max Planck Institute for Brain Research, the Technical University Darmstadt, and the Ernst Strüngmann Institute for Neuroscience for their support, feedback, and friendship. In particular, I am grateful to Dr. William Barnes and Katharina Schmitz for their continuous encouragement and many, many valuable discussions.

I wish to acknowledge the help provided by Dr. Christiane Kiefert, Franzi, Nadine, and the rest of the team in the optimum treatment and care of my cats. My special thanks also are extended to the former or current staff of the mechanical workshop and the IT department at the MPI for Brain Research for their various forms of support during my graduate study.

I would also like to thank all my former undergraduate students for their assistance and their contributions to this research work.

Finally, I wish to thank my mother and Dennis for their patience, support and encouragement throughout my study.

EHRENWÖRTLICHE ERKLÄRUNG

Ich erkläre hiermit ehrenwörtlich, dass ich die vorliegende Arbeit entsprechend den Regeln guter wissenschaftlicher Praxis selbstständig und ohne unzulässige Hilfe Dritter angefertigt habe.

Sämtliche aus fremden Quellen direkt oder indirekt übernommenen Gedanken sowie sämtliche von Anderen direkt oder indirekt übernommenen Daten, Techniken und Materialien sind als solche kenntlich gemacht. Die Arbeit wurde bisher bei keiner anderen Hochschule zu Prüfungszwecken eingereicht.

Neu-Isenburg, den 08.11.2016